THE UNIVERSITY OF OKLAHOMA

GRADUATE COLLEGE

FLUID FLOW PHENOMENA IN DUSTY AIR

A DISSERTATION

SUBMITTED TO THE GRADUATE FACULTY

in partial fulfillment of the requirements for the

degree of

DOCTOR OF PHILOSOPHY

BY

MEHERWAN PHIROZ BOYCE

Norman, Oklahoma

1969

FLUID FLOW PHENOMENA IN DUSTY AIR

APPROVED BY

Edward F. Shamber

Raymond Kaser

Allen H. Weber

K. T. Yang

Maurice Rasmussen

DISSERTATION COMMITTEE

PREFACE

The work reported herein is part of a project supported by the funds from the U. S. Army (ARO-D Project No. 5596-E under Contract No. DA-31-124-ARO-D-349), and was conducted at the Aerospace and Mechanical Engineering Laboratory located on the North Campus of the University of Oklahoma.

Many factors contributed to the successful completion of this project. My particular appreciation goes to the faculty members of the Department of Aerospace and Mechanical Engineering. Of greatest assistance throughout the entire project was the thoughtful consul of Dr. E. F. Blick who was a source of encouragement and inspiration during the total duration of my stay at the Univerisiy of Oklahoma. Also Dr. M. Rasmussen deserves thanks for his assistance with parts of the theory.

Special thanks also goes to Mr. Richard Thorp and Mr. Michael Roe for their untiring aid in the development of photographic techniques for the calculation of the particle velocities. Mr. E. Mallory of Weather Science Incorporated, Norman, Oklahoma deserves thanks for building a special timing device for the photographic techniques involved. Thanks also goes to Captain Ferris Garrett for giving up his vacation and

helping in the fabrication of the experimental setup.

The entire project would not have been possible had it not been for the untiring assistance of my wife, Lola. From the initial stages to the final typing she gave completely of herself in all phases of the project. Her patience, understanding and encouragement contributed greatly to the success of this project.

Finally, I would like to dedicate this dissertation to the memory of my late dear father, Phiroz H. J. Boyce.

TABLE OF CONTENTS

LIST OF TABLES

LIST OF FIGURES

FLUID FLOW PHENOMENA IN DUSTY AIR

CHAPTER I

INTRODUCTION

The development of the various modes of high speed transportation has introduced many new problems in the field of fluid mechanics. One such problem is drag which has been a topic for investigation for a long time.

It is interesting to note that, although we are continually surrounded by a blanket of air, we are only occasionally aware of its resistance to motion. We are reminded, for instance, when riding a bicycle against a moderate to heavy wind that extra muscle power is required to overcome this resistance. This resistance is called drag and acts in a direction opposed to the motion.

This drag force is so commonplace that we accept it without question. Despite the importance of drag, it is interesting to note that experimental measurements and a scientific understanding of drag came several centuries later in history than similar knowledge on the movements of heavenly bodies.

Historical Development

It was not until the late 15th century when the incredible Leonardo de Vinci made a drawing in his sketch book showing flow around a flat plate standing perpendicular to the flow stream, that any one has described the flow around a body. His diagram showed not only the streamlines but also the wake behind the body. Figure (1.1) illustrates the deep insight of this great man, for as we know now it is the wake that is responsible for the majority of drag on such a body.

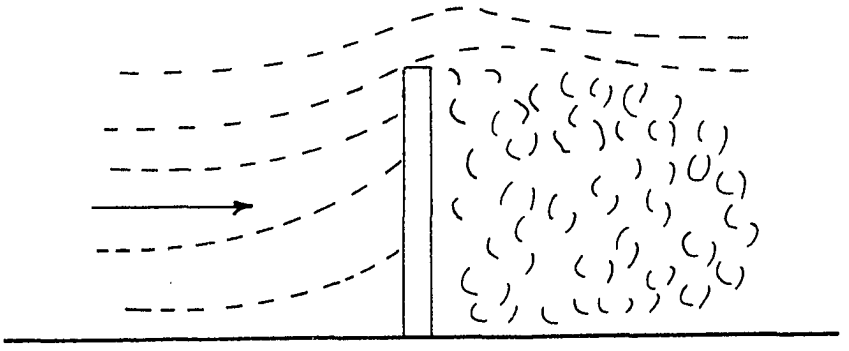

Figure (1.1) De Vinci's Sketch (1490).

In 1687 Newton (1) carried out his now famous experiment from the dome of St. Paul's Cathedral. By dropping spheres of various weights and diameters from atop the dome he found that the drag was proportional to the square of the diameter of the sphere and to the square of the velocity:

$$D \propto V^2 \, d^2 \qquad (1.1a)$$

or

$$D \propto V^2 \, A \qquad (1.1b)$$

This agreed well with the results he had obtained theoretically. Thus from Equation (1.1) a constant now known as the

drag coefficient is obtained:

$$C_d = \frac{D}{\frac{1}{2}\rho V^2 A} \qquad (1.2)$$

It was not until the 18th century that the real importance of air resistance began to be appreciated. Benjamin Robbins (2), whose interest lay in the science of gunnery, or ballistics, carried out a series of tests using cannon balls. Robbins measured the motion of cannon balls by firing them at a ballistic pendulum and was able to deduce that the drag coefficient was not a constant. His results can best be expressed in his own words (2): "The theory of the resistance of the air, established in slow motions by Sir Issac Newton and confirmed by many experiments, is altogether erroneous when applied to the swifter motions of musket or cannon shots; for that, in these cases, the resisting power of the medium is augmented to near three times the quantity assigned by that theory; however, this increased power of resistance diminishes as the velocity of the resisted body diminishes, till at length, when the motion is sufficiently abated, the actual resistance coincides with that supposed theory."

Therefore it was not until the 18th century that an accurate picture of the way in which drag is dependent upon velocity was obtained. Figure (1.2) shows a typical variation of the drag coefficient with velocity. In Robbins' experiments some of the cannon balls traveled greater than the speed of sound on a standard day (Mach number greater than one). As shown in Figure (1.2) the rate of increase of resistance sud-

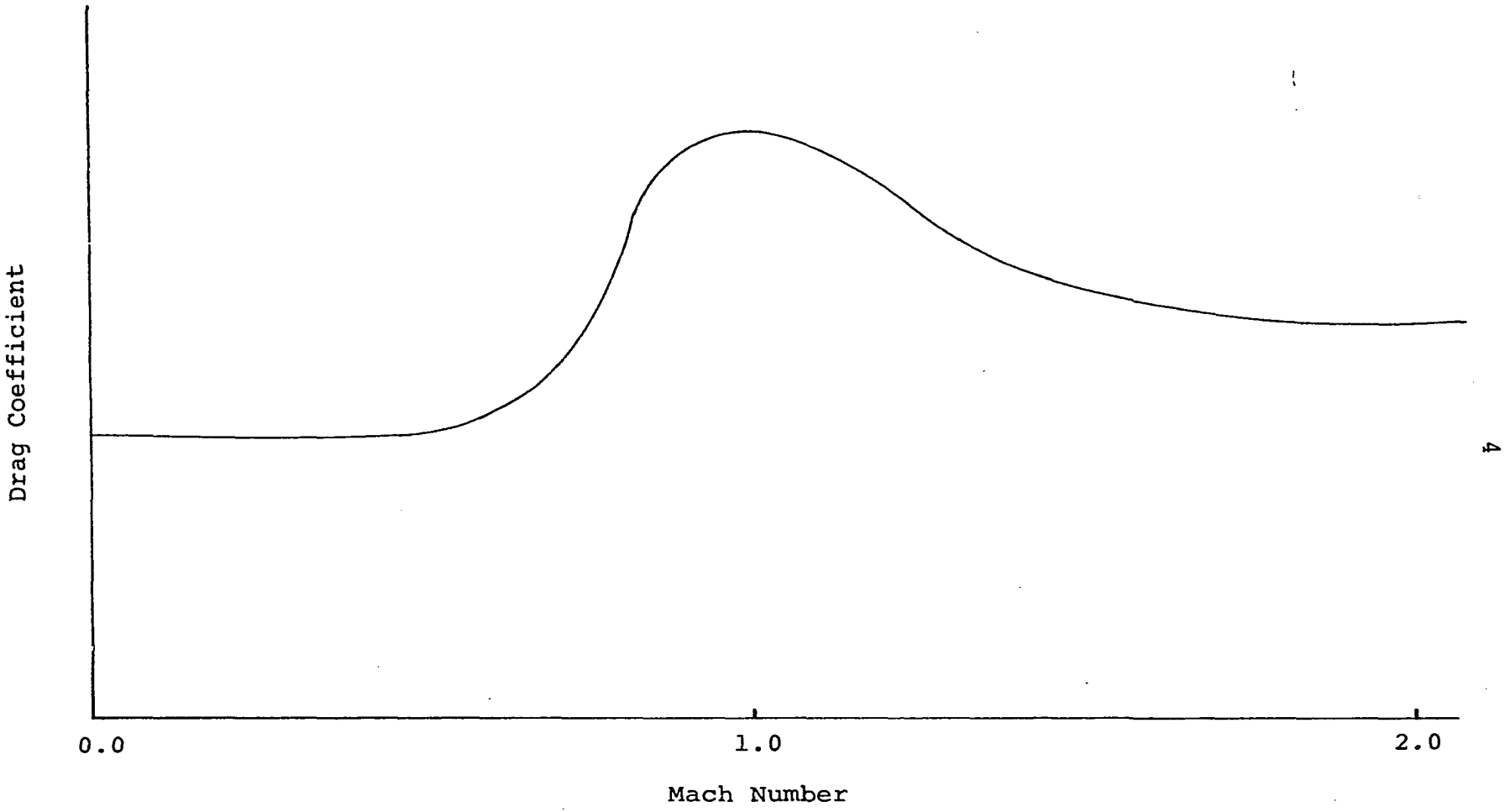

Figure (1.2) Effect of Mach Number on Drag Coefficient.

denly jumps to very large values with the increase in velocity. The sudden increase in drag coefficient was correctly attributed to the elasticity of air. However, the true nature of Robbins' experiments were not comprehended by the close of the 18th century. For example, in Parkinson's System of Natural Philosophy (1785), a treatise on mathematical physics, the following statements are found: "The increase of resistance depends upon the degree of compression (of the air) produced by the body and increases so fast as to render all attempts to augment the velocity of military projectiles, beyond a certain point, very inconvenient or perhaps impracticable. The velocity may be so great as to produce a degree of compression that destroys the body's motion and it will then be reflected in an opposite direction. Thus small shots are often ineffectual or repelled, when fired with very great charges of powder."

Of course we now know this reflection phenomenon, as described in the last sentence, does not really occur. The upper limit on the speed of a body is determined by its melting or ablating temperature. For high enough speeds a body will eventually burn up or vaporize just as a metorite does due to the intense heat generated by friction or as parts of the heat shield of a satellite burn up in the re-entry process.

The importance of the resistance of air to the motion of an object flying through it can be further illustrated by a simple example. If a shell were fired at an

initial velocity of 1700 feet per second and at an angle of 30 degrees to the horizontal the bullet would travel about 12,000 yards in the air (3). If gravity were the only force acting on the bullet it would have traveled 16,000 yards. Thus one can easily see the importance of air resistance in the field of gunnery. To achieve extremely large ranges the ICBM's travel for the majority of their flight at high altitudes where the air is so rarefied that the resistance is extremely small compared with that experienced near sea level.

In the 18th and 19th centuries, before the advent of the airplane, it was the ballisticians who came up with accurate determinations of air resistance. The theoreticians of that time were making great strides in classical hydrodynamics, but their contributions to the problem of fluid resistance were very limited. The hydrodynamicists came up with the same answer, that the drag was zero, for all the multitude of real problems involving direct resistance of fluids such as from the pressure drop in conduits to the movement of cannon balls through air. The famous d'Alembert's paradox, as it is most commonly known, states that "the resistance to a body moving with uniform velocity through an unbounded inviscid fluid, otherwise at rest, is zero." At this point in history fluid mechanics had failed completely in attempting to describe a phenomenon which was so plainly evident. This was indeed a major scientific puzzle of the 18th and 19th centuries.

The pieces to this puzzle were put in place in 1904 when Prandtl presented a theoretical paper to the Third International Congress of Mathematicians in Heidelburg entitled "Fluid Motion With Very Small Friction"(4). In this paper Prandtl reconciled the difference between the actual flow and the theoretical flow. He introduced the concept of a thin layer of fluid around the body in which the tangential velocity component increases with gread rapidity from zero at the body surface to the velocity of the main stream a very short distance above the body. This thin layer is known as the boundary layer (Grenzschicht). Prandtl concluded that this thin layer of fluid with large velocity gradients was due to the viscosity of the fluid and the viscosity had virtually no influence outside this layer. These assumptions, which were based on observations, allowed Prandtl to reduce the complexity of the fluid equation of motion to a form which could be solved.

The viscosity of the fluid in the boundary layer causes a friction drag force to be exerted on the body and causes the streamlines not to follow the surface of the body back to the rear end. Instead the streamlines separate from the surface at some point, thus forming an eddying region downstream known as the wake. This new theory now explains the nature of drag and avoids the paradox of d'Alembert.

The above is not to say that theoretical hydrodynamics does not fulfill an important role, because outside the wake there is still a theoretical streamline motion.

This theoretical analysis can also be applied with good results on shapes (such as properly designed airfoils) where the breaking away of the boundary layer is close to the trailing edge.

In a series of lectures in 1941 and 1942 at Luftfahrtforschungsanstalt Hermann Goring, H. Schlichting brought to the forefront the problem of the boundary layer and with it the problem of skin friction drag. The series consisted of sixteen two hour lectures which dealt with boundary-layer problems in both laminar and turbulent flow.

Boundary-layer theory was developed initially for an incompressible fluid in the laminar flow region, and was later extended to include turbulent, incompressible boundary layers which are more important from the practical view point. A rational theory describing the fully developed turbulent flow is still non-existent owing to the extreme complexity of such flows. It was in 1914 that experiments performed by Prandtl on spheres showed that the boundary layer could be either laminar or turbulent and that this phenomenon governs the problem of separation and drag.

Before we can proceed to describe and discuss the flow around bodies we must review some of the fluid mechanics principles involved in these studies.

Laminar and Turbulent Flow

In 1883 Osborne Reynolds (5) demonstrated that there were two distinctly different types of fluid flow. The appa-

ratus used by Reynolds consisted of a straight pipe which had a bell mouth entrance on one end which in turn was connected to a large resevoir full of water. A valve at the discharge permitted him to regulate the flow of water. By injecting a fine thread-like stream of colored dye he was able to trace a streamline in the flow. When the flow velocity was small the colored dye was a straight line throughout the entire length of the tube. But as the velocity was increased by opening the discharge valve there was a point where the flow pattern was altered. He observed that the line would first become wavy and then, as the velocity was further increased, the line, at some short distance from the entrance, would break into numerous vortices beyond which the color would be diffused in the entire region so that the streamlines could no longer be observed.

The first type of flow as observed by Reynolds is what is now known as laminar flow. The particles in this type of flow move in smooth parts or streamlines and the flow is characteristic of highly viscous fluids. The second type of flow that he observed is known as turbulent flow. This type of flow has no fixed characteristics, in fact it is distinguished by its irregularity. Mathematical theory which completely describes turbulent flow has been looked upon in the past as an impossible task. A statistical theory, coupled with experimental data, has been somewhat successful in describing the mean or average fluctuating values of the various fluid properties in turbulent boundary layers.

Generally, laminar flow exists at low speeds and turbulent flow at high speeds. It has also been found that the boundary layer just downstream of a stagnation point is laminar while much further downstream it becomes turbulent. The region between laminar and turbulent flow is called the transition region. Reynolds, in his studies, found that a certain non-dimensional number was the key to be used in predicting whether the flow would be laminar or turbulent. This number, now known as Reynolds number ($Re = \rho VD/\mu$), is probably the most important quantity in the field of aerodynamics.

Reynolds, using a bell mouth entrance to his tube, found that a Reynolds number of 12,000 was obtained before turbulence set in (i.e., the thread of injected dye became very irregular and diffuse). Other experimenters, using the same equipment have obtained Reynolds numbers as high as 40,000 before turbulence set in. This was accomplished by letting the water stand for a few days before the experiment and taking care to avoid any vibrations of the water or equipment. It is thus obvious that the onset of turbulence may be caused by vibrations or movement of the tube through which the fluid is flowing. Since, in laminar, flow the energy loss has been found to be approximately equal to the velocity and in turbulent flow the loss has been found proportional to the velocity to a power between 1.7 and 2.2, the transition of the flow from laminar to turbulent is very important. Thus, by controlling the inlet conditions and the

vibration, the onset of turbulence may be delayed. The delay of the transition region between laminar and turbulent flow has been the basis of a majority of the methods for reducing skin friction drag.

Types of Drag

Basically there are only two types of drag, pressure drag and frictional drag. Pressure drag is the component of the resultant of all the pressure forces that is parallel to the direction of motion of the body. Frictional drag is the force parallel to the direction of motion arising from all skin-friction forces acting tangential to the surface. Pressure drag has its origin in two phenomena. One is related to the lift of the body and the other is related to the size of the body's wake. Hence pressure drag can be subdivided into induced drag ("induced" due to lift) and wake drag. Furthermore, some aerodynamicists will add the wake drag to the frictional drag and call this quantity the profile drag because they are determined by the local cross section (profile) of the wing or body.

Induced Drag

Induced drag has been described as the drag that is produced by lift. Lifting bodies have induced drag, non-lifting bodies have no induced drag. Induced drag is a result of the vortices that flow from the tips of lifting wings. The vortices are produced by the flow of air from the high pressure

bottom side of the wing tips to the low pressure upper side. The tip vortices induce a downward velocity of air all along the wing. This causes a reduction in the effective angle of attack. The lift force is always perpendicular to the relative wind. Hence the resultant force measured perpendicular to the relative wind is inclined slightly backward from the perpendicular to the direction of flight. The component of the force parallel to the flight direction is the induced drag. Figure (1.3) illustrates the forces acting on the wing.

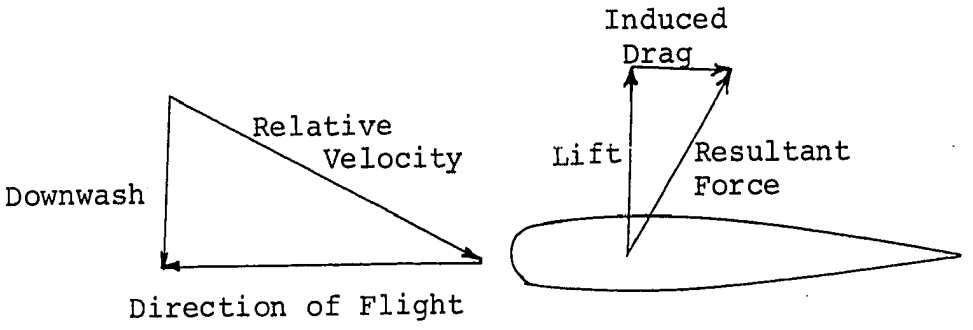

Figure (1.3) Forces on a Wing.

The induced drag coefficient therefore is directly proportional to the square of the lift coefficient and indirectly proportional to the aspect ratio,

$$C_{di} \propto \frac{C_\ell^{\,2}}{AR} \qquad (1.3)$$

where AR = aspect ratio = span/chord.

It is obvious that if there is lift, and the wing span is not infinite, then there must exist induced drag.

The remaining problem is to minimize this drag. Max Munk, a student of Prandtl, found that minimum induced drag is obtained if the distribution of lift over the span corresponds to an ellipse. Such a distribution of lift is called an elliptic distribution. If the wing has no twist, the plan form area of the wing will be an ellipse if the section lift curves are independent of span.

Wake Drag

Great strides were made in reducing the wake drag in the 1930's and 1940's by streamlining the body shapes. For modern subsonic aircraft the wake drag is only one-third that of the skin-friction drag. The wake drag may be reduced by careful shaping of the after body so that the flow follows the contour faithfully almost to the trailing edge of the body. This shaping of a body to reduce the wake drag is called streamlining. A good example of this is an airfoil or a fish.

Thus a streamlined body is a body with a very small wake and for such bodies d'Alembert's analysis is almost true since pressure differences between the front and rear of the body are almost entirely eliminated. The streamlined body still experiences some drag because of the effect of viscosity in the boundary layer. Artillery shells are examples of bodies that have sharply truncated tails (Figure (1.4)) and have a large wake drag owing to their large wake. Such bodies are sometimes called bluff bodies.

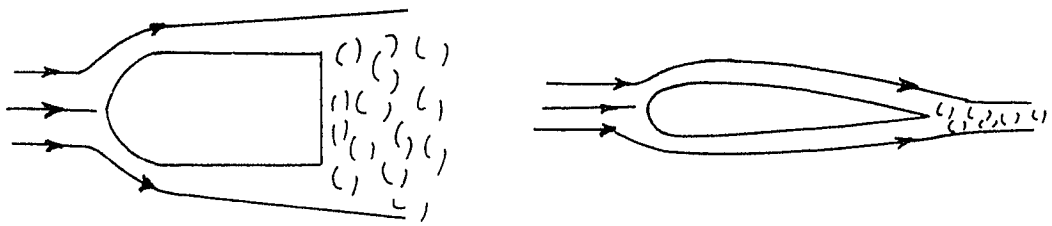

Artillery Shell
Large Wake Drag

Airfoil or Trout
Small Wake Drag

Figure (1.4) Wake Drag.

Many of the dramatic increases in airspeed were due, in large part, to reductions in wake drag obtained by means of cantilevered wings, retractable landing gears, fairing the lines of cockpit, and attaching fillets to the junction between wing and fuselage. The wake drag of a modern high speed airplane has been reduced to a very small value.

Skin-Friction Drag

The drag that arises due to the fluid sticking to the surface of a moving body (because of viscosity) and forming a boundary layer is called skin-friction drag. Figure (1.5) shows the improvement in the reduction of skin-friction drag over the years. From the figure it is obvious that the drag of the aircraft has been reduced to a point where, unless some type of boundary-layer control is introduced, a further reduction in drag is not possible. Skin friction can be reduced, but never eliminated, by making the surface of the body very smooth. The drag of a carefully shaped airfoil may be reduced

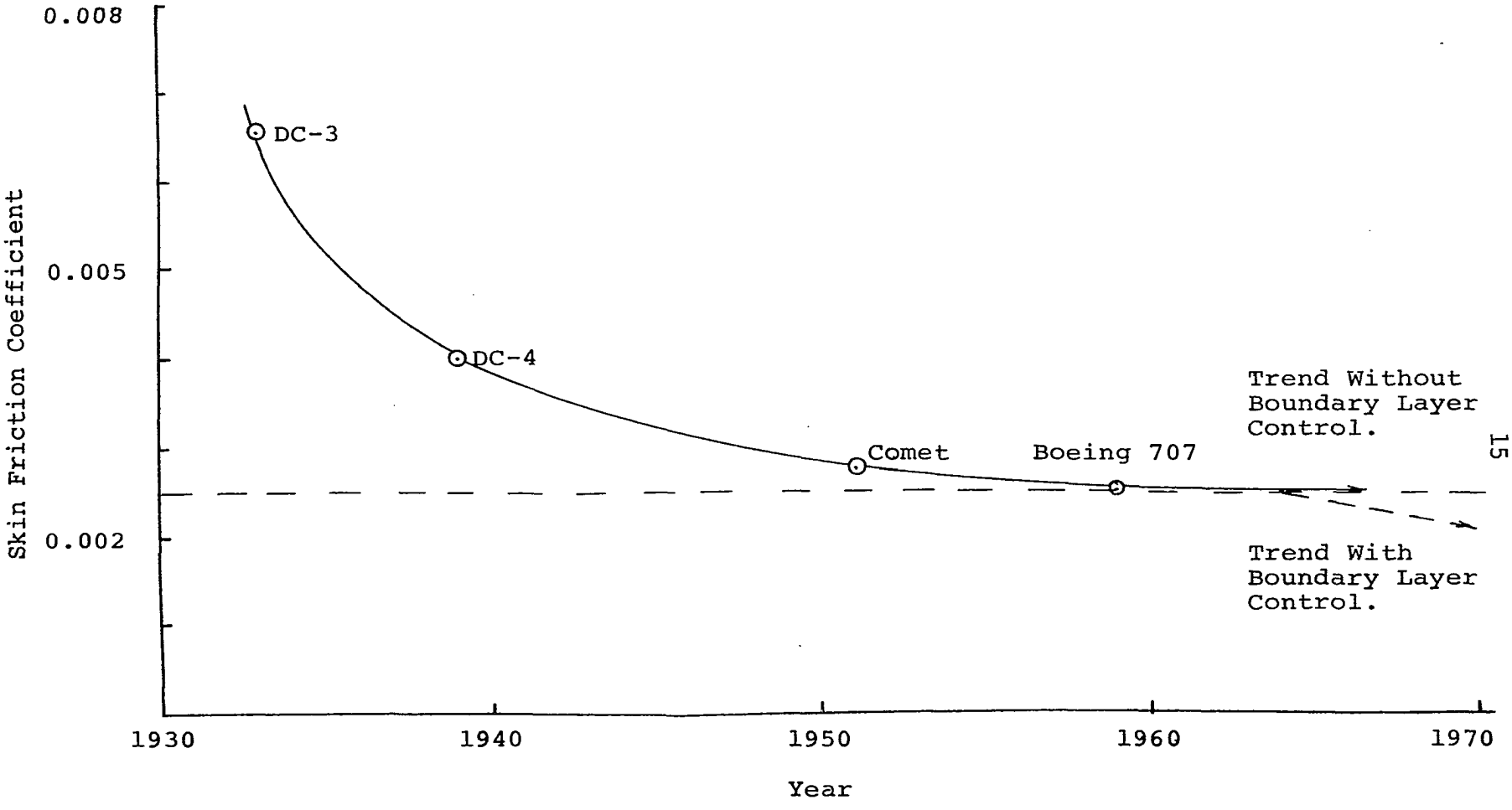

Figure (1.5) Progress of Drag Reduction Through the Years.

to a value less than 1/50th that of a disk having the same diameter. The drag on the airship is almost all skin-friction drag with a small percent of pressure drag, while the drag on the disk is almost all pressure drag. Modern subsonic aircraft have been refined to such an extent that 75 percent and occasionally even more of the profile drag can be attributed to skin-friction drag.

Thus it is apparent that skin friction must be reduced if higher and higher airspeeds are to be attained. Previously in this chapter laminar and turbulent flow were described. These two diametrically different types of flow are important phenomena in skin friction. Laminar flow is characterized by a very smooth steady flow, whereas turbulent flow is of an oscillatory irregular nature.

An important characteristic of the turbulent boundary layer is the fact that the violent intermingling of particles enables the turbulent layer to remain attached to the surface better than laminar flow, which contains less kinetic energy and leaves the surface earlier. This explains why engineers have placed dimples on a golf ball or vortex generators on certain portions of airplanes. The dimples on the golf ball cause the boundary layer to be turbulent, which results in a smaller separated flow region (wake) and hence lower wake drag. On a sphere the wake drag is much greater than skin-friction drag; hence the dimples cause a reduction in the overall drag of the ball as shown in Figure (1.6).

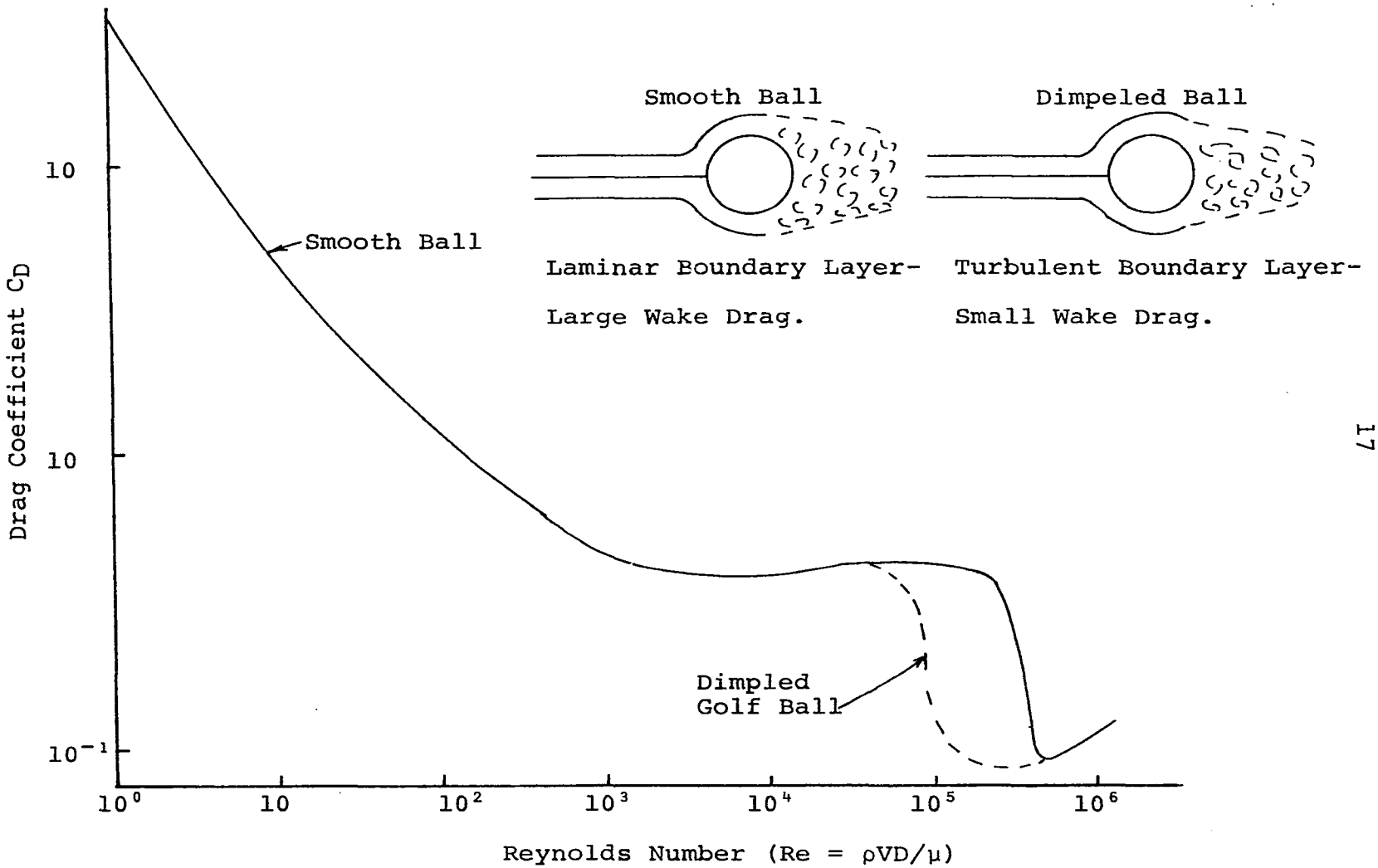

Figure (1.6) Comparison of Drag Coefficients for Smooth and Dimpeled Balls (7).

The vortex generators are similar in that they induce a turbulent boundary layer causing less separation, more lift, and less wake drag.

It should be pointed out that for the same Reynolds number, laminar flow has a smaller skin-friction coefficient than turbulent flow as shown in Figure (1.7). Thus it is obvious that turbulence works against the engineer as far as skin friction is concerned.

The question which naturally arises is, can engineers, in some way, cheat nature and maintain the boundary layer in a laminar state up to higher than usual Reynolds number, thus reducing the skin friction drag coefficient? Many methods have been introduced to "cheat nature"; the newest is introduced in this dissertation. The next section will now review the past methods and see what levels of reduction were achieved.

Laminar flow airfoils. In the period just before and during World War II much attention was given to laminar flow airfoils. These airfoils are so designed that the lowest pressure on the surface occurs as far back as possible (6,7). The reason for this design is the fact that the stability of the laminar boundary layer generally increases when the external flow is accelerated, i.e., in the flow with a pressure drop, while the stability decreases when the flow is directed against increasing pressure. Considerable reduction in skin friction is obtained by extending the laminar region

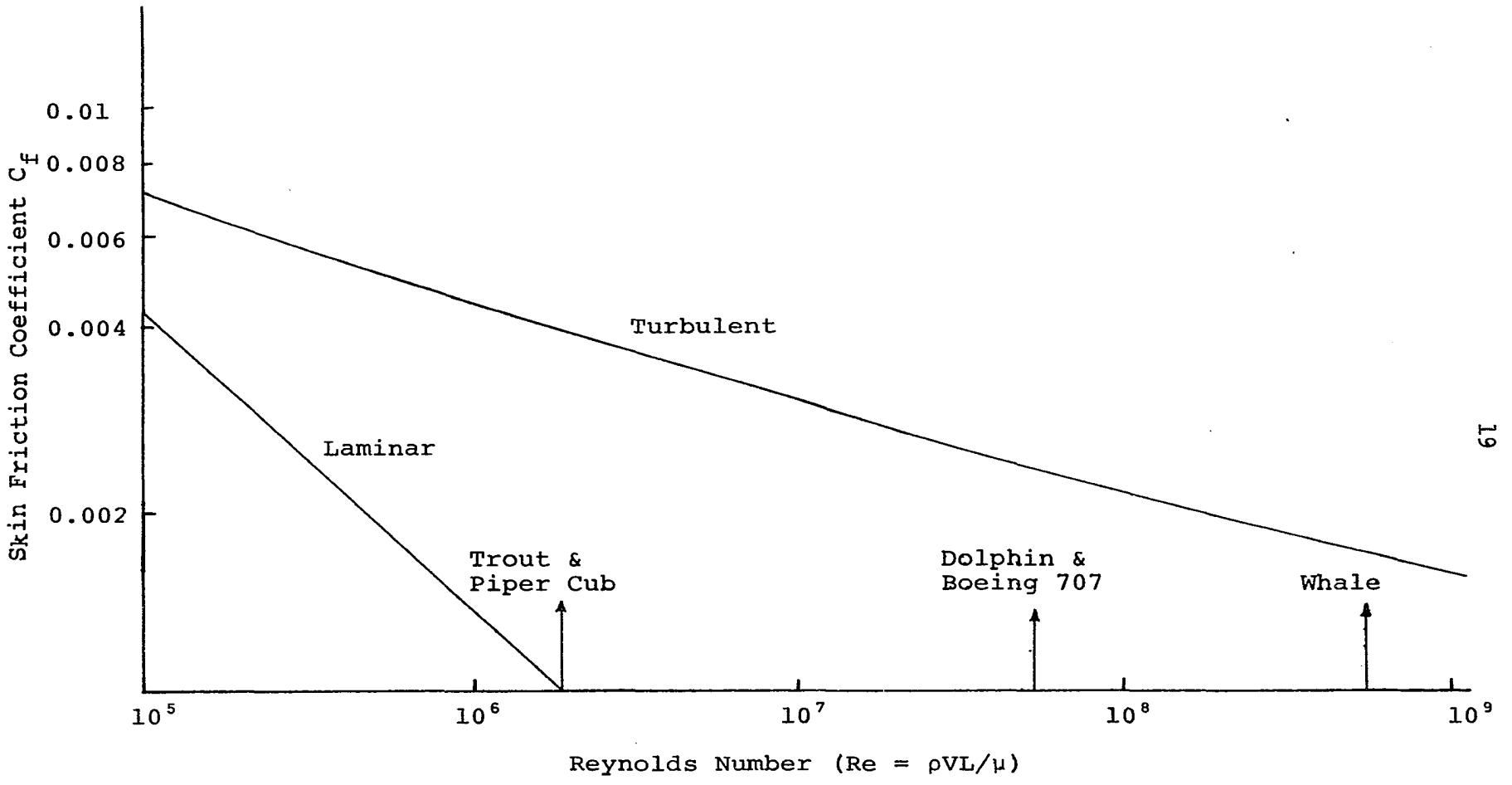

Figure (1.7) The Effect of Turbulent and Laminar Flow on the Skin Friction Coefficient

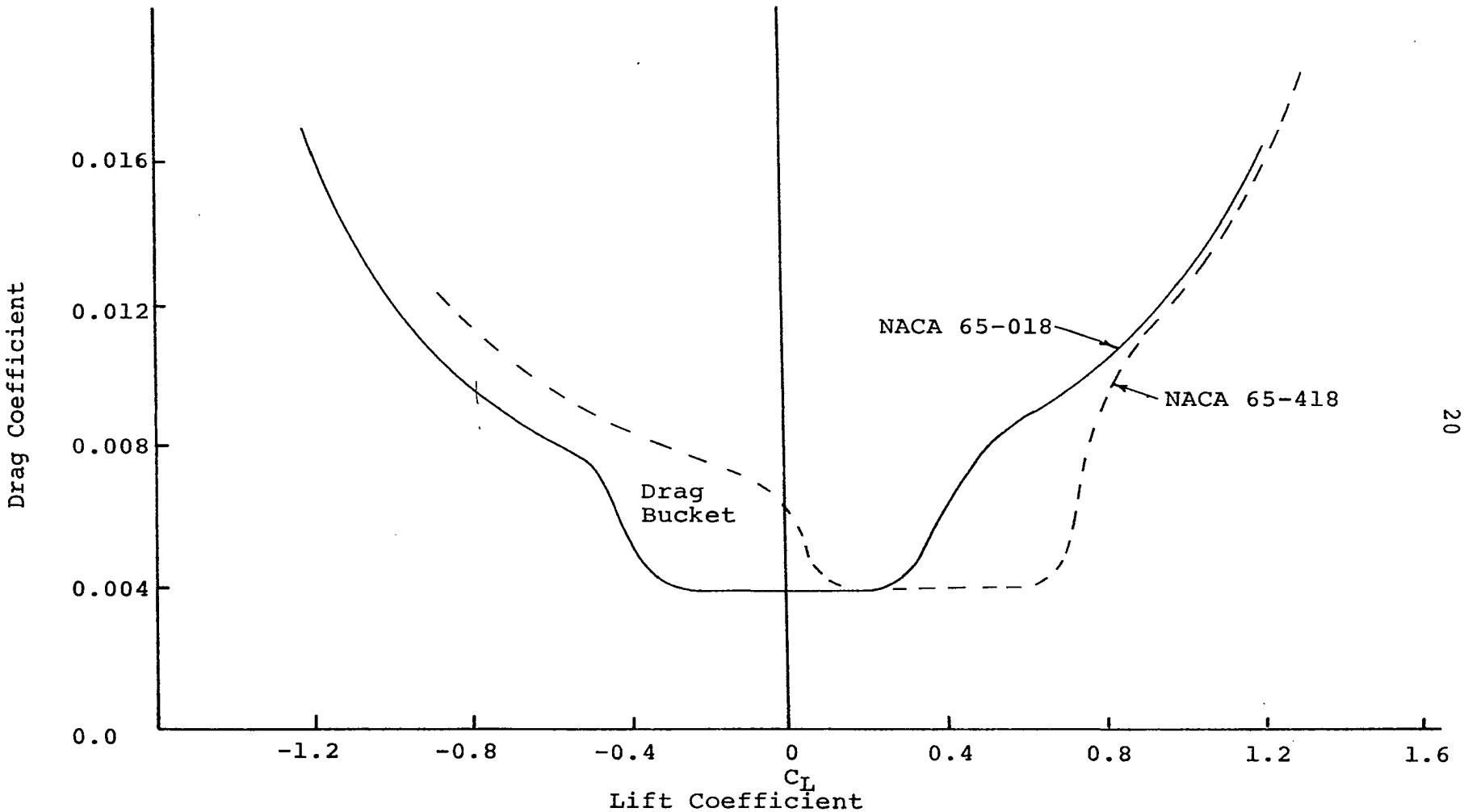

Figure (1.8) NACA Measurements of Drag Coefficients For Two Laminar Airfoils.

in this way provided that the surface is sufficiently smooth.

A disadvantage of this type of airfoil is that the transition from laminar to turbulent flow moves forward very suddenly at small angles of attack. This results in a very narrow low drag bucket which means that the drag at moderate to large angles of attack is much larger than the angle of attack as shown in Figure (1.8). This phenomenon can be attributed to the fact that the point of minimum pressure moves forward, therefore the point of transition between laminar and turbulent flow is also advanced toward the nose as shown in Figure (1.9). It is evident that the more an airfoil is surrounded by turbulent airflow, the higher will be its skin friction.

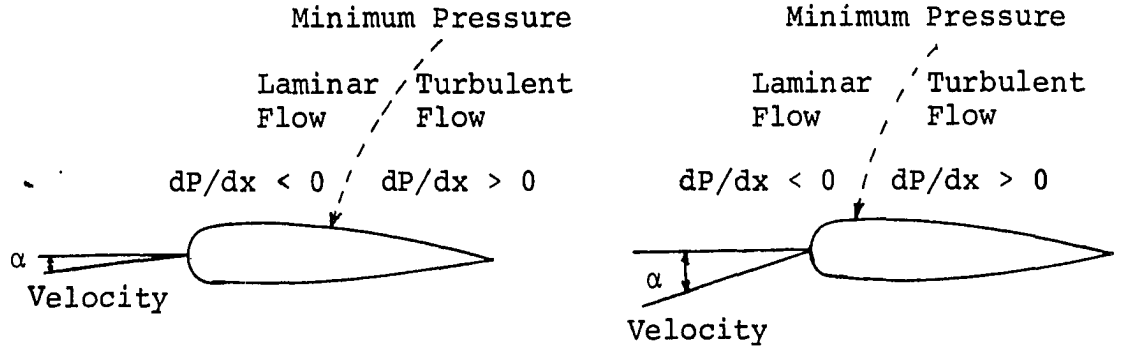

Low Angle of Attack High Angle of Attack

Figure (1.9) Laminar Flow Airfoils.

Laminar flow control. Laminar flow control has been one of the most dramatic techniques developed in the reduction of skin-friction drag. This technique reduces the thickness of the laminar boundary layer by removing fluid from the bound-

ary through slots or holes in the wing surface. The sucking away of slower velocity changes the form of the velocity distribution causing the layer to be more stable. This is a similar effect, mentioned in the laminar flow airfoil case, as obtained by a pressure drop. Thus the critical Reynolds number of the boundary layer $(U\delta^*/\nu)_{crit.}$ becomes considerably higher than for the case without suction. This latter circumstance takes full effect if the suction is continuous such as in a porous wall.

The advantages of this method were well understood in the late 1930's, but it has only been investigated extensively in the last eighteen years. The reduction in skin friction by the use of laminar flow control has been very substantial. Full chord laminar flow was achieved on a F-94 airplane up to a Reynolds number of 3.6×10^7 (8). Wind tunnel tests on 30 degree swept wings (similar to those on modern jet transport airplanes) equipped with laminar flow control have shown that the drag is five or six times lower than the typical turbulent wings (9). Similar tests in supersonic flow have shown skin friction reductions of up to 70 percent. Figure (1.10) shows the reduction in skin-friction drag on tests conducted on airfoils by Pfenniger (10), one of the leading authorities on laminar flow control in this country.

There are substantial rewards in using this type of flow control, but there is a penalty to be paid in increased weight and the complexity of the airplane due to the pumps and plumbing. There is also an increase in maintenance

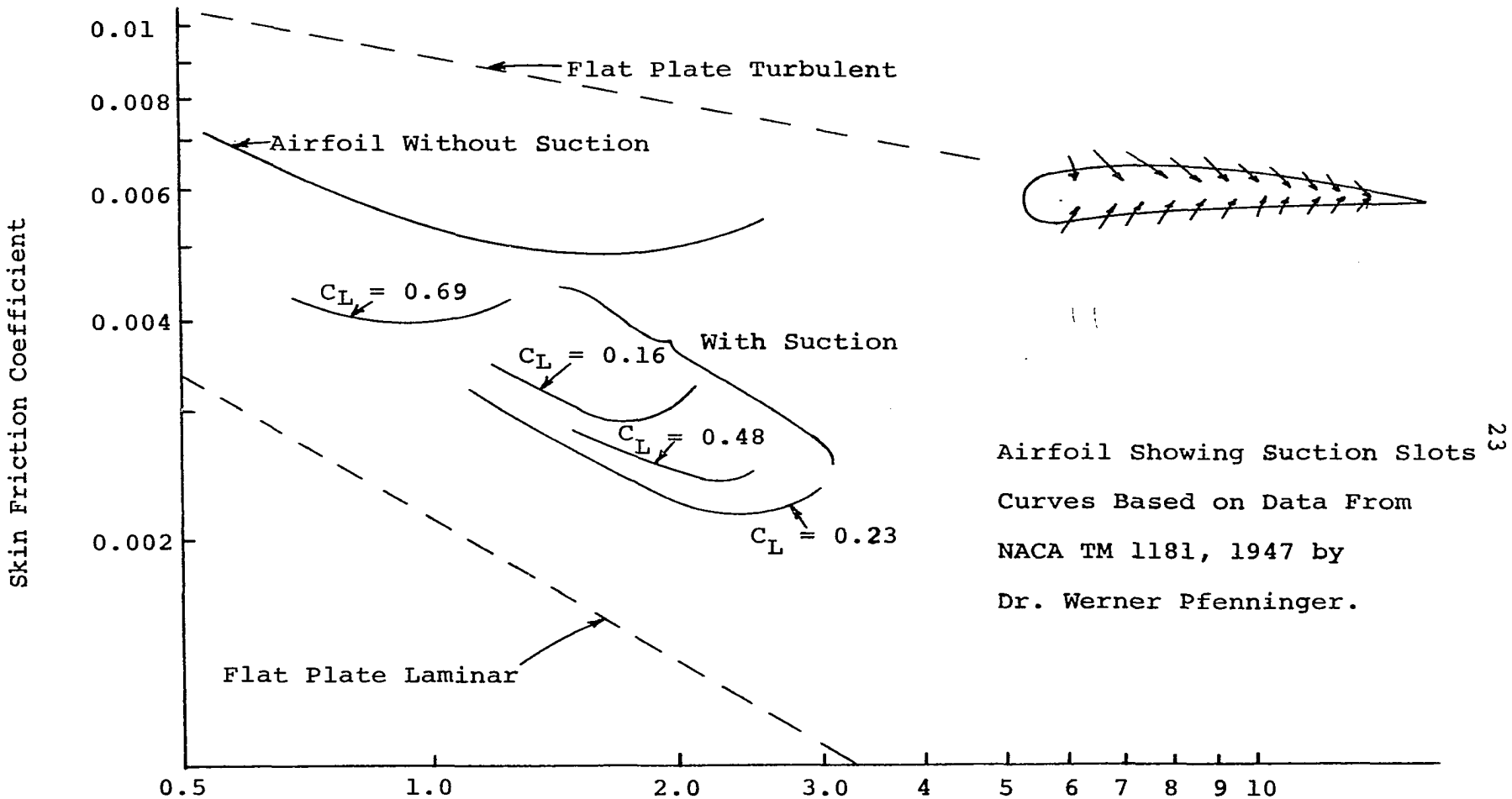

Figure (1.10) Suction Effect-Laminar Flow Control

time by about three and a half hours per flight hour in addition to the fifteen hours already required for current jet transports (11). In addition, the increased weight of the equipment would offset the drag reduction in short range flights.

Another important application of this method is its role in turbomachinery. The method of laminar flow control has been used both in axial and centrifugal flow compressors. In axial flow compressors the theory is the same as outlined for the wing, but in the centrifugal compressor the application is slightly different (12). In a centrifugal compressor the higher velocity from the lower pressure side is introduced into the slower moving air thus energizing the boundary layer on the high pressure side and preventing separation, increasing efficiency, and most important of all, increasing the range of operation as shown in Figure (1.11).

Drag reduction by compliant coatings. Kramer (13, 14, and 15) discovered a new method of drag reduction in 1957. After observing a school of dolphins, on a trip to this country in 1946, he was fascinated by their performance. He began collecting data on the performance of the dolphin, comparing their top speeds with the output of their muscle motor and deduced that the dolphin has solved the problem of drag reduction.

Studying the dolphin's skin, he found that there were two layers, the outer layer about 1/16th inch thick and the inner about 1/4th inch of tough tissue. The outer layer covers the entire body of the dolphin and is so delicate that it can

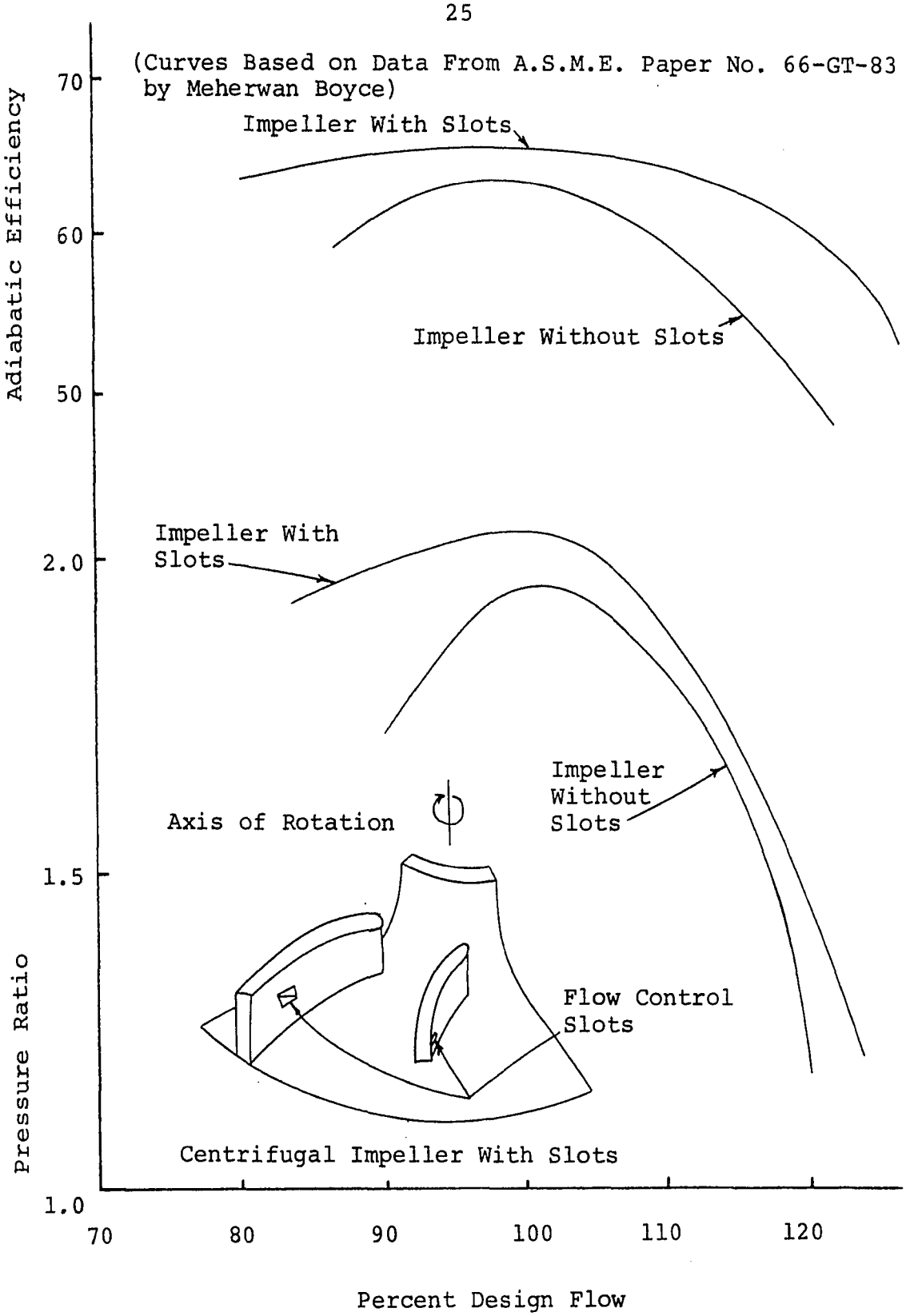

Figure (1.11) Laminar Flow Control-Centrifugal Impeller

be scraped off with a fingernail. It is very pliable and contains a multitude of narrow ducts which are filled with a soft spongy material. When dry, it is brittle but turns soft again when immersed in water. In its dry state the skin weighs one fifth of its weight when wet--an indication of its high water content.

Pictures taken of the dolphin swimming show wrinkles on the skin. Kramer postulated that turbulent fluctuations were damped out by the soft spongy skin and the transition from laminar to turbulent flow is delayed. Kramer then constructed a body which had what he considered the three basic components of the dolphin's skin: one, the smooth pressure sensitive diaphragm, two, the structure supporting the diaphragm, and three, the damping fluid. Preliminary tests indicated that the transition Reynolds number was increased by 140 percent. He also measured a reduction in drag of up to 50 percent at a Reynolds number of 1.5×10^7.

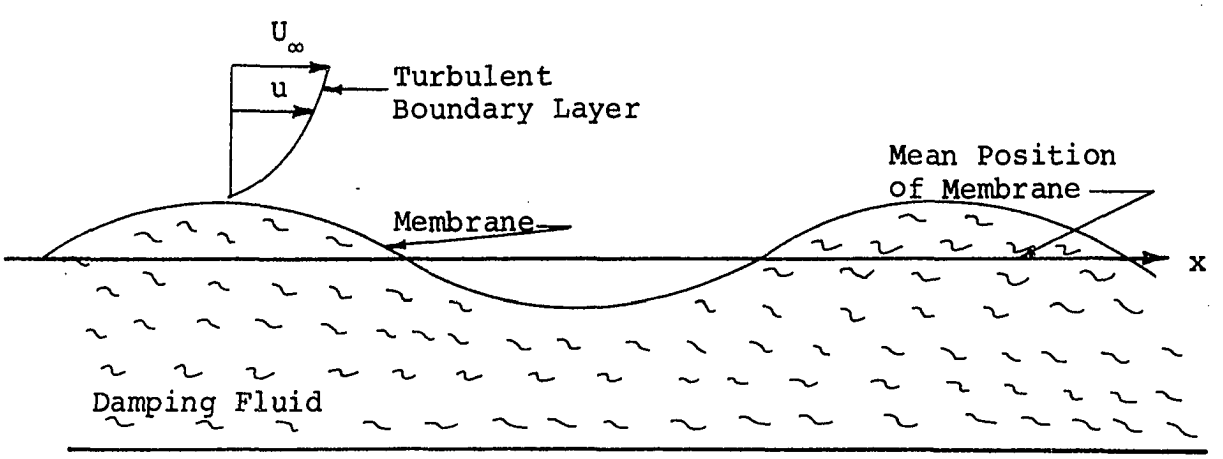

Figure (1.12) Compliant Skin Coating.

Here, at the University of Oklahoma under the direction of Dr. Blick (16), further tests were conducted on a compliant skin in wind tunnels. The compliant coating was constructed by using a 0.0025 inch thick polyvinyl chloride skin stretched over various damping fluids as shown in Figure (1.12). Tests were also run using polyutherane foam instead of the damping fluid; results of these tests are shown in Table (1.1).

Material	Bare	Covered with PVC Skin	Water Saturated Covered with PVC
Rigid Surface	Baseline C_f = 0.0043 0%	---	---
40 PPI Polyurethane Foam	+107%	-26%	-37%
80 PPI Polyurethane Foam	+ 72%	-33%	-21%
27 PPI Polyurethane Foam	+200%	+ 2%	-30%
Foam Rubber	+ 26%	+72%	+95%

Table (1.1) Percentage Changes in Skin Friction Coefficient From the Hard Plate Value (V = 38 ft./sec.).

From the table it is clear that when all three conditions are met, which Kramer felt were important, the reduction in skin friction is the greatest. Figure (1.13) shows a graph of skin-friction coefficient versus Reynolds number for the compliant coating.

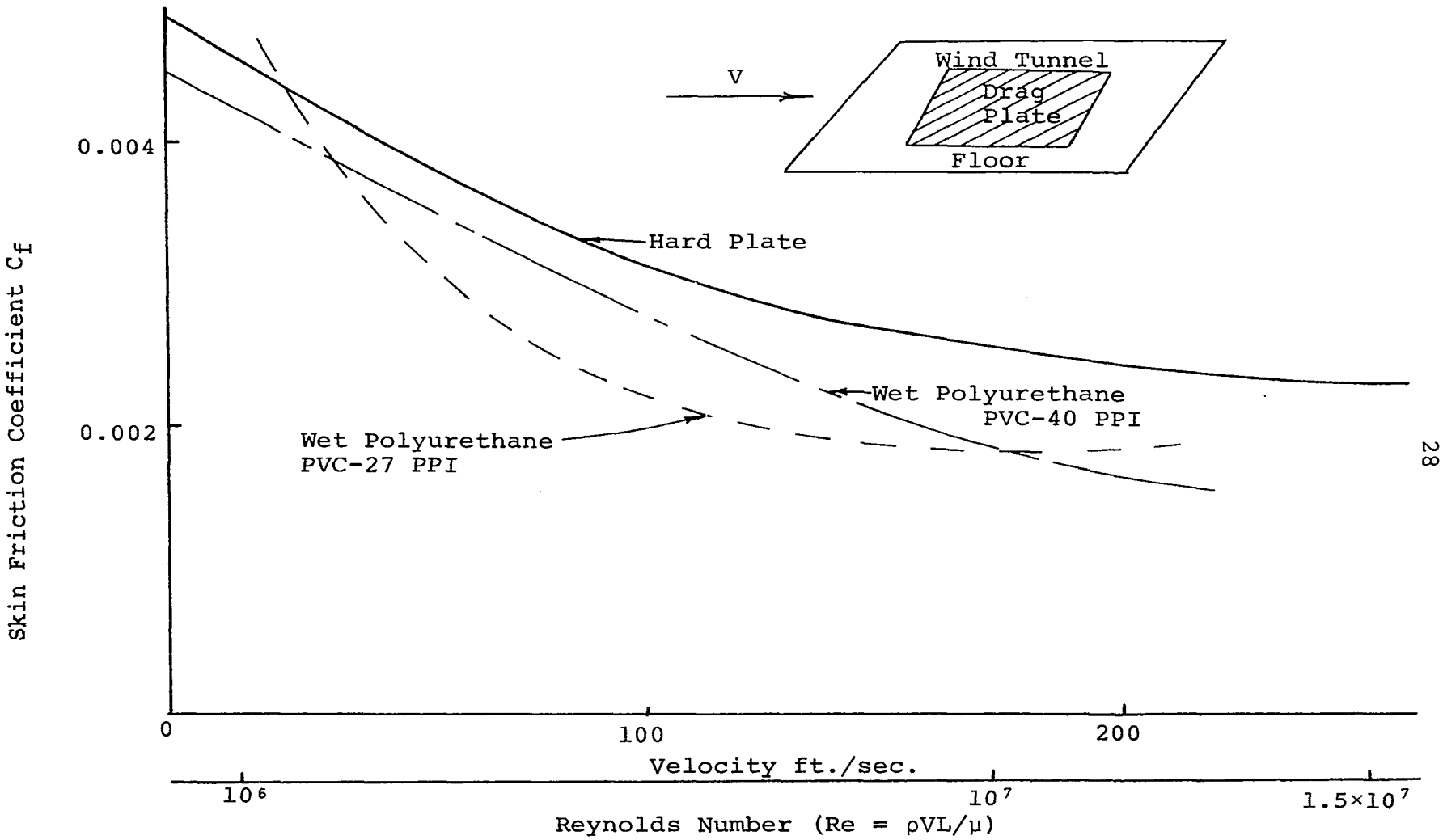

Figure (1.13) Compliant Coating Drag Reduction (16)

Pelt, working on a doctoral thesis at the University of Pittsburg, adapted Kramer's flexible skin to pipe line flow. He found reductions in the pressure drop as high as 35 percent. His experiments were conducted with thick and thin wall rubber tubing, a polyvinyl chloride-polyvinyl acetate copolymer (Tygon tubes), and polyester based urethane resin (Texin tubes) as pipe liner, backed by a damping fluid. The best results, 32 to 35 percent decrease in pressure drop, were obtained by urethane elastomers, followed closely by thick and thin wall rubber tubes respectively and then with Tygon tubes.

Toms' effect. The characteristic of turbulent flow in a molecular fluid continuum (e.g., water, air) can be drastically altered by the addition of macroscopic particles, e.g. dust in air, wood fibers,and plastic beads in water.

In 1948 Toms (17) studied dilute solutions of polymethylmethacrylate in chlorobenzene. He found that the dilute solutions had less drag than the pure solvent, and this occurred only when the flow was turbulent. Hoyt and Fabula (18) found that 10 weight parts per million (wppm) of polyethelene oxide (polyox) produced a 40 percent reduction in driving torque of a rotating disc apparatus operating in the turbulent region. In addition they measured up to 80 percent reductions in turbulent pipe flow for 50 wppm and a 40 percent reduction for 2 wppm. Tests run with scrapped slime from sea fish showed a 14.5 percent reduction in drag.

Many researchers have shown that this drag reduction

ability is proportional to the molecular weight and the length to diameter ratio of the molecule. Polyox has been used by many investigators and has a molecular weight ranging from 0.2 million to over 5 million and a length/diameter ratio ranging from 20.000 to 165,000.

Pruit, Rosen, and Crawford (19) (1966) found that increased coiling and high temperatures (105°to 104°F) decreased the drag reducing ability of the polymers.

Tests on spheres, hemisphere cylinders, and ship models have shown drag reductions of 45 percent, 40 percent, and 30 percent respectively.

Sproull (20) in 1961 conducted tests using air in a viscosimeter and found a "reduction in viscosity" of 40 percent. Table (1.2) shows work done by different investigators and the results they have obtained. The results vary videly from increase in pressure drop to decrease in pressure drop.

The wide discrepancy in data and the narrow range over which these experiments were conducted pointed out the need for further experimentation. Also the fact that no data were available for the flat plate having a sublayer of dust flowing past it was the reason that Dr. Blick initiated this project. The author was assigned this problem in February, 1968 and the following chapters present his work since then.

Type of Flow	Reference	Reynolds Number	$\frac{W_s}{W_g}$	Particle Size Microns	Effect Upon Skin Friction	Comment
Flue gases	Briggs (1945)	10^5	0.21	....	Decrease 13%	Homogenous flow
Glass particles in air	Halstrom (1952)	....	....	200μ	Decrease	Homogenous flow
Pneumatic conveying	Hinkle (1953) Orr (1966) Mehta et al. (1957)	10^3-10^4	1-10	....	Increase	Large axial variations in solids density
Viscosimeter flow of air & talc powder	Sproull (1961)	....	....	10μ	Decrease	Homogenous flow
Heated gas suspensions	DePew and Farbar (1963)	2.5×10^5	<1	....	Decrease	Homogenous flow
Air and MgO suspensions	Soo and Trezek (1966)	1.3×10^5 to 2.95×10^5	0-2	30μ	Decrease	Homogenous flow
Glass particles in air	McCarthy and Olson (1968)	10^5-10^6	<0.6	3-64μ	Decrease	Homogenous flow

Table (1.2) Frictional Losses With Solid Additions in Gases.

CHAPTER II

BACKGROUND LITERATURE

As can be seen from the introductory chapter a vast amount of background information is available. If we were to look under such topics as laminar flow, transition flow, turbulent flow, boundary-layer theory, turbulent energy, and particulate flow in liquids, the background in technical literature is very extensive. However, the study of drag in dusty air in pipes and on flat plates does not have an extensive research history.

In this section a comprehensive review of the work done using particles in liquids and air will be presented. The literature on the latter, however, is very limited. Each of the important articles will be reviewed in depth and the fluid flow theory and research work, which may have a bearing on the results, will be discussed.

In the introductory chapter we mentioned the work and ideas of B.A. Toms and referred to them as the basis for this research project. This type of drag reduction has been referred to as "Toms' effect". Since the basis of this work is the so-called "Toms' effect", it is fitting and important, therefore, that first consideration in this section should be

given to the pioneer work of Toms in this field. The work of Thomas and others will also be discussed here in detail.

The Results Reported by Toms

Toms, in his paper (17) before the International Rheological Congress at Scheveningen, Holland, showed the effects of dilute solutions of polymethyl methacrylate in monochlorobenzene flowing through straight tubes. The results indicated a phenomenon which before then was not observed. It was seen that at high Reynolds numbers the dilute solutions had less drag then the pure solvent. A theory was advanced by Oldroyd in conjunction with Toms' experiment for this flow phenoemna as being due to wall effect. Some of this theory will be presented later in this section.

Description of Apparatus

Toms' apparatus consisted of four straight metal tubes of uniform bore and circular cross section. Three of these tubes were made of brass and the fourth tube of Duralumin. The ends of these tubes were cut off square by means of a lathe. The two ends of the tube were connected to two upright circular cylinderical glass jars (capacity, 2000 milliliters) with the tube in a horizontal position. One end of this tube passes through the vertical wall of each resevoir, near to the base, and projects about 2 centimeters on the inside. The above apparatus was connected to a pneumatic circuit designed so that the air pressure above the liquid surface

in one reservoir could be varied independently of that in the other; thus the liquid could be made to pass through the tube at a constant velocity.

Different concentrations of liquid were tested at different pressure gradients therefore, different velocity and flow rates were observed. By using three tubes, Toms provided a check to insure that uniform flow conditions had been reached and this also served to eliminate "end effects" and correct for kinetic energy effects. The total loss attributable to this was found to be equal to ρv_m^2.

By the use of the Reynolds color filament method described in Chapter I, a critical Reynolds number was obtained. This critical Reynolds number, where the breakdown from the laminar flow region in solutions of polymethyl methacrylate, was found to be Re = 2000.

Results

The results were then plotted as shown in Figure (2.1). The dotted line which corresponds to a Re = 2000 separates the laminar flow region and the turbulent flow region. This division clearly shows the most important part of "Toms' effect"--the increase in the flow rate at a constant pressure gradient, caused by the addition of the polymer, was observed in the turbulent flow region. The maximum effect was most pronounced when the concentration of polymer rose to about 2.5 grams per liter. The trend is reversed when the concentration of the polymer is increased. The reason for this phenomenon was,

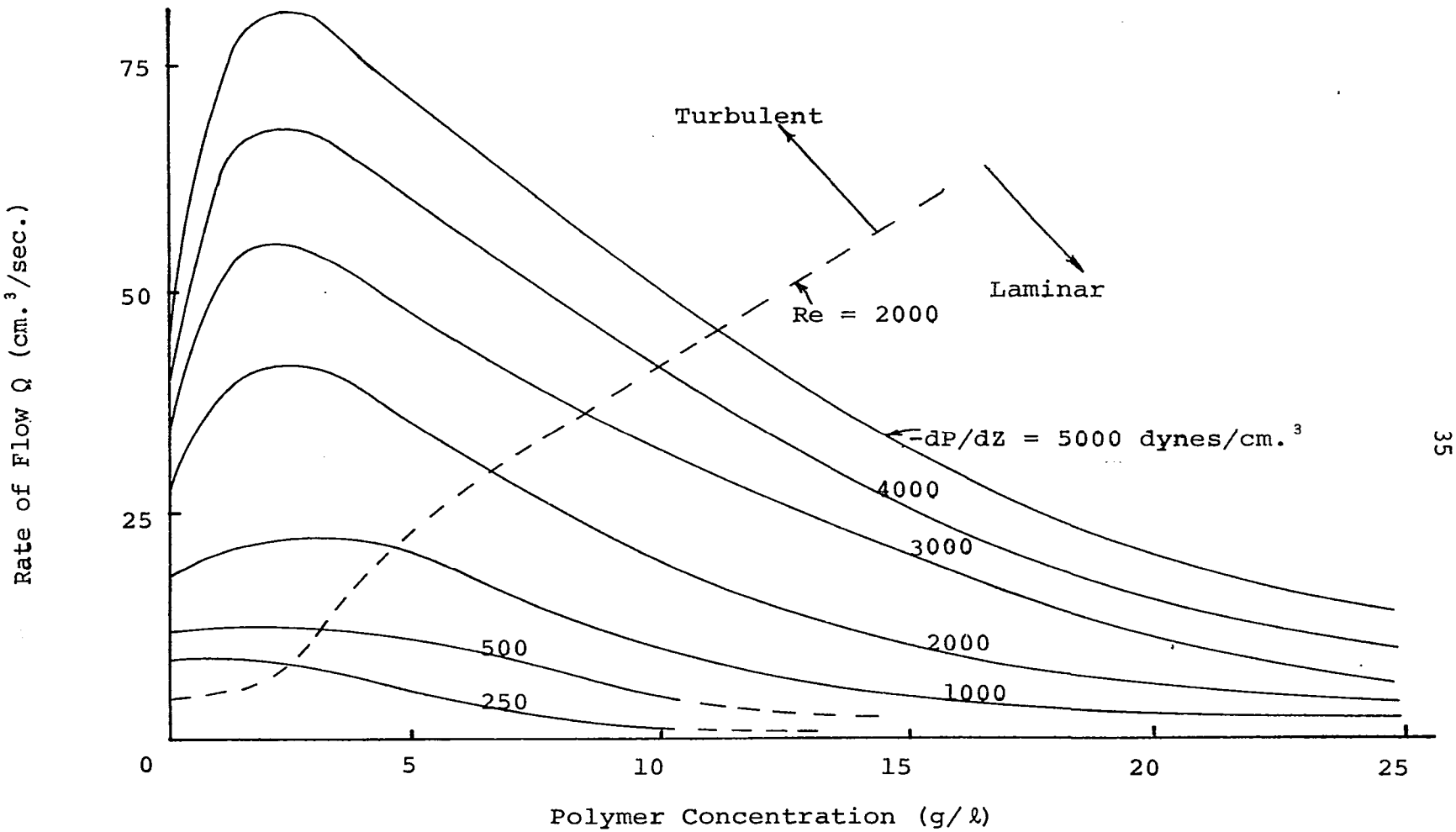

Figure (2.1) Change in Flow Rate With Addition of Polymer as Found by Toms (17).

according to Toms, due to the fact that full turbulence had not been achieved in these liquids even through a Reynolds number of about 4,000 was attained.

Theory by Oldroyd

Oldroyd (21), in conjunction with Toms, derived some theory to explain this phenomenon. The theory put forth suggests that the tube wall may introduce a "preferred direction in a normally isotropic material." Thus, for example, if the liquid is a solution of a linear high polymer, an external constraint is imposed by the wall on the movement of the long chain molecules near the wall. Oldroyd suggests that an "abnormally mobile laminar sub-layer" could exist of a thickness equivalent to the molecular dimensions. The existence of wall effects has been demonstrated in laminar flow and shows itself macroscopically as an effective velocity of slip (ω) at the wall, and depends on the local conditions of stress as defined here:

$$\tau = - \tfrac{1}{2} d \, dp/dz \qquad (2.1)$$

where d is the tube radius and dp/dz is the pressure gradient.

In the turbulent flow region the shear stress in the laminar boundary layer near the wall is still defined by the above equation. Oldroyd hypothesized that if a thin sheath of liquid near the wall behaves differently owing to the presence of the wall, the effect can be measured again by an effective velocity of slip, ω, or by an "effective slip coefficient", ζ, as defined by:

$$\zeta = \omega/\tau \qquad (2.2)$$

Thus ω and ζ can be regarded as functions of the local conditions of stress at the wall.

For Newtonian liquids of density (ρ) and viscosity (μ), Oldroyd obtained a relationship between the flow rate, Q, and the negative pressure gradient (dp/dz) for fully turbulent mainstream flow in terms of two reduced variables:

$$Re = \frac{2\rho Q}{(\pi d\mu)} \tag{2.3}$$

the Reynolds number and,

$$\gamma = \frac{-\pi^2 d^5 \frac{dp}{dz}}{\rho Q^2} \tag{2.4}$$

the resistance coefficient. The relationship takes the form:

$$\gamma^{-\frac{1}{2}} = B \log_{10} (Re\gamma^{\frac{1}{2}}) - C \tag{2.5}$$

where B and C are constants. These constants, as obtained by Goldstein (22) experimentally are B = 4.0 and C = 0.4 for air and water flowing through smooth pipes. Although Equation (2.5) has been justified theoretically for Reynolds numbers exceeding 10^5, experimental results are in agreement for all Reynolds numbers above about 3,000.

The difficulty in extending these results to isotropic viscoelastic non-Newtonian liquids is the redefining of the Reynolds number. Since viscosity is not a constant but a function of shear stress (varying between μ_o for low rates of shears to μ_1 at high rates), the Reynolds number can vary between $Re_o = 2\rho Q/(\pi d\mu_o)$ and $Re_1 = 2\rho Q/(\pi d\mu_1)$. Oldroyd assumed that the only viscosity which need be considered in turbulent flow (and the thin laminar boundary layer at the wall) when the

mainstream is turbulent, is the limiting value at the high rate of shear, μ. With this assumption, and the same reasoning as for Newtonian liquids, he obtains the following equations for viscoelastic non-Newtonian liquids:

$$x = \mu_1 Re_1 \gamma^{\frac{1}{2}} = 2(-d\rho\frac{dp}{dz})^{\frac{1}{2}} \qquad (2.6)$$

$$y = \gamma^{-\frac{1}{2}} = \frac{Q}{d^2}(-\frac{d}{\rho}\frac{dp}{dz})^{-\frac{1}{2}} \qquad (2.7)$$

$$y = B \log_{10} x - (B \log_{10} \mu_1 + C) \qquad (2.8)$$

Equation (2.8), if plotted as $\log_{10} x$ against y, will give a straight line and is independent of tube diameter. Oldroyd points out that one can detect wall effects in fully turbulent flow by plotting $\log_{10} x$ against y and noting whether or not the results of different tubes, at high Reynolds numbers, lie on the graph. If, for different diameters of tubes, the x-y graphs are not distinct curves then there is no reason to suspect anomalous flow at the wall, while on the other hand, if they form distinct curves it can be interpreted as having wall effect.

Oldroyd stated that the observed phenomenon is due to the wall effects. He suggested that if ρ is constant for each solution at different pressure gradients, the values of Q, μ, and ζ will depend on the concentration of the solute, while a, ρ, b, c, and dp/dz remain constant for all solutions. Since y is a constant multiple of Q, and since x is constant for all fluids, then Oldroyd obtains the following relation-

ship:

$$Q = K_1 - K_2 \log_{10}\mu_1 + K_3\zeta \qquad (2.9)$$

where K_1, K_2, and K_3 are constants. As the concentration of polymer increases from zero, the limiting viscosity also increases and, if there is no wall effect, ($\zeta = 0$), Q would decrease as one would expect. However if there is a wall effect when the polymer is present in solution, then it is possible that ζ increases with concentration in such a manner that Q increases. Thus Oldroyd's theory predicts that, under certain conditions, the rate of flow might be increased at constant pressure gradient by the addition of solute. In describing Toms' flow, Oldroyd hypothesized that wall effects, already observed in laminar flow with the same solutions, might persist when the mainstream is turbulent, thereby reducing the Reynolds stress and consequently the wall skin friction in a turbulent flow.

The Results Reported by Thomas

Work done by Thomas (23, 24, 25, and 26) was in conjunction with his research on atomic reactors. He utilized a form of thorium for this investigation that is used in an aequeous homogenous power reactor. It is restricted, for the most part, to the suspension of thorium oxide in water. The results obtained by Thomas bore out the work of Toms and indicated a reduction in the skin-friction coefficient in turbulent flow.

Apparatus and Results

The apparatus used by Thomas to carry out his experiments consisted of three circular pipes: 1.03 inch, 0.318 inch, and 0.124 inch in diameter. The slurry was pumped through the pipes and measurements of pressure drop were taken in the horizontal section of the pipe. Transition from laminar to turbulent flow occurred at a Reynolds number of 1.7×10^3 for the 0.318 inch diameter pipe and at 3.3×10^3 for the 1.03 inch diameter pipe, as would have been expected.

Figure (2.2) shows that there is a marked reduction in skin-friction coefficient in the turbulent region, while in the laminar flow region an increase of skin friction occurred when the particles are suspended in the flow. An important point to note here is that the maximum reduction of the skin-friction coefficient occurs near the transition region from laminar to turbulent flow. This phenomenon, as will be discussed in later chapters, was found to exist in the experiments carried out by the author.

In order to determine whether the change in the skin-friction coefficient in the turbulent flow from the "Newtonian" curve was due solely to the suspension of particles or to the non-Newtonian characteristics of the mixture formed by introduction of the particles, Thomas carried out the following experiment. In the mixture, sodium silicate was added, thereby reducing the yield stress. Thus the silicate reduced the non-Newtonian characteristics and at the same time the skin-friction coefficient in the turbulent flow

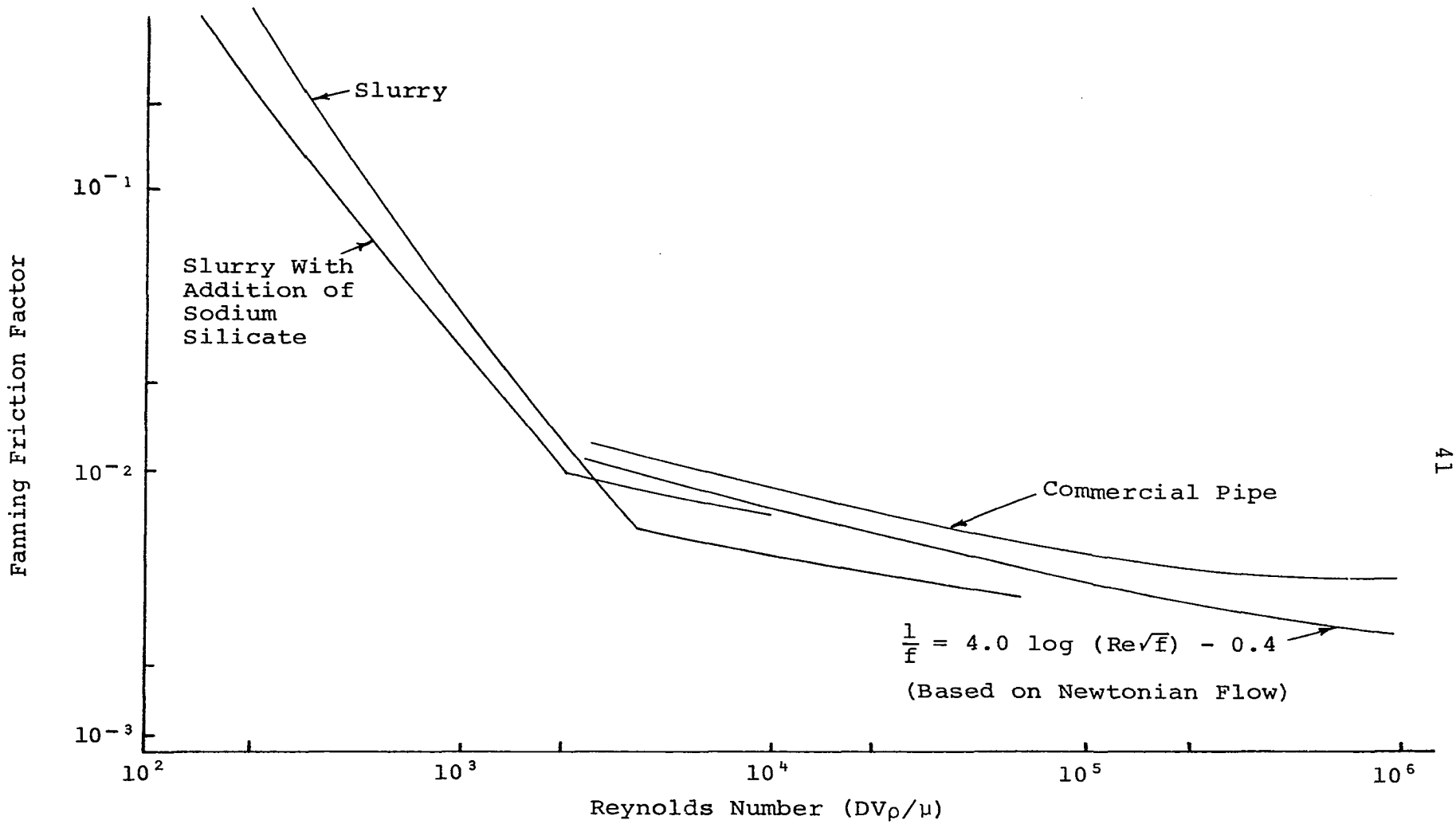

Figure (2.2) Friction Factor-Reynolds Number Plot for Aqueous Thorium Oxide-Thomas (23).

was increased towards the smooth tube Newtonian friction factor curve. This seemed to indicate, perhaps not conclusively, that the flow deviations "are truly the result of non-Newtonian characteristics."

In later experiments conducted by Thomas the yield stress was increased and he noted a very interesting fact: although in both cases the friction factors were less than those for Newtonian fluids, the trends with increasing Reynolds numbers were different. Figure (2.3) shows, for high yield values (greater than 0.5 pounds per square foot) that, as the Reynolds number increases, the friction factors tend to diverge from the Newtonian fluids. This is a direct contrast to what was found in the low yield case.

It may be reasonable to assume that the reason for these two seemingly contradictory phenomena is that, for the low yield stress case, the departure from the Newtonian fluids is the result of the laminar wall layer that was thickened by the non-Newtonian characteristics, thus making the laminar boundary layer exist into high Reynolds numbers. As the Reynolds number increases, the stability of the laminar layer decreases, causing the skin-friction factor to approach the Newtonian curve. For the high yield stress case it is believed that the damping of the turbulent fluctuations increases with the volume fraction of solids and with the ratio of the attractive force between particles to the disruptive forces due to turbulent fluctuations. This reduced the tur-

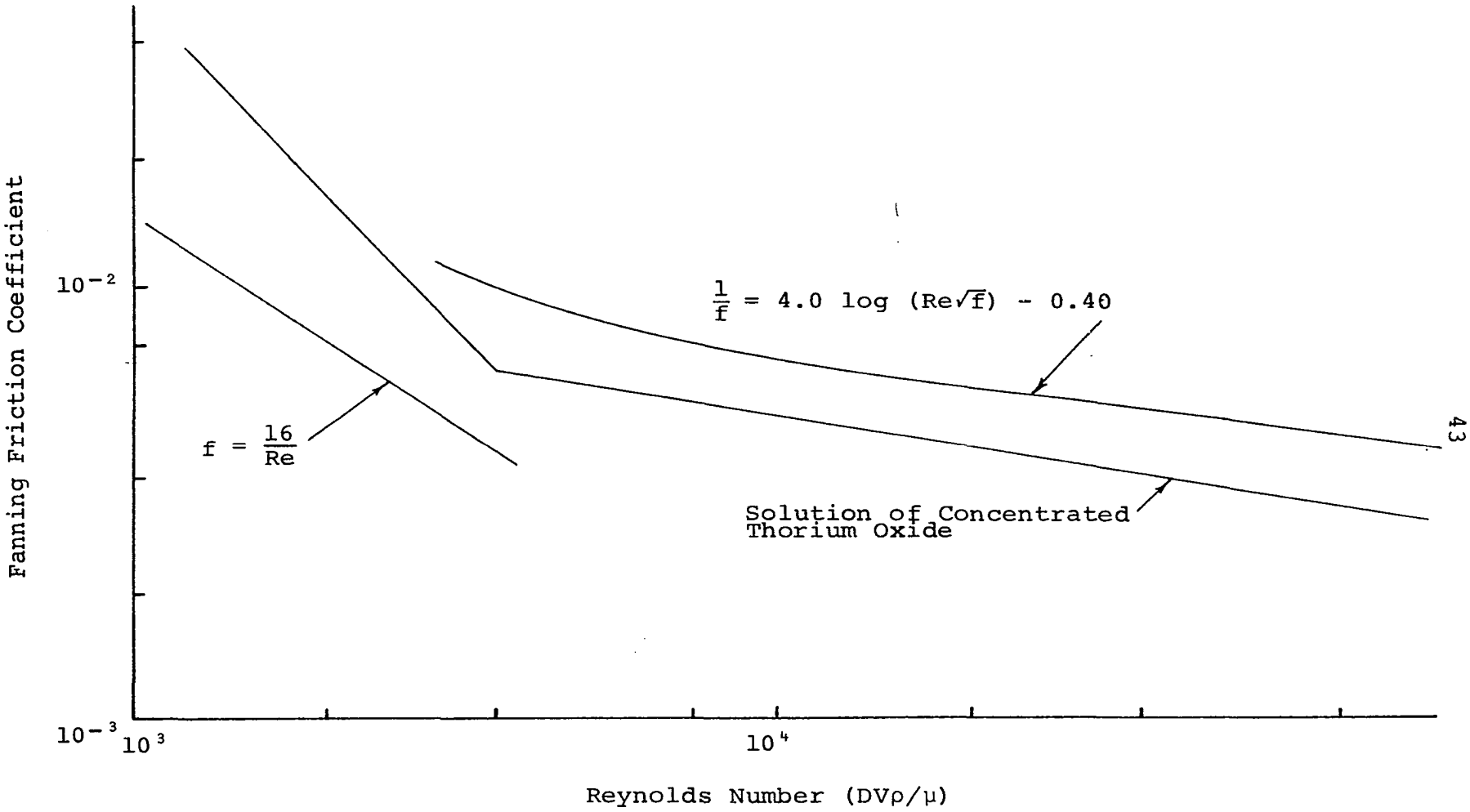

Figure (2.3) Fanning Friction Coefficient Factor for Concentrated Suspensions of Thorium Oxide-Thomas (26).

bulent boundary layer to laminar, thus reducing the Reynolds stresses and the skin-friction coefficient.

Theory

The theory put forth by Thomas was based on Martinelli's analogy, which was developed following von Karman's assumption of a buffer layer between the laminar sublayer and the turbulent core. The Martinelli Equation (23), as used by Thomas, related the heat transfer factor to the Fanning friction factor as shown here:

$$Nu = \frac{\frac{\varepsilon_h}{\varepsilon_m}\sqrt{f/2}\ (Pr)^{2/3}\ \frac{T_w - T_o}{T_w - T_b}}{5\left[\frac{\varepsilon_h}{\varepsilon_m}Pr + \ln\left(1 + 5\frac{\varepsilon_h}{\varepsilon_m}Pr\right) + 0.5\ F_1 \ln\frac{Re}{60}\sqrt{f/2}\right]} \qquad (2.10)$$

where Nu = heat transfer factor, f = Fanning friction factor, and ε_h and ε_m = thermal diffusivities of heat and momentum.

In their book, Kundsen and Katz (27) have tabulated values of F_1 as a function of Reynolds and Peclet numbers. For Thomas' data the values of F_1 were between 0.99 and 1.0. Values of $(T_w - T_o)/(T_w - T_b)$ have also been tabulated as a function of Reynolds and Prandtl numbers, and for Thomas' data the values were between 0.958 and 0.963. Thomas took the ratio of $\varepsilon_h/\varepsilon_m$ as unity. With the above assumptions Thomas was able to reduce the Martinelli Equation to:

$$\frac{\sqrt{f}}{Nu} = 2.120 \ln Re\sqrt{f} + 17.48 \qquad (2.11)$$

for Prandtl number of 8 and to:

$$\frac{\sqrt{f}}{Nu} = 1.715 \ln Re\sqrt{f} + 19.07 \qquad (2.12)$$

for a Prandtl number of 11. The deviation of the actual runs from the above equations was a maximum of 17 percent in the positive and 36 percent in the negative. Thus it is obvious that even in the liquid and solid phase one has to go far before predicted results will agree with actual tests. Even the above equation is mainly an empirical equation since values of some of the major parameters were obtained from experimental tests. Once again one is confronted with an inadequate knowledge in the turbulent flow region.

The Results Reported by Sproull in Dusty Gases

Description of Apparatus and Results

The work of Sproull (20) is one of the first published articles showing the effect of reduction in the skin-friction coefficient when the gas is dusty. Sproull conducted tests using a viscosimeter having a vertical sensing cylinder suspended coaxially within a rotating cylinder. The annulus between the cylinders could be varied between 5 millimeters and 7.5 millimeters. Two types of dust were used. One was limestone containing 40 percent, by weight, of particles smaller than 10 microns in diameter and the other was dust 99 percent, by weight, smaller than 10 microns.

Sproull measured the torque on the inner sensing cylinder and found it to be less when the gas was dusty then when the air was clean. Table (2.1) shows the values obtained by Sproull.

Test Series	Dust	Approx. Concentration gm./m.^{2}	Cylinder Speed (r.p.m.)	Annulus Width (mm.)	Observed Viscosity Reduction Percent
1	Limestone	240	50	7½	40
2	Talc	240	50	7½	38
3	Talc	60	50	7½	10
4	Talc	60	50	5	10
5	Talc	240	50	5	35
6	Limestone	240	50	5	24
7	Limestone	240	25	5	24

Table (2.1) Results Reported by Sproull.

The last column indicates reduction in viscosity. This is because Sproull equated the measured reduction of torque directly to the reduction of viscosity of the gas. Sproull attempted to explain the large reduction in viscosity of the dusty gas by resorting to the kinetic theory of gases.

Theory

From elementary kinetic theory the viscosity μ is given by:

$$\mu = \frac{1}{3}\rho\bar{C}\lambda \qquad (2.13)$$

where ρ is the gas density, $\bar{C}$ the average molecular velocity, and λ is the mean free path. Now with dusty air at constant

temperature, the mean velocity remains constant, but the density increases. Therefore if one is to get a reduction in viscosity, the mean free path length must be reduced. The mean free path length as given by kinetic theory is:

$$\lambda = \frac{1}{\sqrt{2}\pi N a^2} \tag{2.14}$$

where N is the number of particles per cubic centimeter and a is the diameter of the molecules. Now if the dust cloud is regarded as a second gas mixed with the true gas, then the expression of the mean free path length of the gas in the dust laden gas is:

$$\lambda_g = \frac{1}{\sqrt{2}\pi (N_g a_g^2 + N_d a_d^2 \sqrt{1 + m_g/m_d})} \tag{2.15}$$

where N_d is the number of dust particles per cubic centimeter, a_d is the diameter of the particles, and m_d is the mass of the dust particles. Examining the above equation shows that m_g is negligible as compared to m_d; therefore the final radical reduces to unity. Also note that $N_d a_d^2$ is small compared to $N_g a_g^2$. Unless one can show that this is not so, the equation reduces to that of the single gas. The only way that $N_d a_d^2$ could have the same magnitude as $N_g a_g^2$ is if a_d is assumed to be much larger than the actual dust particle diameter. If this "effective diameter" caused $N_d a_d^2$ to have the same magnitude as $N_g a_g^2$ then this could cause λ_g to be reduced by approximately 50 percent. Thus the viscosity would be reduced by 50 percent.

To obtain this effective diameter Sproull suggested that each dust particle was surrounded by a boundary layer of gas adhering to it. This diameter was calculated by means of Stokes' law which gave an expression of the diameter,

$$\delta = \sqrt{\frac{\mu a}{\rho V}} \qquad (2.16)$$

where V is the difference in the gas velocity on opposite sides of the particle. Knowing the velocity gradient across the annulus Sproull calculated the velocity, V, for a one micron particle. This gave him a diameter between 100 and 500 microns, thereby making his term, $N_d a_d^2$, the same magnitude as $N_g a_g^2$.

Sproull, in summarizing, said that the suspended particles are surrounded by a gaseous boundary layer some 50 to 100 times as great as its actual diameter. Also he notes that the couple on the dust particle would tend to rotate the particle and would act "like the balls between the races of a bearing." This ball bearing concept also could contribute, according to Sproull, in the reduction of viscosity.

Theory by Saffman

The theory advanced by Sproull came under heavy fire by Saffman (28 and 29). Saffman pointed out that Sproull's theory contradicts the Einstein formula for the viscosity of a suspension, according to which the viscosity will increase with the bulk concentration of the dust.

Saffman obtained an equation for the torque per unit length of the cylinder as:

$$G = 2\pi\mu r^3 \frac{\partial}{\partial r}\left(\frac{V}{r}\right) = 2\pi m N \tau r V^3 + G_1 \qquad (2.17)$$

where μ is the viscosity of the air and G the torque per unit length on the inner cylinder. The parameter, σ, is a measure of the time for the velocity of the particle to become adjusted to changes in the velocity of the air. Using Stokes' Equation one can derive an expression for σ:

$$\sigma = \frac{m}{6\pi\mu a} \qquad (2.18)$$

To summarize, Saffman advanced the idea that when the particles are large σ will be comparable to or greater than the time scale of turbulent fluctuations. The relative velocity of air and dust cause an extra dissapation that extracts energy from the turbulence and damps it. This damping effect of the coarse dust may be enough to stabilize the laminar flow of the air which is otherwise very unstable. This damping action reduces the Reynolds stresses and the loss of pressure. For the case of the very fine dust for which σ is much less than the turbulent time scale, the dust follows the air motion more closely and its main effect is to increase the effective density of the air therefore increasing the Reynolds number of the air.

Evaluation of Saffman and Sproull Theories

The preceding two theories are of a contradictory

nature. Saffman's explanation agrees with the explanation put forward by Thomas in his investigation of suspensions in liquids. Sproull's theory of an effective diameter is not entirely incorrect, but the effective diameter he obtains (between 100 and 500 times the diameter of the particle) seems to be too large. This can be attributed to two facts. First, the equation of the boundary layer obtained from Stokes' law holds true for low velocities and when there is no interaction between the spheres. In Sproull's case both of these premises were violated, therefore the use of this equation is not correct. Second, the velocity on opposite sides of the particle was based on the velocity gradient of the viscosimeter annulus. Utilizing this velocity without taking into account such parameters as wall effect and variations in particle size would give an erroneous parameter in circular pipes at high Reynolds numbers.

The Results Reported by Soo and Trezek in the Investigation of Dusty Air in Turbulent Pipe Flow

The research on this topic by Soo and Trezek (30) was also conducted at high Reynolds numbers within a range of 1.3×10^5 to 2.95×10^5. The dusty gas used consisted of 30 micron magnesium oxide particles suspended in air. The experimental apparatus consisted of a 5 inch diameter brass pipe which was connected to a large air supply. Particles were injected into the air stream and care was taken to see that the

particles were thoroughly diffused throughout the entire flow.

The addition of solid particles led to a decrease in pipe flow friction factors up to a certain mass flow ratio of solid to gas, but increased again as mass ratio was increased as shown in Figure (2.4). Again caution should be exercised when evaluating these data and it should not be extrapolated outside its range of Reynolds numbers. Soo and Trezek also found that a "tenacious" layer of thickness of magnesia particles was deposited on the wall of the tube. This would form a layer of roughness thereby changing the skin-friction coefficient.

Theory

Theory regarding the reduction of skin-friction coefficients was not present in the paper of Soo and Trezek. However Soo, in his book (31), has developed some theory for this case. The shear stress as expressed by Prandtl for air in terms of the mixing length ℓ is given as:

$$\tau = \ell^2 \rho \left(\frac{du}{dy}\right)^2 \qquad (2.19)$$

In the case of this experiment Soo and Trezek found that the gas phase followed closely the 1/7th velocity law even though solid particles were suspended in the flow. Thus Soo concludes that the shear stress in the gas due to the presence of solid particles can be given by:

$$\tau_{gp} = \ell_p^2 \rho \left(\frac{du}{dy}\right)^2 \qquad (2.20)$$

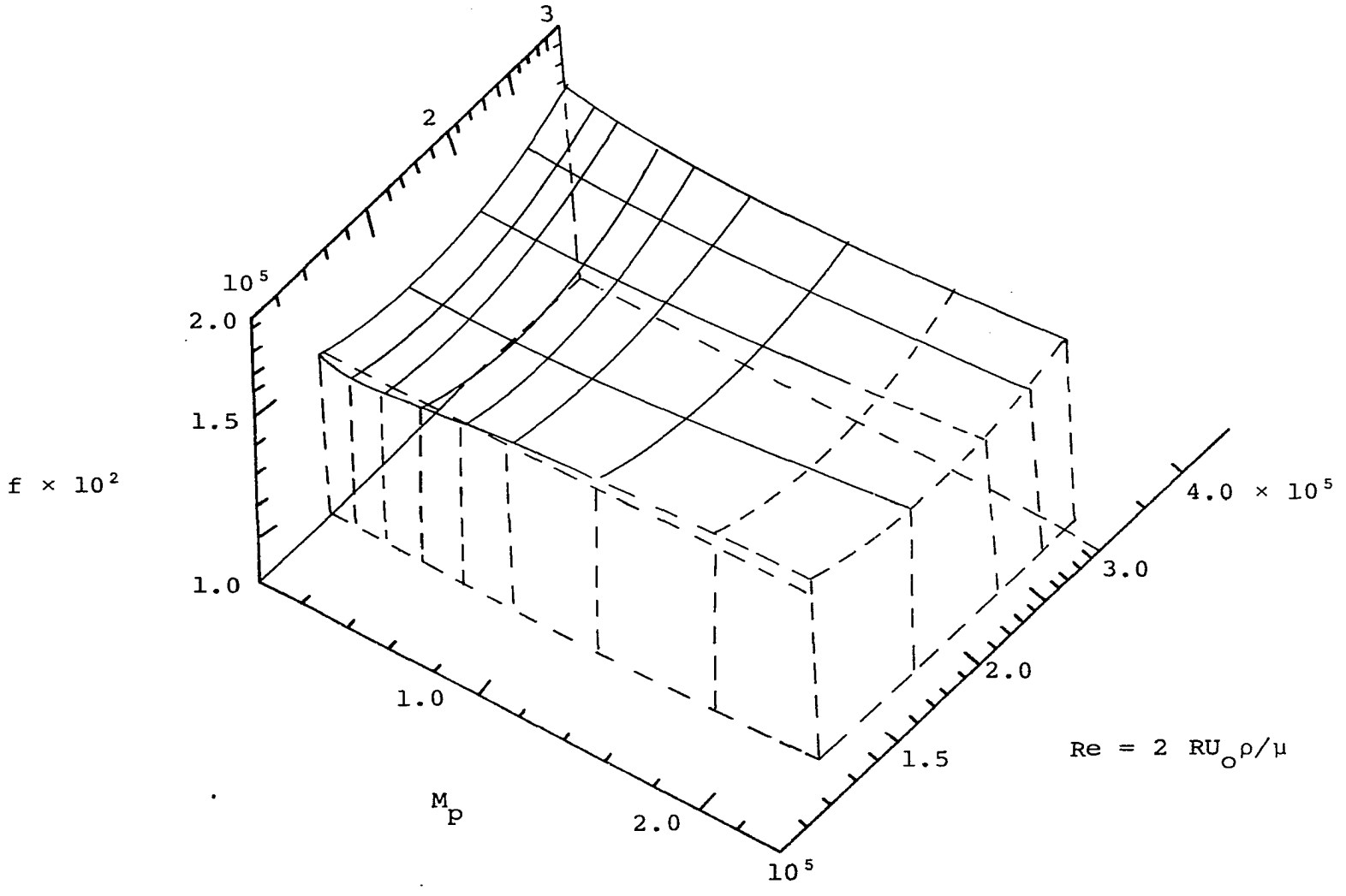

Figure (2.4) Friction Factors at Various Reynolds Numbers and Mass Ratios-Soo & Trezek (30).

where ℓ_p is the mixing length due to the presence of solid particles. Hence,

$$\frac{\tau_g}{\tau_{gp}} = \frac{\ell^2}{\ell_p^2} \tag{2.21}$$

Thus the decrease in friction factor according to Soo, due to the presence of solid particles, may be attributed to the reduced mixing length because of dissipation by the solid particles. The effect of solid particles on the pressure drop and mixing length are shown in Figure (2.5).

The eddy viscosity for turbulent flow as given in Hinze (32) is:

$$\varepsilon_m = \ell^2 \frac{du}{dx} \tag{2.22}$$

With this formula, Soo obtains the following equation for the skin-friction factor:

$$C_f = 2\varepsilon_m \frac{1}{V^2} \frac{du}{dx}$$

$$C_f = \frac{2\ell^2 (du/dx)^2}{V^2}$$

The Results Reported by McCarthy and Olson for Flow of Dusty Air in Circular Pipes at High Reynolds Numbers

Recent Work done by McCarthy and Olson (33) for flow of gas solids in a circular pipe indicated a reduction in skin-friction coefficient when solids are added to the gas in turbulent flow.

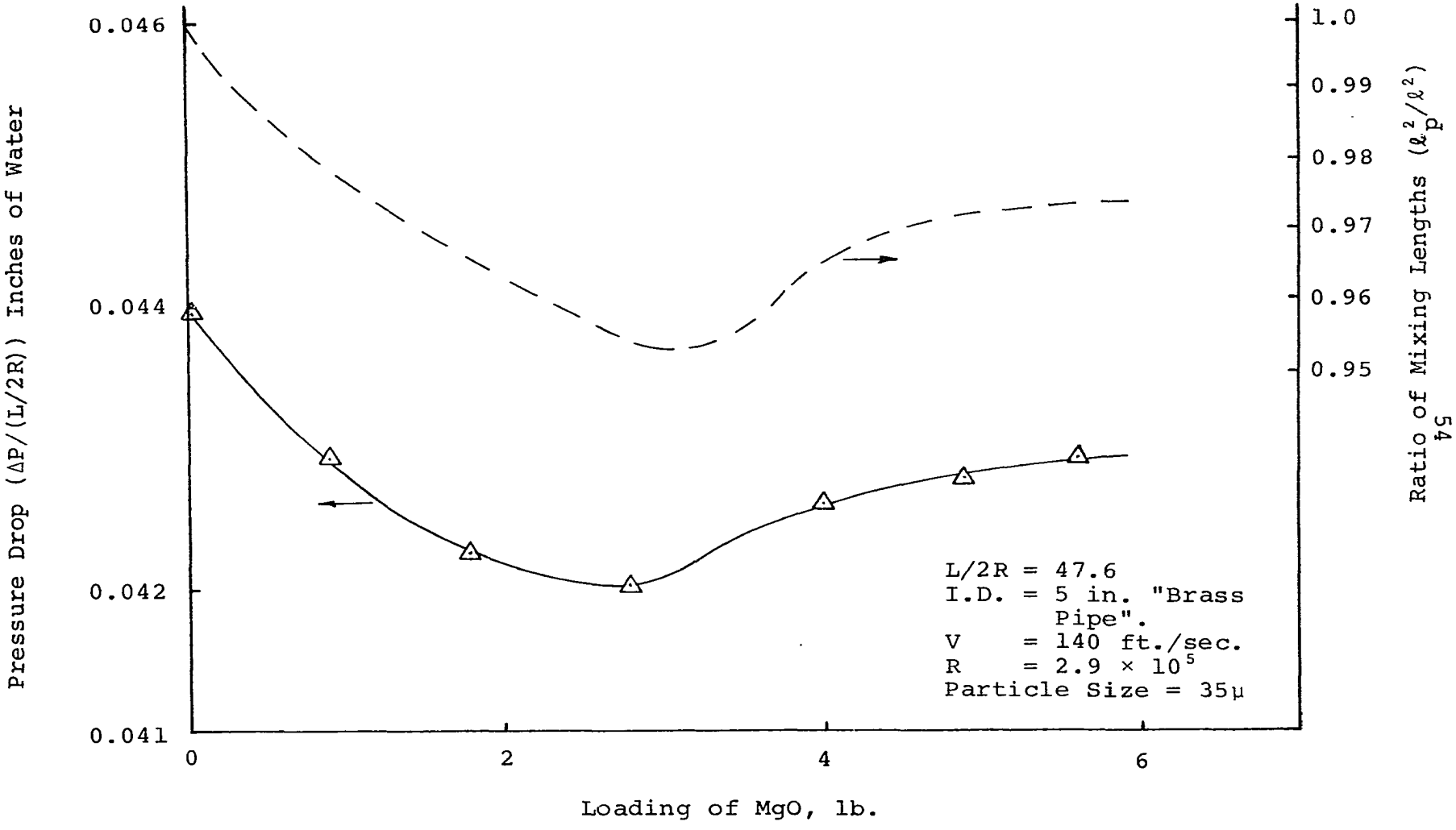

Figure (2.5) Effect of Solid Particles on Pressure Drop and Mixing Length in Pipe Flow-Soo(31).

Apparatus and Results

The apparatus consisted of a horizontal glass pipe connected to a large compressor. Solids were fed into the flow from a specially built feeder. Pressure drops across the pipe were recorded with and without solids suspended in the air stream. A lesser drop in pressure was recorded for the same flow rate when particles were suspended in the air stream than with clean air.

The particle sizes used by McCarthy and Olson were 3 micron and 64 micron. Since these particles are both very small, the difference in their sizes did not make a marked difference on the skin-friction factor at the high Reynolds numbers at which the experiment was conducted. Figure (2.6) shows the effect of particle flow on the friction factor. The rate of decrease in the friction factor decreased with increasing weight ratio. The maximum reduction of the skin friction coefficient was observed to occur around a weight flow ratio (W_p/W_g) of 0.8.

Theory

The theory proposed by McCarthy and Olson to support their experimental results was based on the assumption that the slip velocity $(V_g - V_p)$ is negligibly small. Thus in a system where gas and solid velocities are equal, and the friction loss represented is shear stress at the wall, the con-

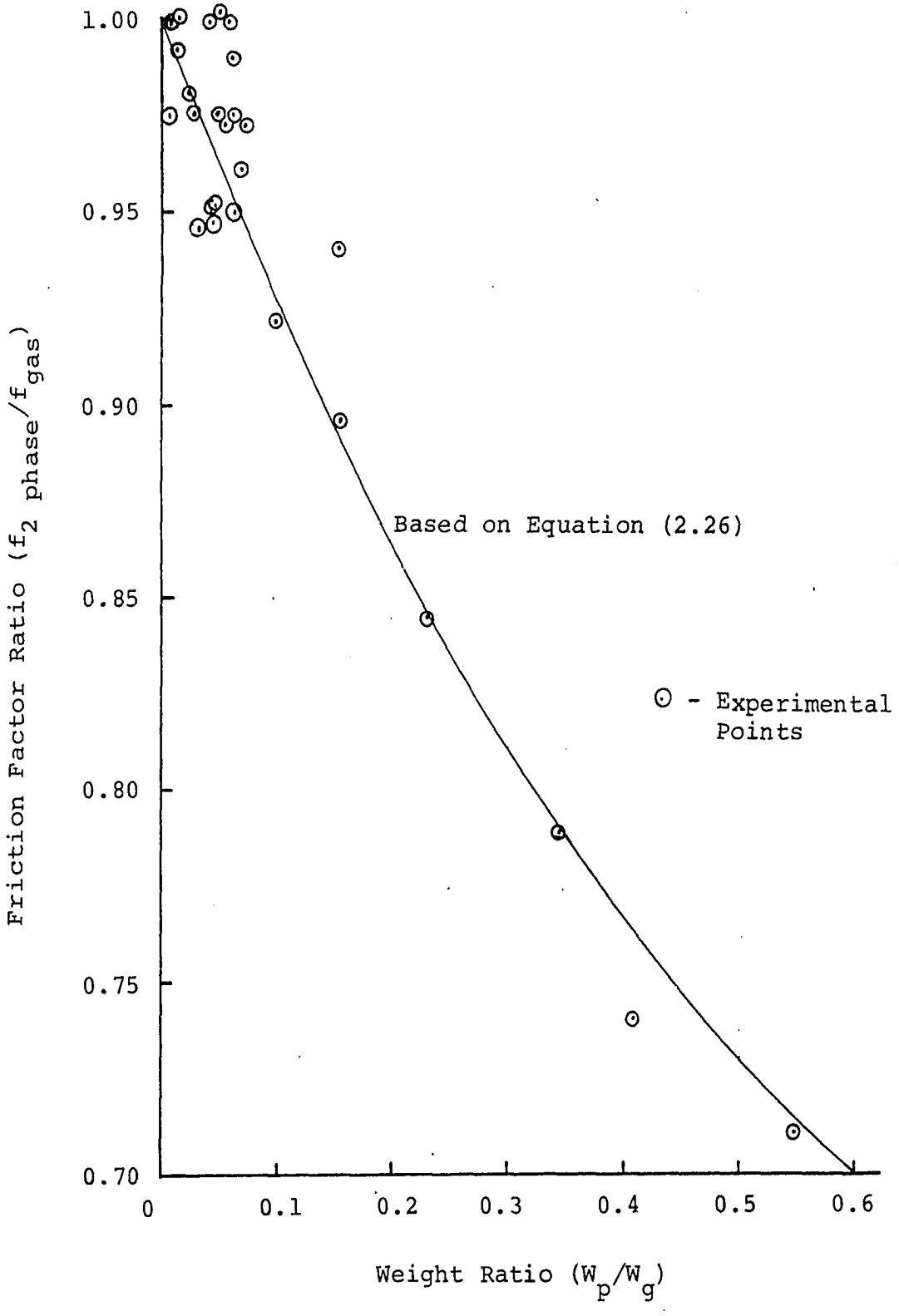

Figure (2.6) Two-Phase Friction Factor as Influenced by Weight Flow Ratio, McCarthy and Olson (33).

tinuum model yields:

$$\frac{\rho_m}{g_c} V_m \frac{dV_m}{dz} = \frac{dP}{dx} - 2 \frac{\tau_w}{r} \tag{2.24}$$

which may be written as,

$$\frac{G_m}{g_c} \frac{dV_m}{dz} = - \frac{dP}{dz} - \frac{2fG_m V_z}{Dg_c} \tag{2.24a}$$

where G_m, g_c, f, and D are constant. Solving this equation for adiabatic flow McCarthy and Olson obtained the following relationship:

$$P = \{1 - \frac{2\beta \frac{C_p}{R}}{\psi^2} + [(1 + \frac{1}{\psi^2})^{\frac{1}{2}} - P(P^2 + \frac{1}{\psi^2})^{\frac{1}{2}}]$$

$$+ \frac{1}{\psi^2} (1 - \frac{\psi}{\alpha}) \ln \frac{[(1 + \frac{1}{\psi^2})^{\frac{1}{2}} + 1]}{[(P^2 + \frac{1}{\psi^2})^{\frac{1}{2}} + P]}\}^{\frac{1}{2}} \tag{2.25}$$

where

$$\psi = \frac{g_c c_p P_o}{RG\sqrt{2g_c c_p T_o}}$$

$$\alpha = \frac{P_o g_c}{G\sqrt{2g_c c_p T_o}}$$

and

$$\beta = \frac{2fL}{D}$$

Solving this equation for the two-phase friction factor, they obtained the following equation:

$$\frac{f_{2\ phase}}{f_{gas}} = 1.011 + 0.82 \frac{W_p}{W_g} + 0.479 (W_p/W_g)^2 \tag{2.26}$$

This equation agreed remarkably well with the data points taken, but one must be extremely careful before any general-

izations are made. The assumption made here was that the slip velocity is negligible. This means that the particles are very small and the equation would fail for coarser particles. The experiment was carried out at high Reynolds numbers and so a simple relationship gives accurate results. At lower Reynolds numbers the effect of Reynolds number is significant, and the diameter of the particles are factors that have also to be accounted for.

Miscellaneous Background Information

Dusty Air Study by Halstrom

Halstrom (34) was one of the first to report that the addition of solid particles in the flow caused a decrease in the skin-friction coefficient below that of clean air. The test was conducted in a straight section of glass pipe of 2 inches in diameter. Figure (2.7) shows the results as tabulated by him. No theory was presented and the data were presented without comment.

Dusty Air Study by Briggs

The work of Briggs (35) was conducted in the laboratories of the Western Precipitation Division, Joy Manufacturing company and, although it was not published, it was referred to by Sproull. Briggs found that by the addition of about 1/4 kilogram per cubic meter of dust, the pressure difference required to maintain the flow was decreased by about 13 percent.

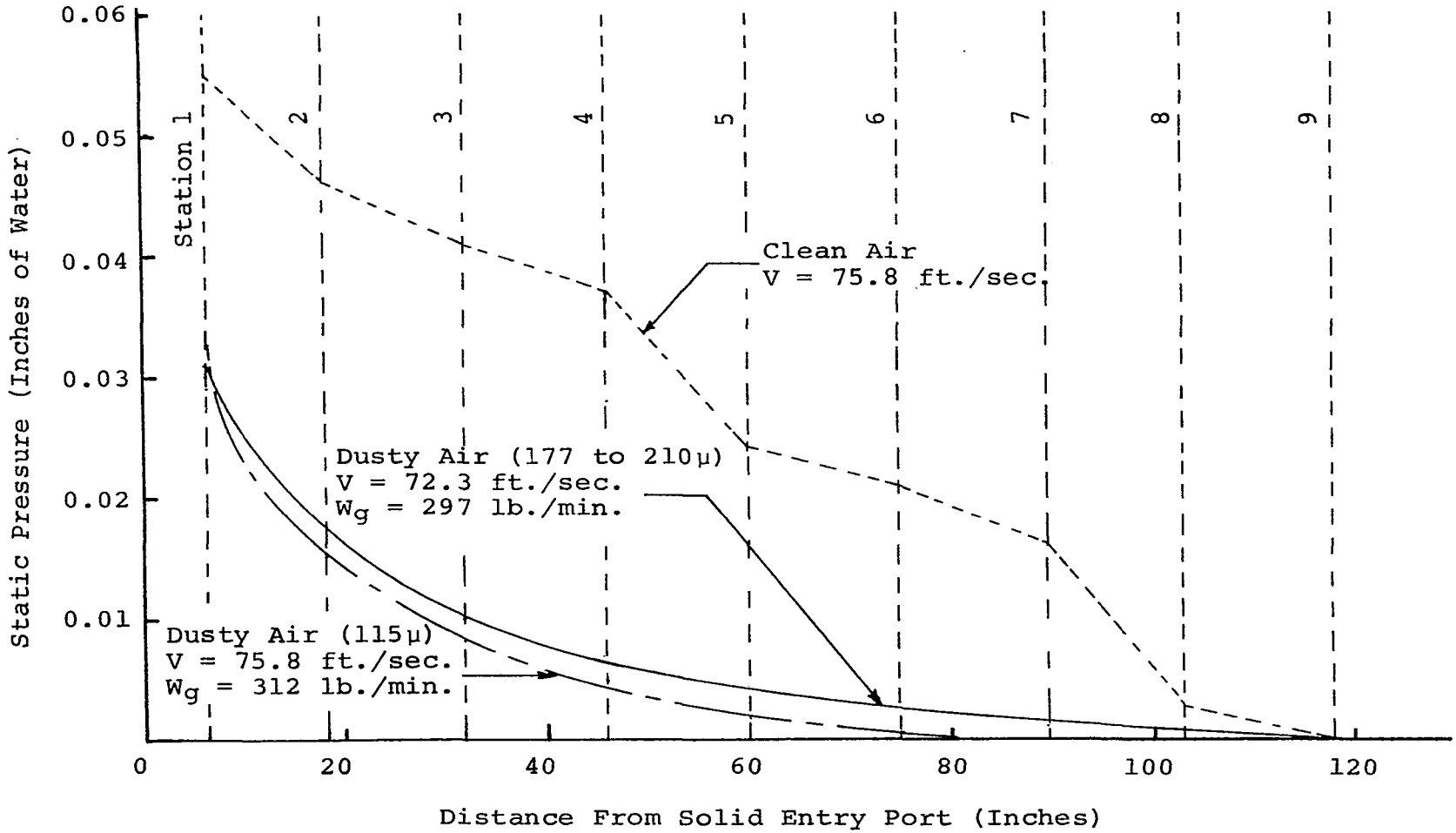

Figure (2.7) Pressure Drop in Pipe With Dusty Air-Halstrom (34).

With the pressure difference maintained constant, the addition of dust increased the flow rate by about 6 percent.

Proposed Theory by Lumley

Lumley (36) proposed that the phenomenon where particles or fibers in flow have been responsible for drag reduction may be due to the Reynolds number similarity. Reynolds number similarity can be violated but this is not a "straight forward matter." By increasing viscosity there is no major change until the dissapative and energy terms are nearly equal, at which point the turbulence can no longer extract the energy required to maintain itself and thus the flow becomes laminar. This results in a lower skin-friction drag. According to Lumley this phenomenon is then one of stabilization. Therefore to influence Reynolds similarity, the fluid particle system must, in the energy equation, have those terms arising from that part of the stress which is not pressure, and which are appreciable in the "energy containing range of wave numbers without being dissapative in character, so as not to turn the turbulence off." The only fluid particle system that supports these properties is a "viscoelastic" system. This has been shown by Fabula (37) although its exact mechanism is not understood.

Lumley observed that results by several investigators indicated an increase in the observed intensities. He suggested that this was due to the fact that the Reynolds number similarity was violated by the introduction of other time scales. Length scales are directly affected by the long fibers, while

velocity scales are introduced by settling effects and time scales by the response time of the particles. This last mechanism is similar to viscoelasticity. This idea had also been previously mentioned by Saffman, as discussed earlier in this chapter. In fact, Lumley's theory and Saffman's are quite similar, with Lumley's being the more elaborate of the two.

CHAPTER III

OBJECTIVES OF THE EXPERIMENTAL WORK

To facilitate the movement of objects through a medium, engineers have sought various ways to control the fluid surrounding the object. This has led to various types of boundary-layer control, some of which have been described previously.

The flow of liquids and gases in pipelines is an important mode of transportation. As the velocity in pipes becomes greater the flow becomes turbulent. This turbulence causes greater resistance to the flow, thereby increasing the pumping costs. One of the main objectives of this research project was to investigate the variables of dusty air flow which would reduce the skin friction in pipes.

Another important aspect of the field of transportation is the aircraft. Skin-friction drag, as pointed out earlier, is the major drag encountered by the aircraft, and so reduction of this drag would result in considerable savings in fuel. The other main objective of this research project was to investigate the variables of dusty air flow which would reduce the skin friction on flat plates. This should

provide basic data which could then be adapted for an aircraft wing.

The original goals thus were to investigate the reduction of skin-friction drag on a circular pipe and over a flat plate. As the project advanced changes were made to the initial proposal to investigate intermediate findings. Also difficulties encountered in certain phases of the test program made it necessary to make changes in the approach. Nevertheless the basic objectives of the original proposal were all met.

The investigation of the flow phenomena was to be carried out over a large range of Reynolds numbers. It was decided, after a close investigation of the published literature, that the region to be investigated should be from the laminar or transition region to the fully developed turbulent flow. As indicated in Chapter II the region most frequently investigated by prior researchers was only in the fully developed turbulent flow, a region between Reynolds number of 10^5 and 10^6 for pipe flows. Other parameters to be investigated were variation of particle diameter size and the variation of the weight ratio. Finally it was proposed that if tests proved positive then an attempt would be made to explain this phenomenon in terms of fluid dynamic principles. Also other interesting side effects developed throughout the project and they received their share of attention. Careful attention was given to every possible observation, and each was thoroughly checked to see if it contributed, in any way, to the basic objectives of the research.

Important Parameters to be Observed

Reynolds Number

As mentioned earlier, it was decided to investigate the region from laminar flow to fully developed turbulent flow. It was observed by Thomas (23 and 26), as mentioned in Chapter II, that the effect of particles suspended in liquids was very prominent in the transition region. The apparatus therefore was designed with this in mind so that it would fully cover the transition region.

McCarthy and Olson (33), Soo and Trezek (30), all investigated the flow at very high Reynolds numbers. At these high numbers the effect of Reynolds number did not contribute significantly to the percent change in the skin-friction factor as is borne out by Equation (2.26) obtained by McCarthy and Olson. Thus it was felt that in an exploratory research program, such as this, an important parameter such as Reynolds number should be further investigated. There was no desire to repeat investigations already conducted by other able experimenters.

Particle Size

This important parameter seems generally to be ignored or treated very lightly by past reserchers. The trend has been to investigate very small particle sizes, usually between 3 microns and 70 microns, and draw the conclusion, which we believe to be erroneous, that particle size was not an im-

portant factor.

To prove that particle size is a very important parameter it was decided to vary particle size from 2 microns to 1600 microns. It was also decided to use glass spheres as particles since they were available and flowed out of the hopper smoothly and evenly.

Weight Ratio (W_p/W_g)

This parameter has been one which has been investigated in depth by most researchers on this subject. Although most of the past research has been usually done keeping this ratio less than unity, we felt, once again that for an exploratory research project, we should vary the weight ratio to the maximum achievable without clogging the apparatus.

From past data obtained by other researchers it is obvious that this parameter is one of prime importance. Thus care was taken to see that the measurement of this parameter was very accurate. Past data, at high Reynolds numbers and very small particle size, indicated an optimum weight flow ratio of 0.8 but it was felt that this would not be true as particle size was increased.

Slip Velocity

The difference in velocity between the gas and the particles ($V_p - V_g$) is generally known as the "slip velocity". In the past researchers have assumed that this velocity is negligible. It is, however, expected to play rather an impor-

tant part as the particle size is increased.

The violation of the Reynolds similarity parameter has, in recent publications, been indicated as the probable cause of skin-friction reduction. This was done by the introduction of length and time scales. As pointed out earlier the time scale is introduced by the characteristic time of the particles, i.e., the response time to the step function is relative velocity.

To measure this slip velocity a rather complicated photographic setup is needed. A description of the setup will be given in detail in a later chapter.

Velocity Profile

To check the flow for turbulence, velocity profiles in the circular pipe and over the flat plate must be obtained. These velocity profiles also come in handy in calculating the slip velocity once the particle velocity was measured, as mentioned previously.

These velocity profiles, when compared to profiles of other experimenters, not only will enable one to say whether the flow is laminar, turbulent, or in the transition region, but also will provide a confidence check on the apparatus.

CHAPTER IV

DESCRIPTION OF TEST APPARATUS

In the previous chapter the test objectives have been outlined. The next task was the design and construction of suitable equipment to conduct the tests.

The test equipment was carefully selected to adequately obtain the test objectives. The main effort was directed towards the design and construction of the two flow assemblies required to meet our basic objectives. The two flow loops are required since our test objectives deal with two different flow problems, viz., flow in a circular pipe and flow over a flat plate. After the two main assemblies were completed, other test equipment was obtained or constructed to obtain the test data required to meet all the objectives of the project.

This chapter will describe, in detail, the various pieces of equipment used to obtain the necessary data. Since this project was of an exploratory nature, it was felt important to describe the equipment as fully as possible. This would enable future researchers on this subject to accurately evaluate the findings and facilitate future efforts along this line.

The equipment was chosen with two main principles in mind. First, that it be entirely adequate, and second, if possible, that it be from existing equipment. If large funds had been available some parts of the system would have been designed differently, but it was felt that the equipment used was entirely adequate for this research program.

Flow Test Loop Assembly

To meet the objectives of this research project two entirely different flow loops had to be assembled. The flow in the pipe was rather simple to set up as compared to the flow over a flat plate which entailed the setting up of an entire wind tunnel.

Flow Test Loop for the Circular Pipe Experiment

The flow test loop required a long straight circular pipe, a blower, a control system, a metering method, a pressure drop measuring device, a system for feeding the glass particles, and a system for the recovery of the particles.

The particles were poured into the inlet of the blower where the particles were thoroughly mixed with the air. The gas-solid mixture then enters the transition section which joins the blower to the circular pipe and also acts as a control system by the presence of a valve which regulates the flow rate. The circular pipe is constructed of plexiglas with an internal diameter of 2-3/4 inches. The test section is 42 in-

ches in length and is located 6 feet 10 inches from the transition section to assure completely undisturbed flow. The circular pipe then exits into a large collection chamber. Figure (4.1) shows a schematic of the flow loop, and Figure (4.2) is a photograph of the same. Each component of the assembly is described in detail in the following paragraphs.

Feed system. A hopper was designed using a plastic waste basket into which a hole was cut through the bottom. Through this hole a circular 3 inch diameter pipe exits to within several inches above the blower inlet. Inside the waste basket is a hollow inverted truncated cone. The larger diameter of the cone is equal to that of the basket and the smaller diameter is equal to that of the 3 inch diameter pipe. This cone facilitates the flow of the particles. A sliding valve regulates the flow rate. This system worked well for particles larger than 100 microns in diameter. Particles of 2 microns tend to coagulate and another method of feeding had to be found for these particles.

For these smaller particles a system was devised which used the principle of a "flour sifter", i.e., a mesh with rotating blades just above it to break up the coagulation of the particles. Thus for the 2 to 30 micron particles a flour sifter with an extended container was used with certain other slight modification. The flow rate was regulated by the speed at which the blades just above the wire mesh are rotated.

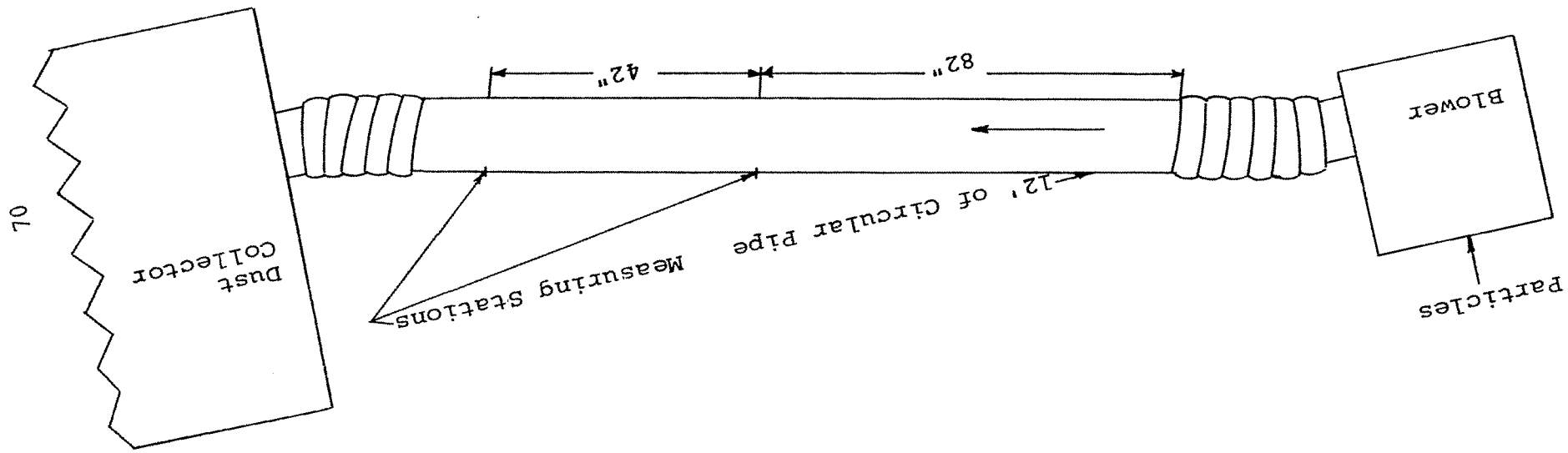

Figure (4.1) Circular pipe Apparatus.

Figure (4.2) Circular Pipe Setup.

The flow rate of particles, by either of the two above mentioned methods, was measured by weighing the hoppers before and after each test run and noting the run time.

Blower. The blower used was a RexVane Vent Set, Size R-16, Design 9, manufactured by B. F. Sturtevant Co., Boston, Massachusetts. The blower has an impeller of the squirrel cage type. Figure (4.3) is a photograph of this type of impeller. The squirrel cage type impeller was chosen because of its excellent diffusion characteristics. Particles and air were taken in by the blower from the same inlet. This assured a complete diffusion of the particles in the air stream. The blower was mounted on its back so that the inlet of the blower faced the ceiling. This was done so that the particles could be fed in by gravity. This exit from the blower was at a 90 degree angle to the inlet.

Most of the problems encountered during the operation of the blower were minor. One of the major problems encountered was during the feeding of the large particle sizes (840 microns and above). The problem arose because the larger particles had a tendency to hit the blades and some of them would bounce out of the blower. To prevent this a cardboard inlet lip was added to the inlet of the blower. This prevented many of these particles from bouncing out. A large plastic sheet was also placed around the blower which enabled any particles that may have escaped to be collected in it. These particles were collected after each test run and weighed.

Figure (4.3) Impeller of Blower.

This weight was then subtracted from the weight calculated by subtracting the initial weight from the final weight and thereby giving an accurate weight of the particles that actually went through the blower.

The other problem encountered was the occasional particle getting into the bearing of the blower. To prevent this, a vacuum hose was placed next to the bearing and this prevented any further problems along this line. The amount of particles that fell in this region was so negligible that it was felt that there was no need to try and compensate for this loss.

Another problem which was anticipated and so taken into account early in the project was choking the inlet. This was due to the placing of the hopper too close to the inlet. A series of tests were conducted by placing a piece of cardboard in front of the inlet at a known height above the inlet. By these tests it was possible to ascertain the closest distance at which the hopper could be placed from the lip of the blower inlet without affecting the flow rate of the blower.

Metering section. The metering section, which controlled the flow rate of the air, was also a transition section which connected the rectangular exit of the blower to the circular pipe. A butterfly valve was placed in the circular section of the transition piece. This valve was used to regulate the flow rate by increasing the back pressure on the blower.

The metering section was joined to the blower by a hinge type hookup and to the circular pipe by a piece of flexible hose. This setup was chosen so that after each run the metering section could be inspected to make sure no particles were caught in it. The problem would usually arise at low flow settings, i.e., the valve being nearly closed, thereby causing a slight accumulation with large particle sizes. This accumulation, when it occurred, would be taken into account and the particle flow rate would be corrected.

Circular pipe and test section. The circular pipe was made out of plexiglas and had an internal diameter of 2-3/4 inches. The wall thickness of the pipe was 1/4 inch. The length of the pipe was 12 feet. It consisted of two sections, each 6 feet long and "butt welded" together. This process had to be done with great care to avoid any discontinuity in the surface.

To achieve this "butt welded" union a piece of solid plexiglas, 2 inches in length was machined to an inside diameter slightly larger than the external diameter of the circular pipe thus enabling a press fit. Before the two pipes were press fitted together the two ends were treated with a solution known as "Plastic Weld" which actually melts the plastic and fuses the two pieces together. This method provided an entirely true fit without any discontinuity in the surface. To make sure that no glue or edges, due to the pieces being pushed together, were in the flow path a rod with a piece of very fine

sandpaper wrapped around the top was pushed through the pipe.

The test section of the pipe was 42 inches in length and was located 82 inches from the metering section. The location was chosen where the effects of the blower or the butterfly valve would not show up in the flow. To measure the static pressure at the beginning and end of the test section, four holes 1/32 inch in diameter and 90 degrees apart were drilled at both points. At a location 1-3/4 inch from the first ring of static pressure taps, a tap was located for a pitot-static tube. This location was planned so that the leading edge of the pitot-static tube was in the same plane as the ring of static pressure probes. The ring of static pressure taps was connected to a mixer by pieces of Tygon tubing so as to come out with an average static pressure reading. Care was taken to see that the amount of Tygon tubing used for the static pressure rings at the beginning and end of the test section were of equal length, so as to cancel any effects due to this tubing. Figure (4.4) is a photograph of the test section showing all the instrumentation used.

Inclined manometers were used to read the various pressures. These manometers could be read accurately to 0.005 inches of water, although in some cases it was read as close as 0.001 inches of water. This was done at the low flow reading with special markings on the manometer.

Dust collector. The dust collector consisted of a large sheet-metal container, 4 feet by 6 feet by 6 feet,

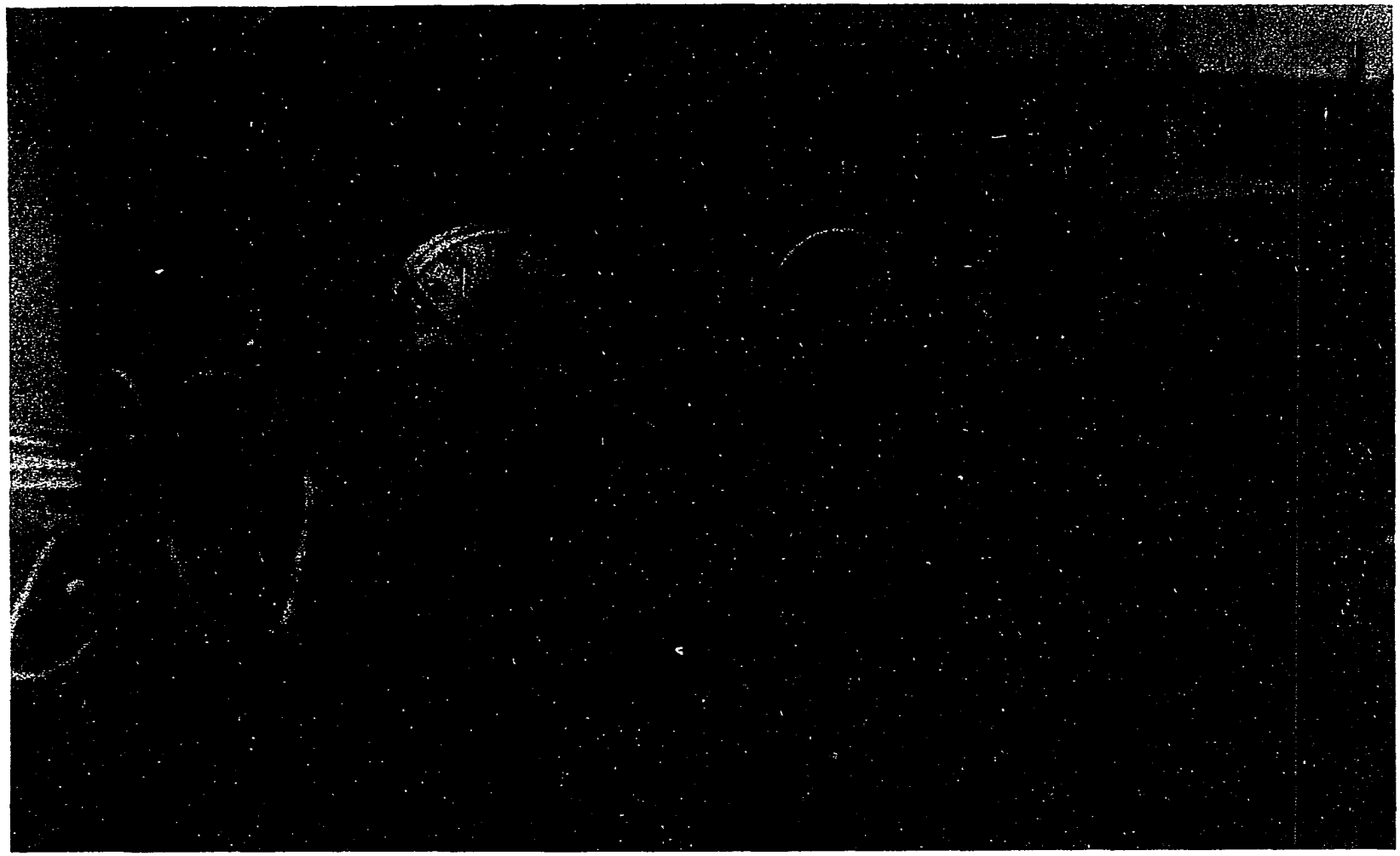

Figure (4.4) Test Section of Circular Pipe.

mounted on a frame 3 feet above the ground. The collector was connected both to the wind tunnel and to the circular pipe as shown in Figure (4.5), a sketch of the dust collector.

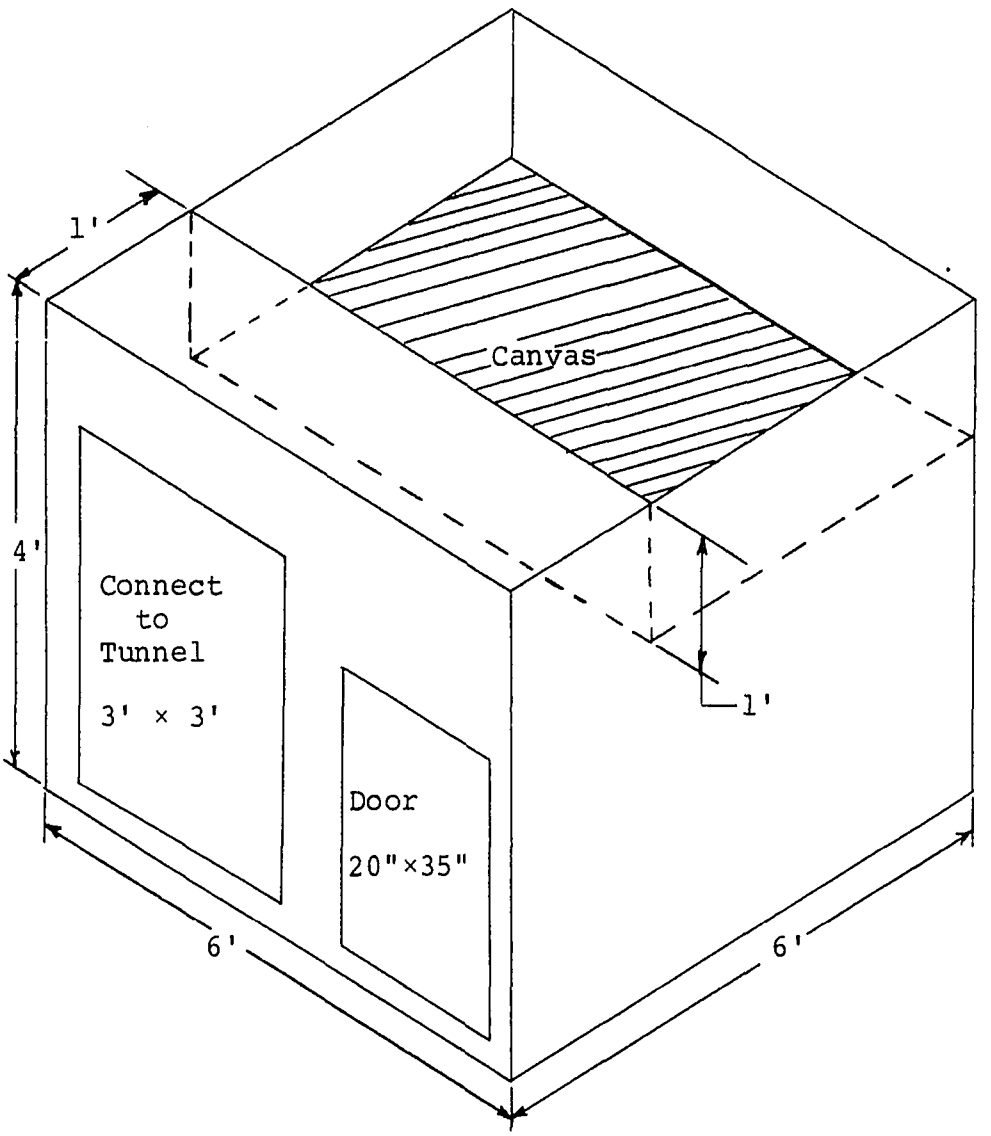

Figure (4.5) Sketch of Dust Collector.

Table (4.1), compiled by Frank (38), was used to estimate the settling rates of different sizes of particles. This was helpful in deciding on the size of the collector and the size of the exit. A canvas was stretched across the exit

Diam. of Particles μ	Rate of Settling in ft./min. for Spheres ρ=1; 70°F	Types of Settling	Laws of Settling in Relation to Particle Size (lines of demarcation approx.)	
8000		Particles Fall With Increasing Velocity		
	1750			
4000				
2000				
1000	790			
	555			
400				
200				
100	59.2	Particles Settle With Constant Velocity	$C = 24.9\sqrt{Ds_1}$	C = Velocity ft./sec. D = Diam. of Particle in Microns s_1 = Density of Particles $\lambda = 10^{-5}$cm. (mean free path length) r = Radius of Particle in cm. K = 0.8 to 0.86
	14.3		Stokes Law for air at 70°F $C = 0.00592 s_1 D^2$	
40				
20				
10	0.592			
	0.148			
4				
2				
1	0.007		Cunningham's Factor $C = C'(1 + K\frac{\lambda}{r})$ C'= C of Stokes	
	0.002			
0.4				
0.2				

Table (4.1) Particle Settling Rate Compiled From Table by W. G. Frank (38).

which measured 6 feet by 5 feet.

To enhance the settling rate the walls of the dust collector were sprayed by a chemical solution, manufactured by the Madison Chemical Corporation, known as "Attract". As described in the literature, "Attract is a clear, violet colored, pleasantly aromatic complex compound. It is formulated with biodegradable emulsifiers for water flushability when desired." It also has an "Anti-Static Chemical" which removes the electric charge from the particles to the nearest ground. Thus the "Attract" treated walls attracted the particles and held them there. Before every set of runs the walls of the dust collector were sprayed with this chemical. In addition the surrounding area was sprayed so as to prevent any escaping dust to spread throughout the entire room.

Particles. Five sizes of glass particles were used varying in size from about 2 microns to 1680 microns. The particles were glass beads and are manufactured from a high grade optical crown glass. They are lead-free and are of the soda lime type, with a minimum silica content of 68 percent. They are designed to resist wear and fracture upon impact and are annealed in their spherical shape to equalize internal stresses. The specific gravity of this media is approximately 2.5.

Table (4.2) shows the standards that must be met by the particles. These standards are the standards set forth by the U. S. Air Force in their MIL-STD-852(USAF).

Bead Size		5	7	12	16
U. S. STD Screen	Size Opening Microns	60% Round	65% Round	80% Round	90% Round
12	1680	95-100			
14	1410	0- 15			
20	840	0- 5	95-100		
30	590		0- 15		
40	420		0- 5		
60	250				
70	210			95-100	
100	149			0- 15	
120	125			0- 5	
140	105				95-100
170	88				
200	74				0- 15
230	62				0- 5

Table (4.2) Distribution of Paritcles.

For the silica flour (smallest particle) the distribution is shown in Table (4.3).

The particles used were manufactured by the Flex-o-Lite Division, General Steel Industries, Inc. of St. Louis, Missouri. The silica flour was obtained from the Halliburton Corp., Duncan, Oklahoma.

Percent	Microns
8.2	over 50
8.6	40-50
15.3	30-40
16.9	20-30
34.5	10-20
12.2	5-10
14.3	0- 5

Table (4.3) Distribution of Particle Size in Silica Flour.

Flow Test Loop for the Flat Plate Experiment

The flow test loop for this experiment, as compared to the one for the circular pipe, is a more complicated one. The flow loop required a wind tunnel, a blower (which was the injection system), a drag measuring device, a flow regulation method, and a dust collector.

The particles, which were poured into the blower, entered the wind tunnel just after the inlet ramp. Air, with particles mixed with it, flowed over the flat plate which was placed flush with the floor of the tunnel. The flat plate was cantilevered on a rod which was used to measure the deflection and hence the drag. The air and the particles were then sucked through the large fan, which operates the wind tunnel,

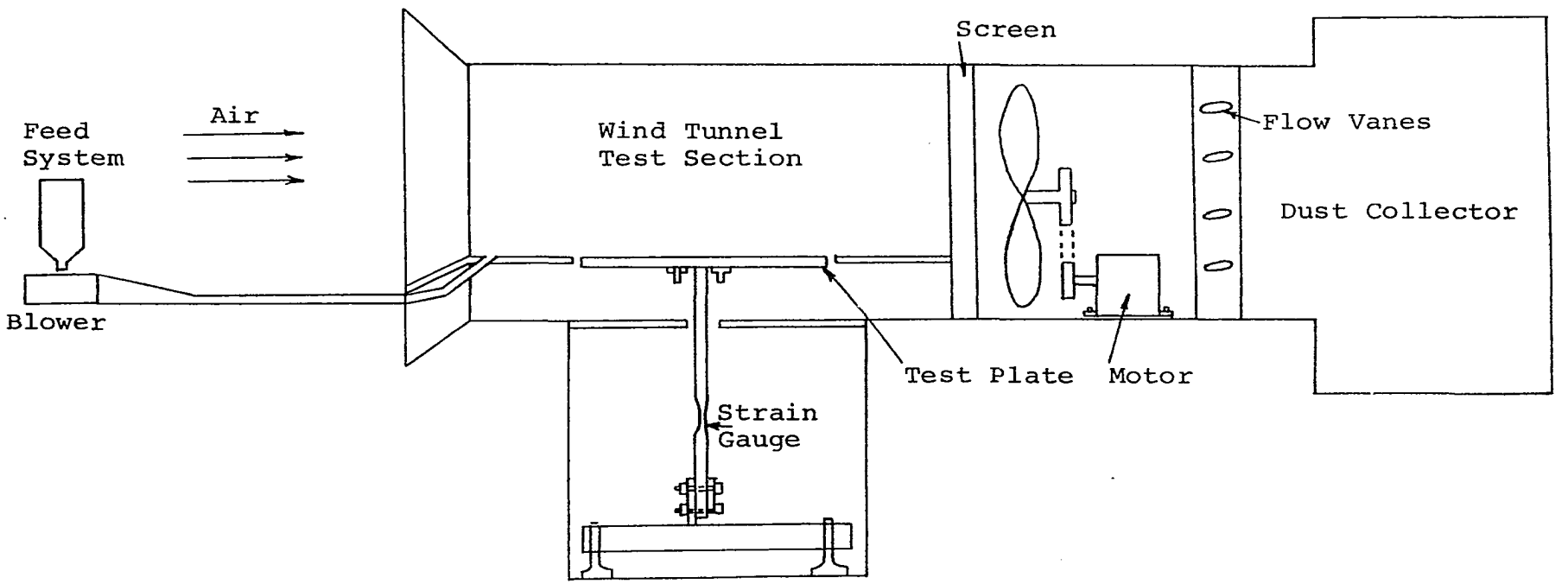

Figure (4.6) Schematic of Flat Plate Test Apparatus

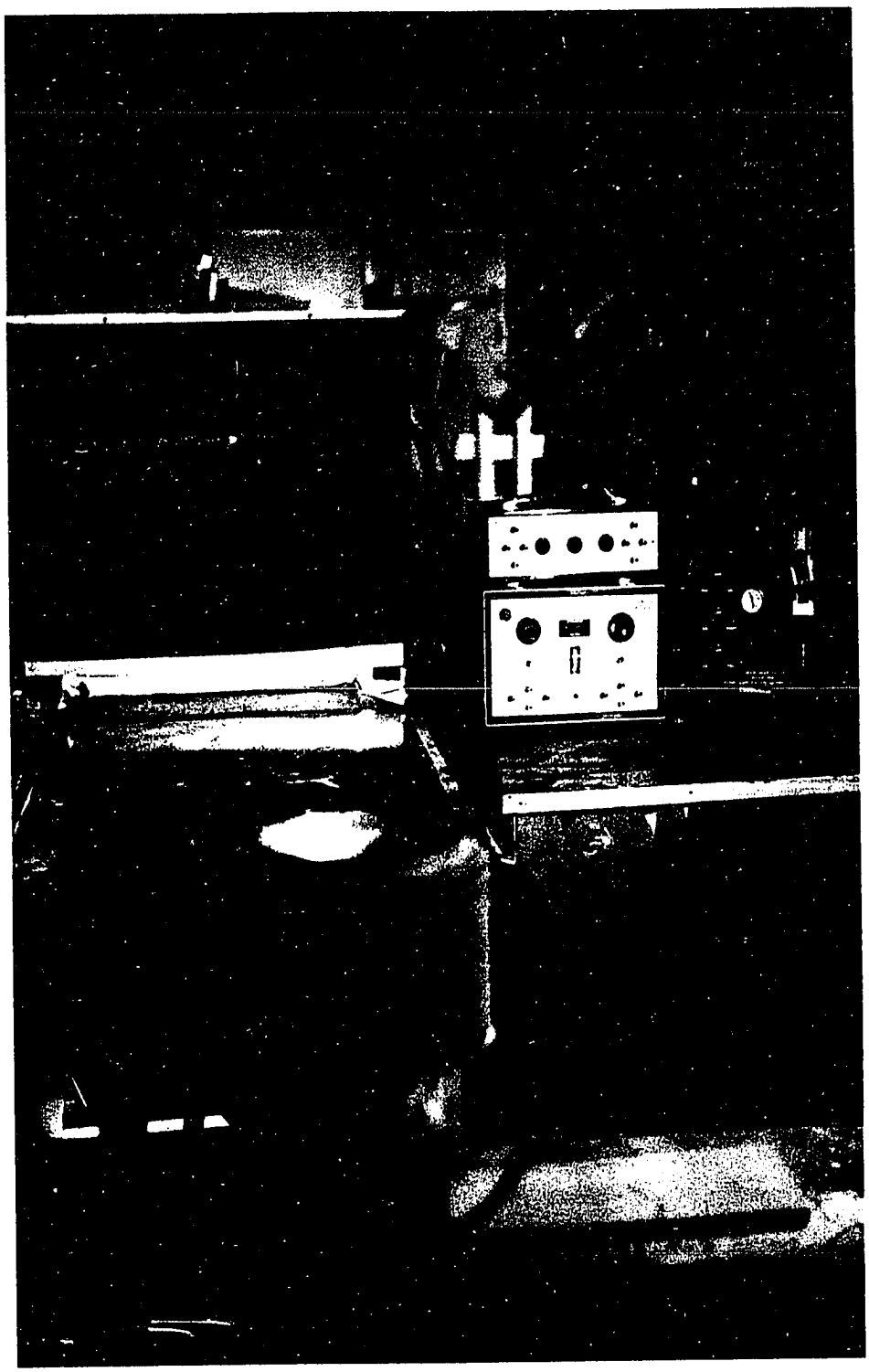

Figure (4.7) Flat Plate Test Setup.

through the flow regulating vanes, and finally into the dust collector. Figure (4.6) shows the schematic of the entire test setup for the flat plate and Figure (4.7) is a photograph of the same. Each component of the assembly is described in detail in the following paragraphs.

The particle injection system. This system consisted of three components: the feed system, the blower, and the transition duct leading to the wind tunnel. The feed system to the blower was the same as for the circular pipe section. The blower used was also of the same type but smaller in size. It was a RexVane Vent Set, Size R-18, Design 9, also manufactured by the B. F. Sturtevant Co., Boston, Massachusetts. The transition piece was made out of sheet metal and connected the blower to the floor of the wind tunnel. Figure (4.8) shows a sketch of the transition piece.

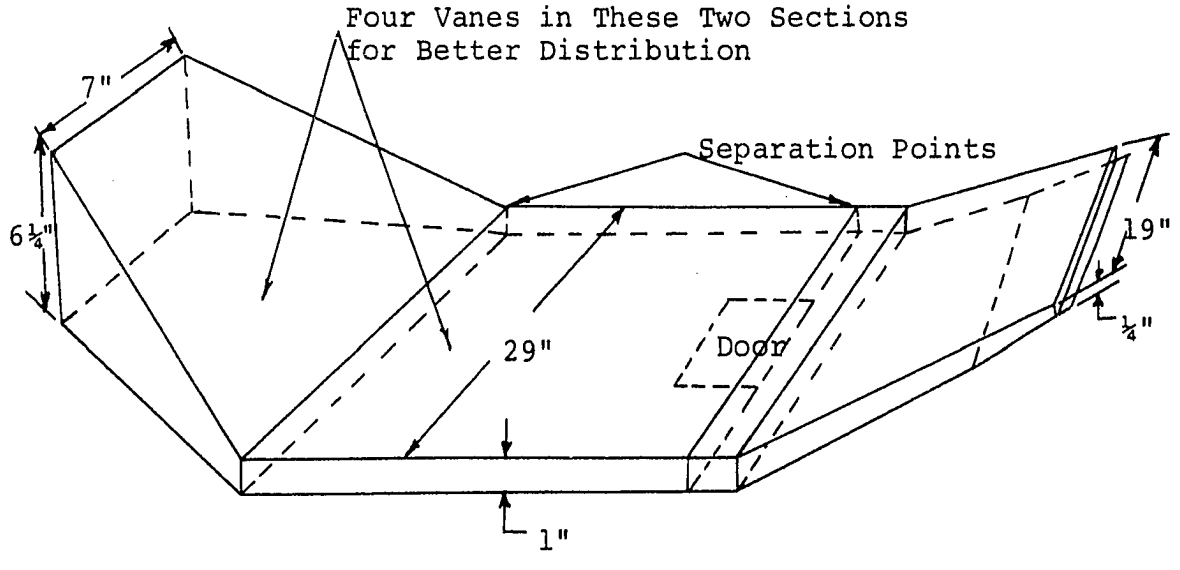

Figure (4.8) Transition Piece.

The particles leave the blower exit which is rectangular in shape and has dimensions 7 inches by 6-1/4 inches. The transition piece is designed so that it can be separated into three main sections with a minimum of effort. This was done in order to remove any accumulated particles that may have become trapped in it after each set of runs. A trap door, as shown in Figure (4.8), allows us to check for any accumulated particles in this piece. The transition piece goes under the inlet ramp of the wind tunnel and exits at the floor just behind it. The particles are discharged along the entire breadth of the floor at an angle of 20 degrees. The high speed air moving over the floor of the wind tunnel carries the particles over the flat plate which is about 15.5 inches behind the ramp of the tunnel. In this manner the majority of the particles remain in the layer of flow next to the floor. Another important consideration in the design of this piece was the complete diffusion of the particles across the entire breadth of the wind tunnel. This was achieved by placing vanes in the transition piece to guide the flow.

Wind tunnel. The tunnel used had been a U. S. Navy open-circuit display tunnel which had been modified by previous graduate students, Walters (39), Looney (40), and Smith (16). The overall dimensions of the tunnel were 33 inches wide by 5.5 feet high by 8.79 feet long. The test section measured 19.875 inches square by 42.5 inches long. One side of the tunnel had a glass window to permit observation and photo-

graphs during the tests while the other side had two square access doors. Figure (4.9) shows the original tunnel configuration before modifications were made for this experiment.

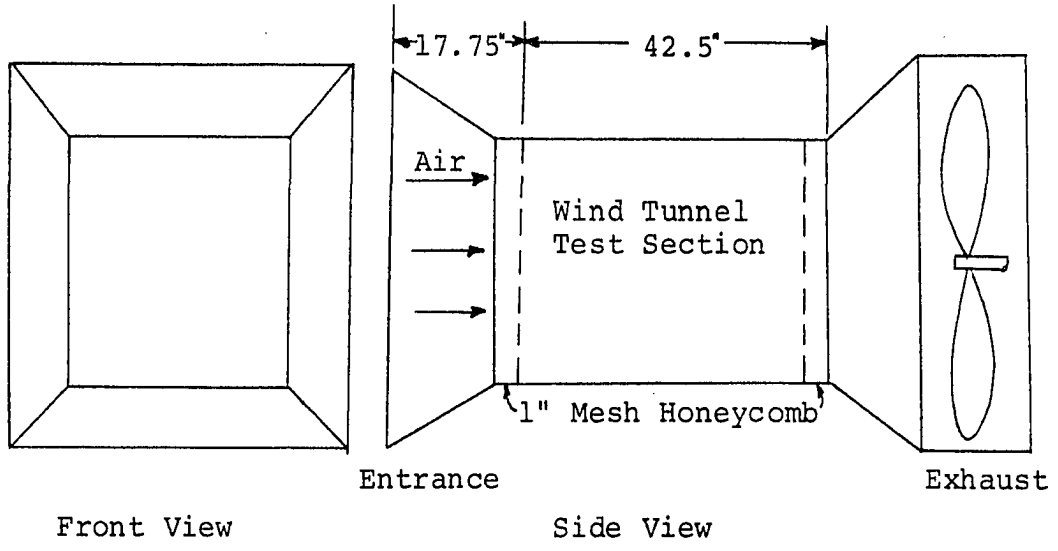

Figure (4.9) Original Wind Tunnel Configuration.

The tunnel was extensively modified for these tests. An extension to the tunnel was constructed to connect it to the dust collector and in the center of this extension a set of vanes was placed to regulate the flow rate and the air speed. The 1-1/2 horsepower, 220 volt, three-phase, constant speed motor was remounted to remove most of the vibrations. A 3.5 inch pulley on the motor was connected by a V belt to a 4.5 inch diameter pulley which ran the fan. Thus a tunnel which operated at a constant test section speed of about 38 feet per second was now able to operate between 70 feet per second and 20 feet per second. Figure (4.10) shows these modifications on the overall wind tunnel.

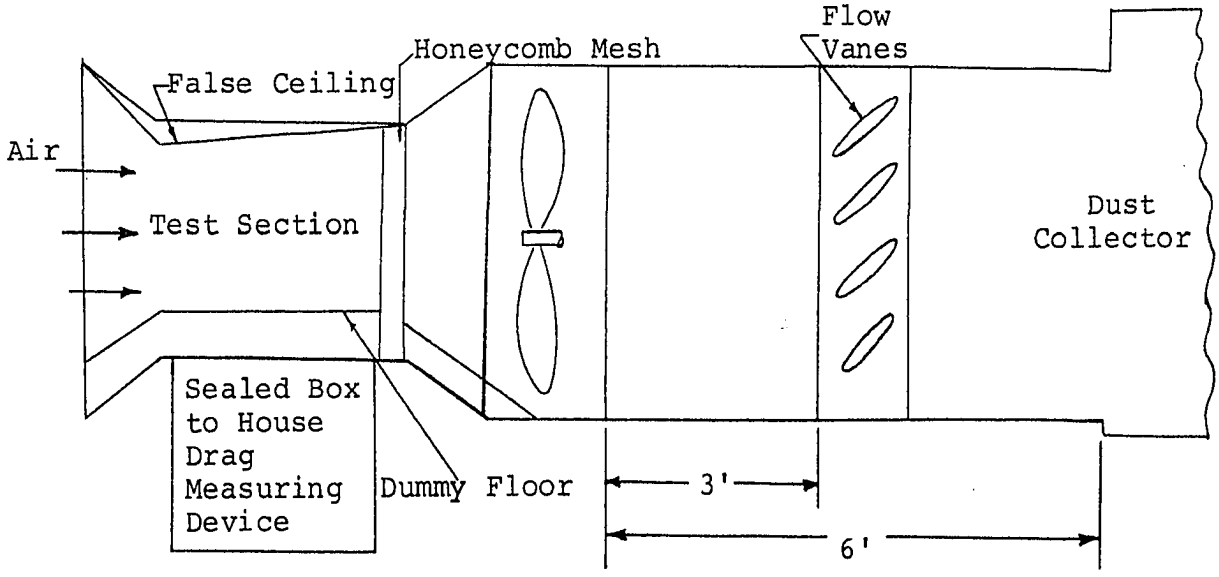

Figure (4.10) New Wind Tunnel Configuration.

A dummy floor was built and placed in the test section. This changed the dimensions of the test section to 13.12 inches high by 19.875 inches wide by 42.5 inches long. This floor was built by previous graduate students, Walters (39) and Looney (40), investigating the flow phenomena over a flat plate with a flexible skin. The floor, for this experiment was taken apart, sanded, and repainted flat black for photographic reasons. Figure (4.11) shows the dimensions of the dummy floor in two views.

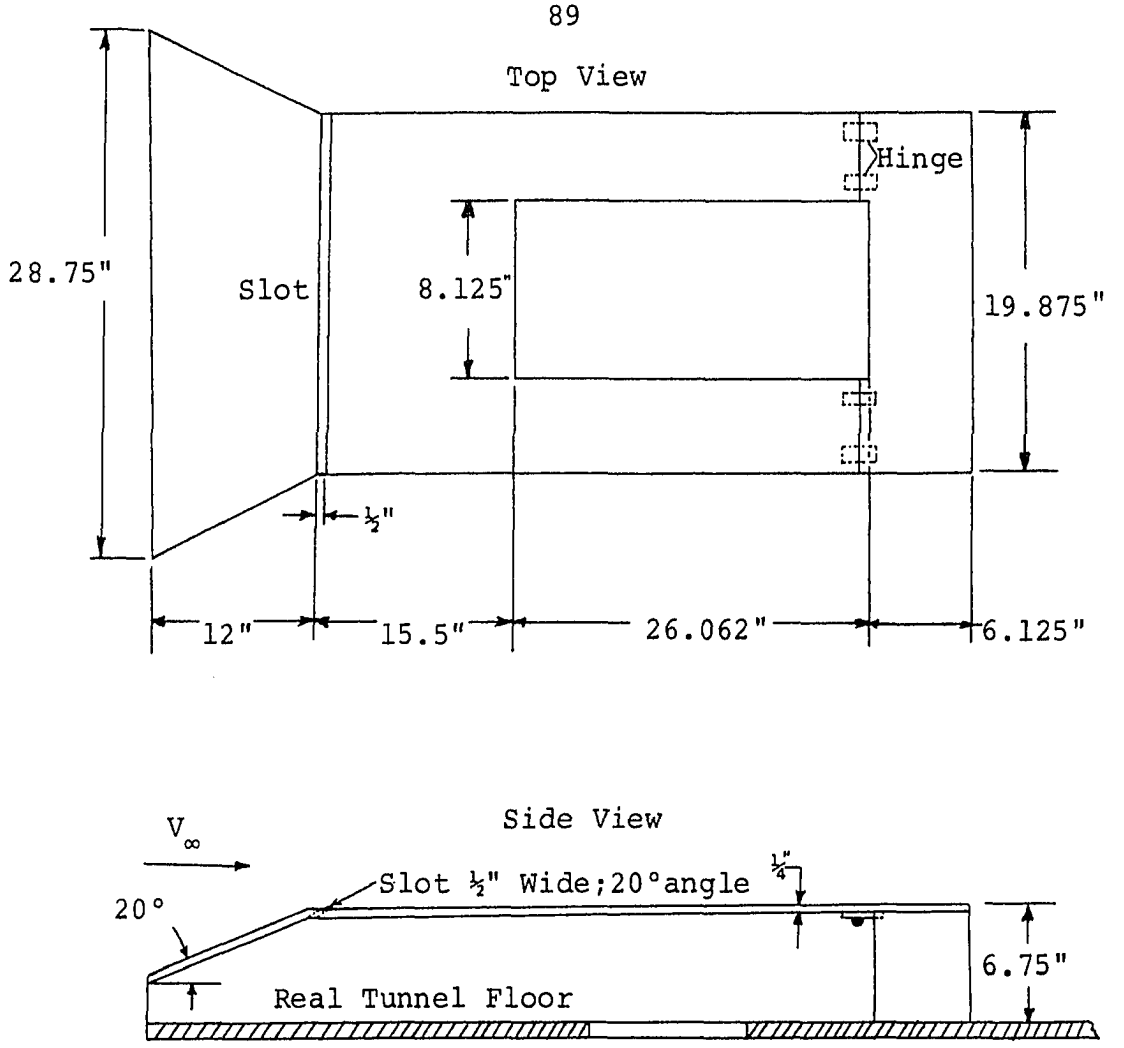

Figure (4.11) Dummy Floor.

Slight modifications were also made on the floor. The rear section of the floor, which previously had simply been placed in the wind tunnel, was now hinged to the front floor thereby preventing any vibration of the dummy floor. Another modification of the floor was a slot located just behind the inlet ramp through which the particles were injected.

A false ceiling was placed in the test section. This ceiling was made out of 1/4 inch plywood so that the flow area

could be modified. This was necessary because of a negative pressure gradient found to exist in the tunnel. It was determined that the negative pressure gradient was due to the boundary-layer thickness generation through the length of the test section. A constant effective flow area was maintained so that there would be a zero axial velocity gradient (du/dx = 0) and hence a zero pressure gradient (dp/dx = 0) throughout the entire length of the tunnel. Figure (4.12) shows a schematic of the false ceiling. The ceiling was said to be in the correct position when the pressure taps indicate the same reading. Since this was a very critical measurement, as will be shown in a later chapter, a micromanometer was used

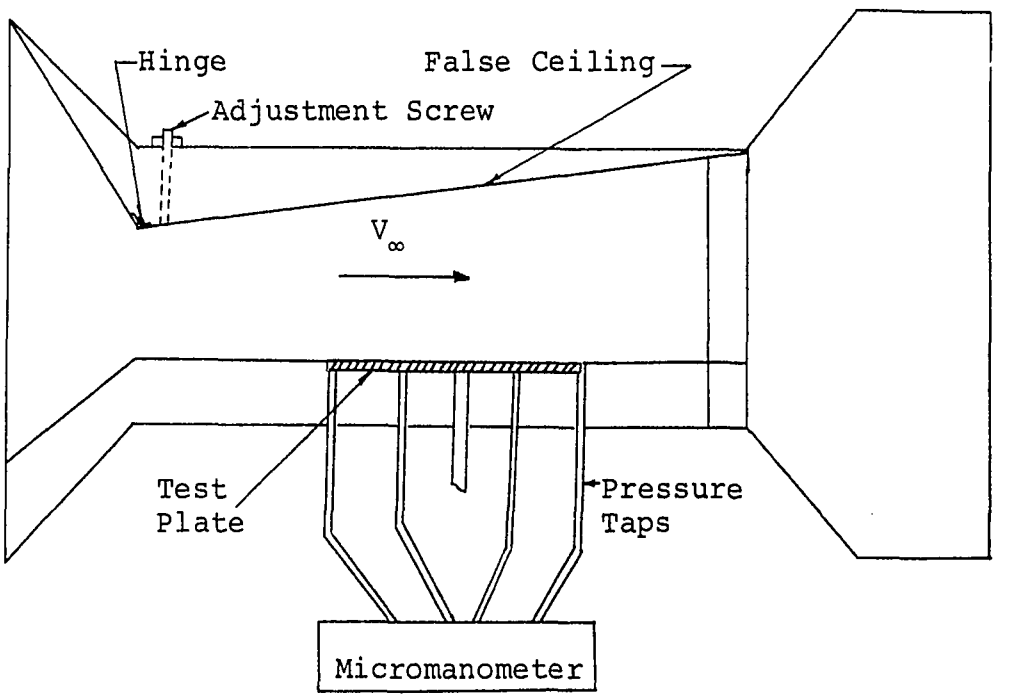

Figure (4.12) False Ceiling to Maintain Constant Effective Flow Area.

to measure the pressure to insure that the pressure gradient along the entire length of the plate was unchanged. Figure (4.13) shows the position of the pressure taps which were drilled along the test plate to monitor the pressure changes. These holes were connected with equal length plastic tubing to the micromanometer which was capable of detecting pressure changes down to 0.000006 psi.

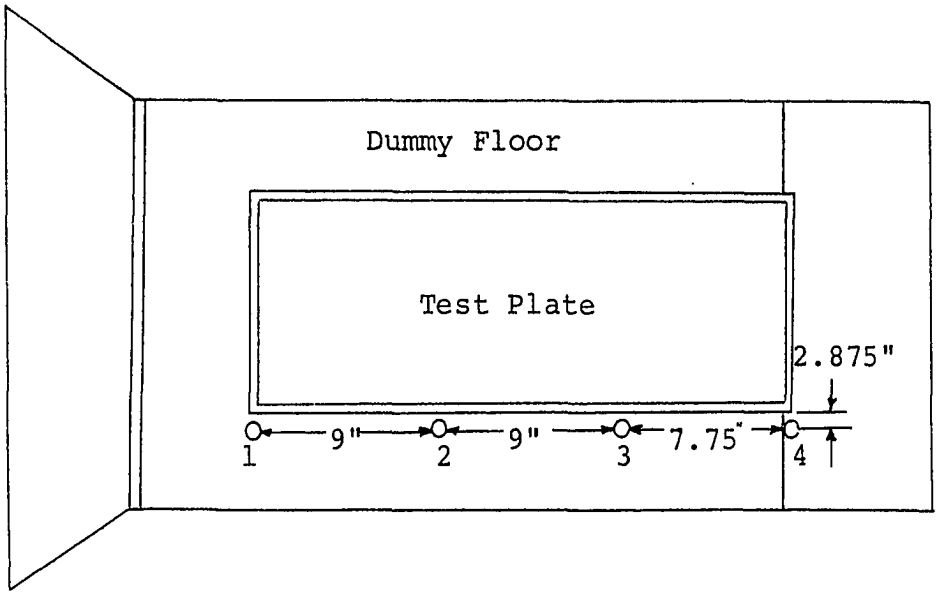

Figure (4.13) Pressure Taps.

Another problem which was encountered during tests of the previous graduate students was the secondary air jets coming up through the slots around the flat plate and mixing with the main stream in the region of the floor of the wind tunnel. To eliminate this effect Walters (39), Looney (40), and Smith (16) had previously enclosed the test plate and the plate support in a plastic bag sealed with zinc chromatic putty. This was not entirely sucessful and leaks sprang up very easily. To avoid this a metal box was designed as shown in Figure (4.14).

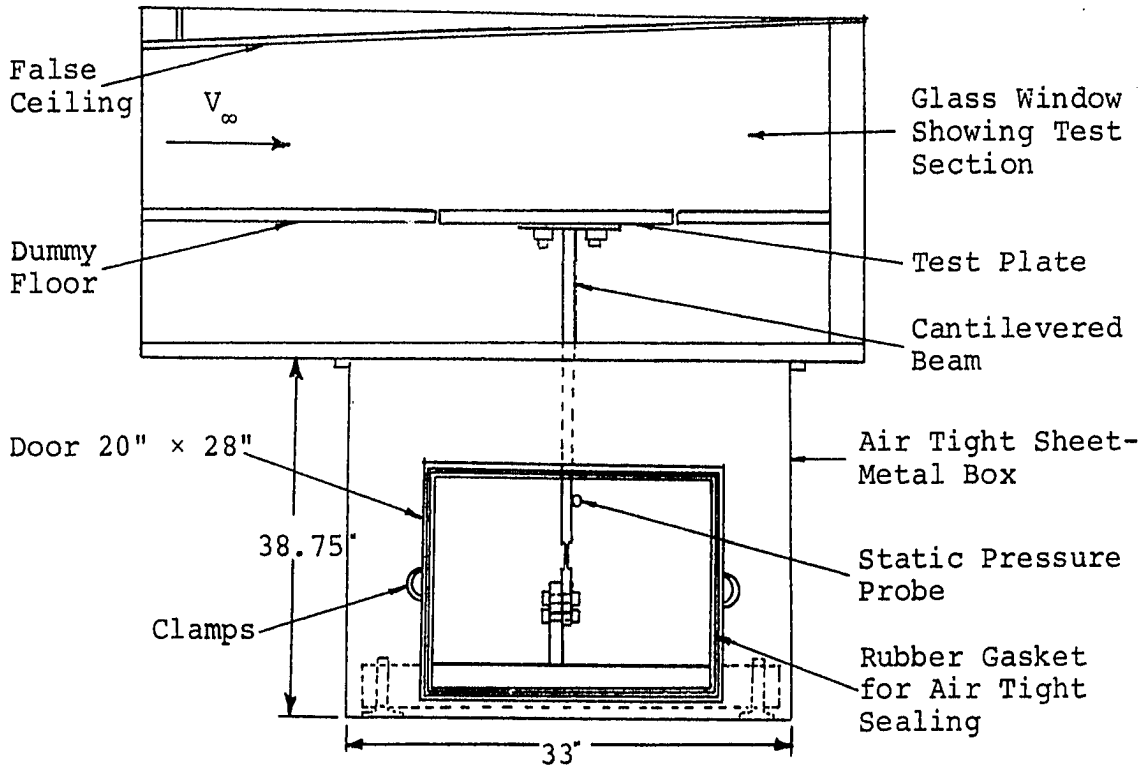

Figure (4.14) Enclosure and Support Mechanism for Flat Plate.

This box housed the entire support mechanism of the flat plate and had a door which made access to any part of the mechanism easy. Figure (4.15) is a photograph of the enclosure and the support mechanism for the flat plate. Easy access was necessary since minor adjustments to the plate had to be made throughout the entire initial phase of the test. The static pressure in the wind tunnel and the static pressure in the metal box were monitored on an inclined manometer which could be read

Figure (4.15) Enclosure and Support Mechanism for the Flat Plate.

accurately to 0.005 inches of water. In this manner it was simple to note any leaks. A smoke test was conducted to check for any existing leads. Sealant was used to insure that there was no leakage between the dummy floor and the side walls.

The entire flow area was sanded and all holes on the walls from previous work were sealed off with plastic wood. Also all old screws were removed and the holes redrilled to countersink the heads. In addition only flat-headed screws were used, and after they were countersunk, plastic wood was used to plug the holes. The entire section was then once again sanded and painted with a flat black paint to prevent glare during photography. Care was taken to check that no disturbance was in the flow stream since slight distrubances can effect the measurements drastically.

Drag measuring setup. For accurate measurements it was felt that a large plate with its large surface area would be most advantageous. The test plate consisted of an aluminum plate onto which was fastened a 1/8 inch hardwood plate with as much surface area as could be placed in the wind tunnel without end effects of the tunnel causing erroneous readings. The plate was 26-1/8 inches long and 8-1/8 inches wide.

A stand was built from which the flat plate was cantilevered so that it was isolated from the wind tunnel. The cantilever beam was chosen after consideration was given to column bulkling and deflection. The frictional force to

be measured was very small and thus the measuring setup had to accurately differentiate forces as low as 0.0006 pounds. After all three parameters had been taken into consideration, an aluminum beam with a cross section of 1 inch by 1/2 inch and a reduced cross section about 2 inches long near the clamped end was selected. The main support consisted of three large 4 inch angle irons welded together to form an "I". The cantilever beam was clamped to the cross member as shown in Figure (4.16) making the effective moment arm 33.75 inches long. The

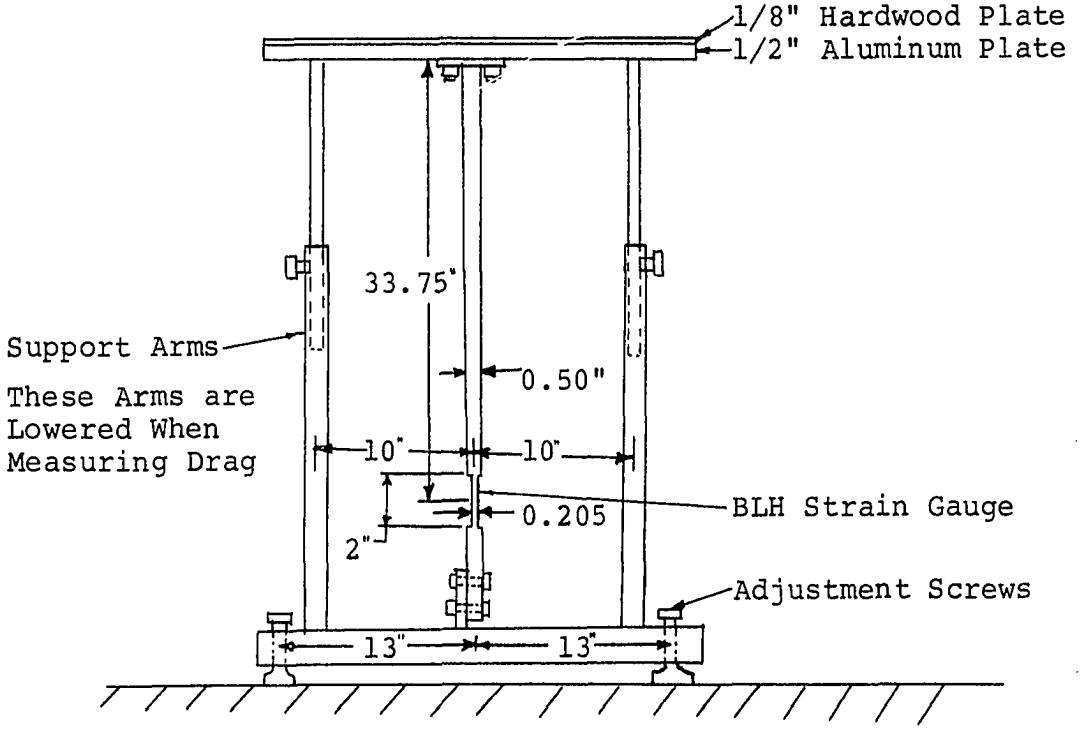

Figure (4.16) Schematic of Drag Measuring Setup.

support could be leveled by the four 1/2 inch by 6 inch bolts placed in each corner of the other two angle irons forming the legs of this support. Four supporting arms, as shown in Figure (4. 16), are used to support the plate when the metering setup is not in use, so as to remove the force from the cantilevered

beam. These supports were made from two sizes of pipe, one sliding into the other, the height of which could be adjusted by the set screws. The outer pipes were welded to other cross-members of the platform as shown in Figure (4.17).

The entire support with the flat plate was then lowered into the metal box previously described. The dummy floor was slid into place in the test section of the tunnel. After the floor was in position, the plate height and level were adjusted so as to insure that the floor of the wind tunnel was absolutely smooth.

Two highly sensitive BLH semi-conductor gauges, type SPB2-20-35 with a gauge factor of 119.7, were mounted on the reduced cross section near the clamped end. The semi-conductor gauges were mounted in a half bridge additive, temperature-compensating configuration. The high gauge factor necessitated adding a BLH strain converter, model 23. The strain indicator used was a BLH, model 120A with a digital type readout of strain in micro-inches. The technique used to measure the strain was to null the strain indicator under a no-load condition and record the read-out. The tunnel is then started and after the strain indicator needle is stabilized, the strain indicator is then nulled and the read-out recorded. The difference in these readings gives the strain in micro-inches. These readings are then converted to weight or force which in turn gives the skin-friction drag.

Flow regulator. The flow regulator is a set of metal vanes placed between the fan and the dust collector.

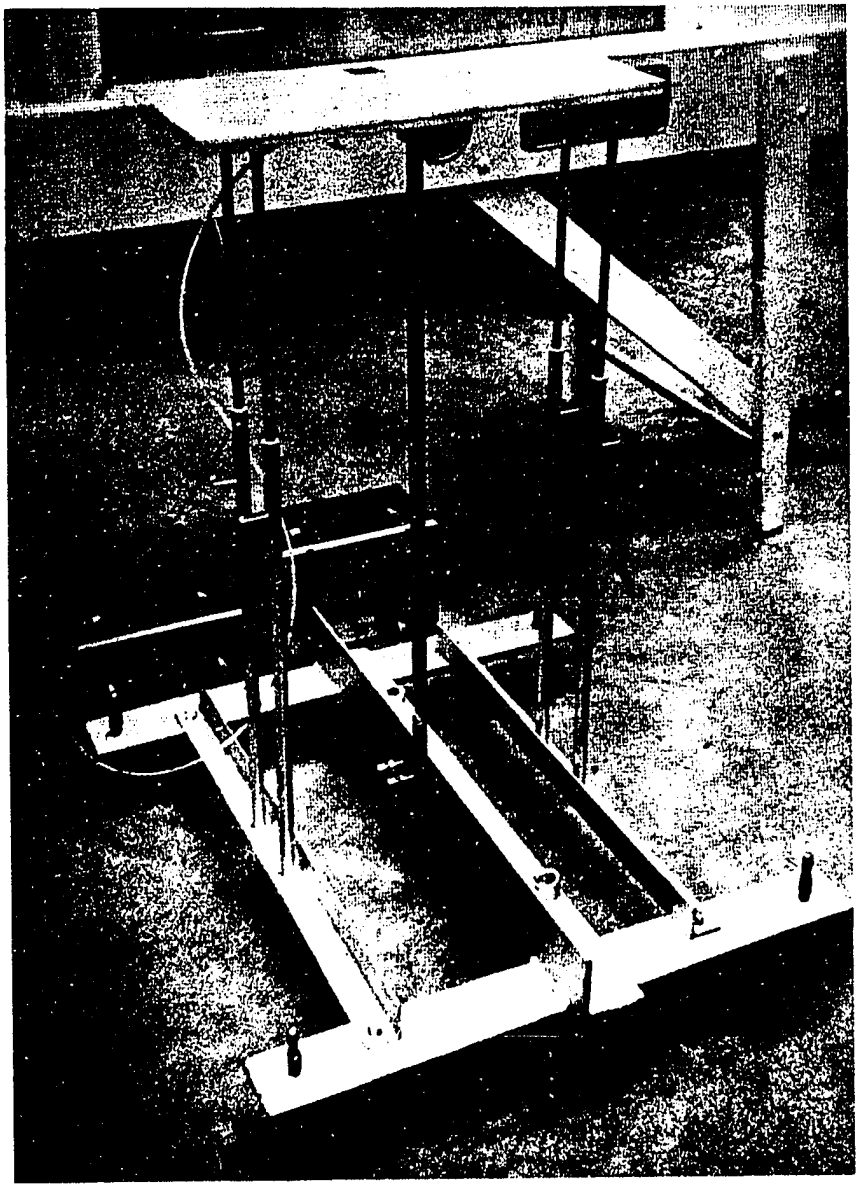

Figure (4.17) Drag Measuring Setup.

The flow is regulated by increasing the back pressure which the fan has to work against thereby reducing the weight flow through the tunnel and consequently the velocity. Since the blower is a constant speed motor and also since the horsepower rating is greater than necessary, the blower can maintain the same r.p.m. as the back pressure is increased.

Figure (4.18) shows a typical curve of a fan. From this curve it is obvious that, as the back pressure is increased at a constant aerodynamic speed, the weight flow is decreased.

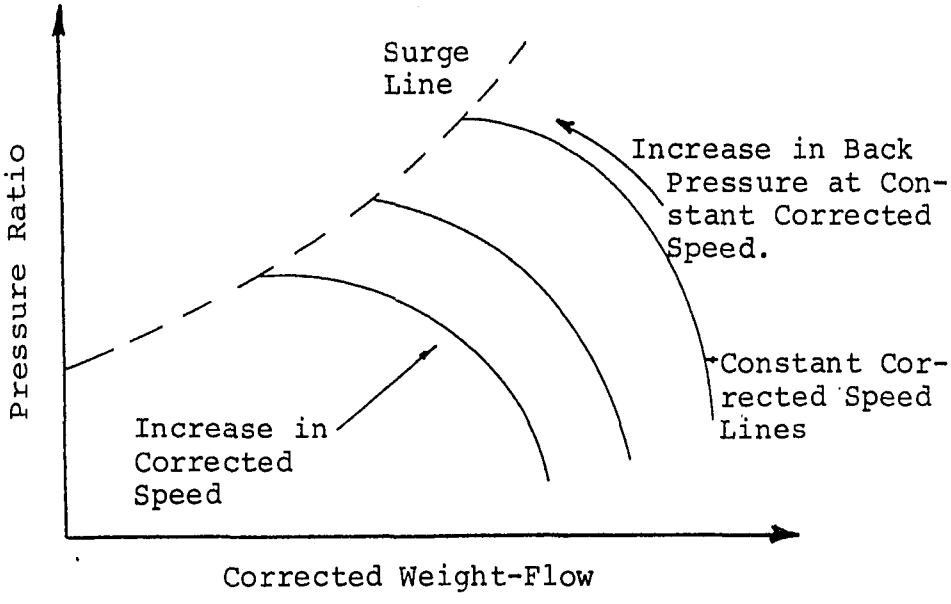

Figure (4.18) Typical Curve of a Fan.

The speed of the fan was checked before each run by the use of a stroboscope to insure no slipping of the fan.

Dust collector. The dust collector used was the same one used for the circular pipe experiment. In fact, both experiments were hooked into the dust collector at the same time.

CHAPTER V

CALIBRATION AND EXPERIMENTAL PROCEDURES

Since the proper operation of the equipment described in the preceding chapter is very important, this chapter will undertake to explain, in detail, all procedures followed by the author.

Circular Pipe Experiment

Calibration Procedures

The first step was to check out the instrumentation. It was decided that the best way to do this would be to run tests with clean air and calculate the velocity profile and skin-friction coefficient for the smooth pipe, and compare the results previously obtained by other researchers.

Velocity profile in a circular pipe. The first experiment was the investigation of the velocity profile in the test section. The purpose of this study was to make sure that the flow in the test section was turbulent. A pitot-static tube was used to calculate the velocity profile in the circular pipe.

The velocity profiles, as measured in the circular pipe, are shown in Figure (5.1). The profiles shown vary from an average velocity of 46.5 feet per second and a Reynolds number of 6.3×10^4, to an average velocity of 7.0 feet per second and a Reynolds number of 0.945×10^4. Figure (5.2) shows that the velocity profiles vary from close to the turbulent profile obtained by Nikuradse (41) to the laminar flow profile obtained by Szymanski (42). Although with this setup it was not possible to reduce the velocity so as to be in the laminar flow region, Figure (5.2) shows that as this region is approached the profiles change in the right direction. This good agreement with previously measured data was very encouraging and the experimental setup passed its first test.

Skin-friction coefficient in a circular pipe. The main purpose of this entire report is to establish the effect of particles suspended in air on the skin-friction coefficient of bodies. Thus before one can determine this effect, one must first verify whether the equipment can accurately obtain data with clean air which agrees with data previously obtained.

The skin-friction drag was obtained by measuring the pressure drop at the test section. The test section, 42 inches long, has been described in the preceding chapter. To calculate the skin-friction coefficient the equation proposed by Darcy, Weisback, and others was used in the form:

$$f = \frac{\Delta P}{\frac{1}{2}\rho V^2} \frac{d}{L} \qquad (5.1)$$

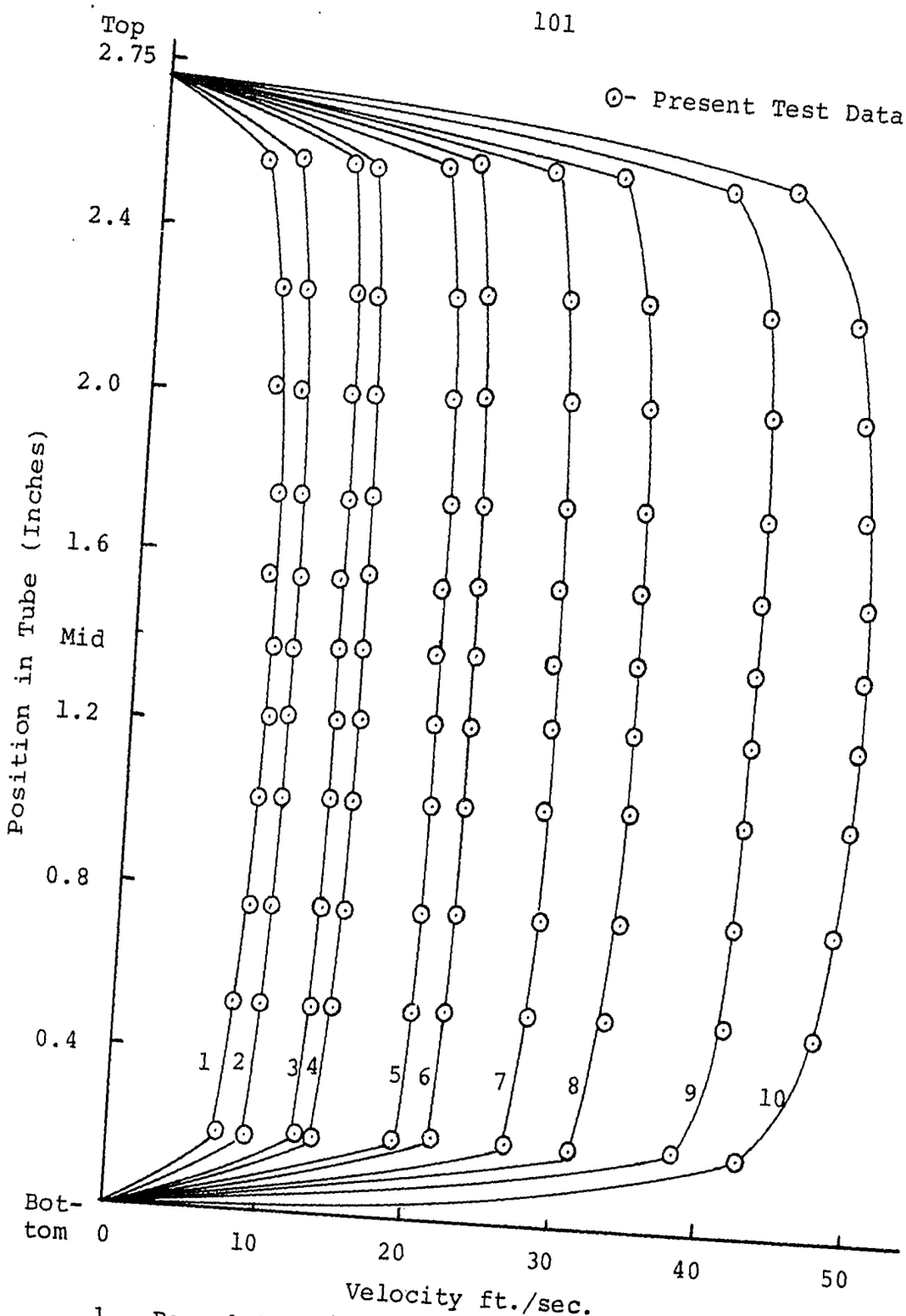

1. Re = 0.945 × 10^4
2. Re = 1.2 × 10^4
3. Re = 1.75 × 10^4
4. Re = 1.82 × 10^4
5. Re = 2.43 × 10^4
6. Re = 2.82 × 10^4
7. Re = 3.5 × 10^4
8. Re = 4.04 × 10^4
9. Re = 5.4 × 10^4
10. Re = 6.3 × 10^4

Figure (5.1) Velocity Profile in Smooth Circular Pipe for Various Reynolds Numbers.

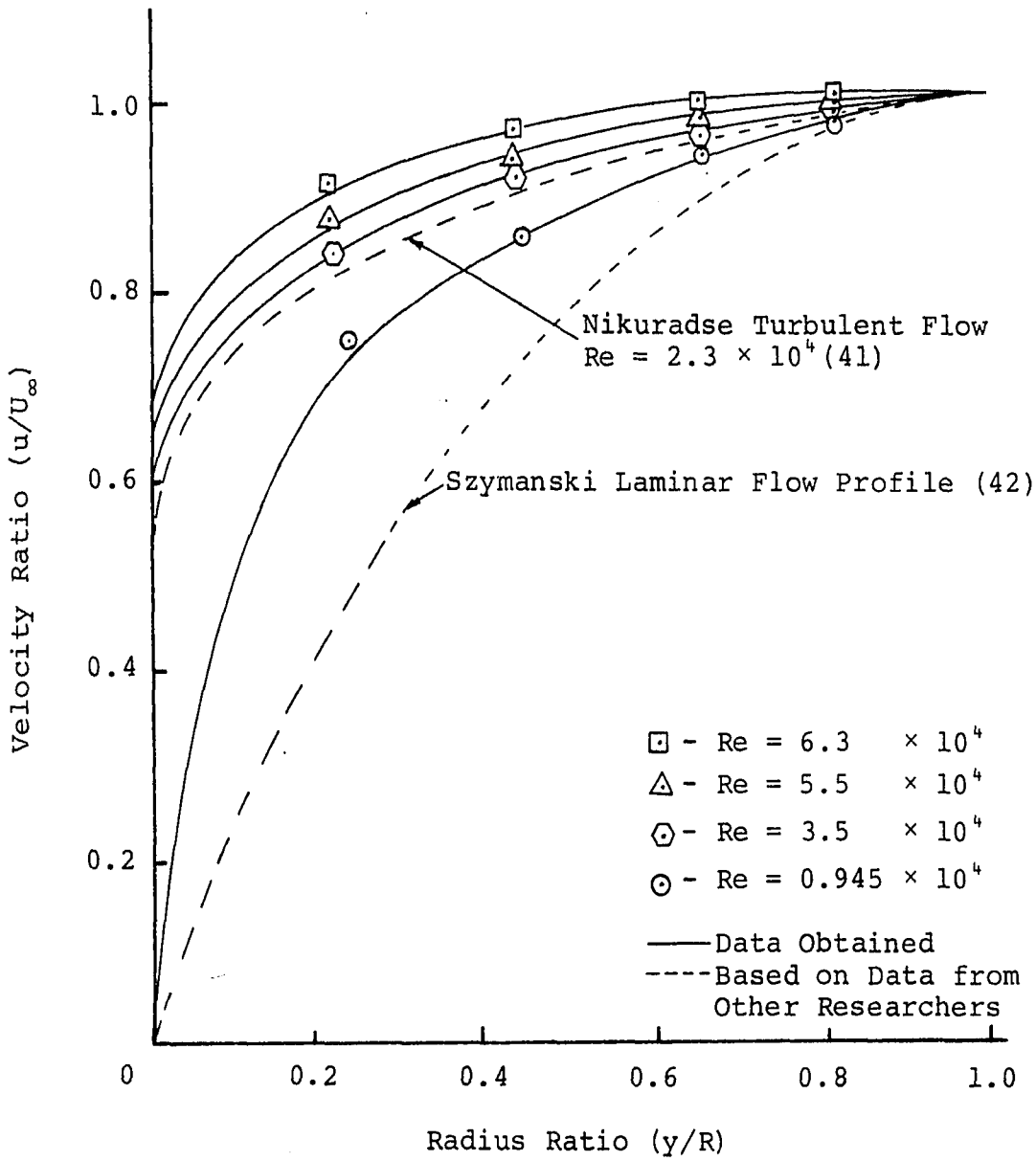

Figure (5.2) Velocity Distribution in Smooth Pipes for Varying Reynolds Number.

The above equation does not take into accout compressibility effects as shown in the following equation (43):

$$(M_1/M_2)^2 = 1 - \gamma M_1^2 [2 \ln \frac{M_2}{M_1} + f \frac{L}{d}] \qquad (5.2)$$

or as may also be written,

$$P_1^2 - P_2^2 = \frac{m^2 RT}{A^2} [2 \ln \frac{V_2}{V_1} + f \frac{L}{d}] \qquad (5.3)$$

where M is the Mach number, m is the mass flow rate, R is the gas constant, T is the temperature, A is the flow area, and V is the velocity. The flow in the pipe is considered to be isothermal. Equation (5.3) reduces to Equation (5.1) if one was to assume that the pressure drop is very small and the velocities at the two measuring stations are the same. The difference in the calculation of the friction factor by Equation (5.1) and by Equation (5.3) was negligible even at the highest velocity at which the test was run. Hence Equation (5.1) was used to calculate friction factors and it was determined that the error involved in neglecting the potential energy between the two pressure-measuring stations amounts to approximately one half of one percent. Figure (5.3) shows the excellent correlation between the test data obtained and the empirical curve established by Blasius. Blasius obtained this curve by making a critical survey of the numerous test data available to him in 1911. He arranged this data in a dimensionless form according to Reynolds similarity rules and obtained the following empirical equation:

$$f = \frac{0.3164}{(Re)^{\frac{1}{4}}} \qquad (5.4)$$

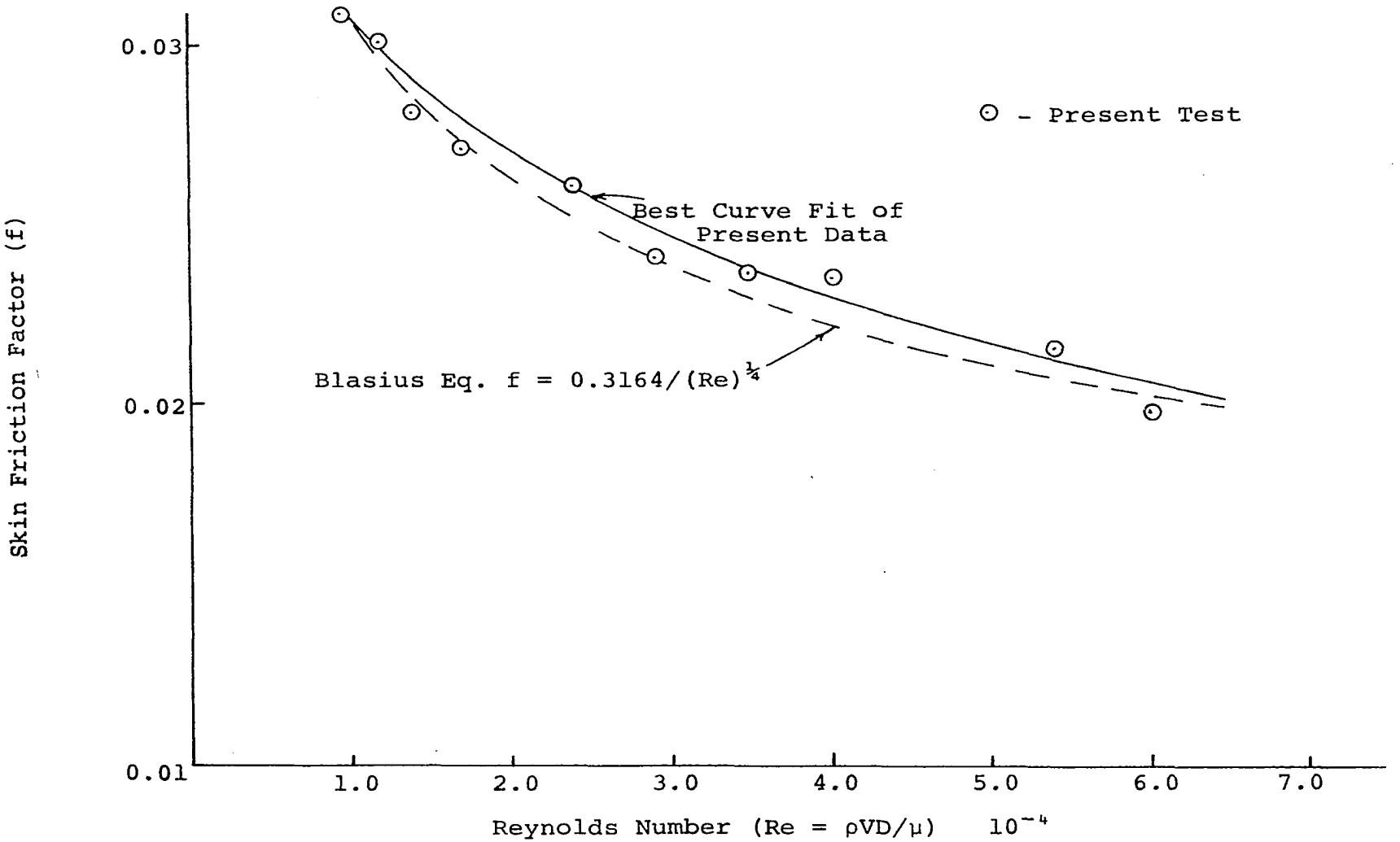

Figure (5.3) Comparison Between Blasius Turbulent Flow Eq. (5.4) and Test Data.

The above equation is known as the Blasius formula and is valid for the frictional resistance of smooth pipes. The Blasius equation has been found to be valid for a range of Reynolds numbers less than 100,000. Therefore it was adequate for the range of Reynolds numbers at which the tests were conducted. The good agreement found between the test results and Equation (5.4) was another indication of the accuracy of the setup.

Velocity calibration. A pitot-static tube was used to measure the velocity at the different stations in the pipe. The static pressure was kept constant and recorded for each traverse. The pitot-static tube used was manufactured by the Dwyer Company, Michigan City, Indiana. Figure (5.4) shows the pertinent dimensions of the pitot tube.

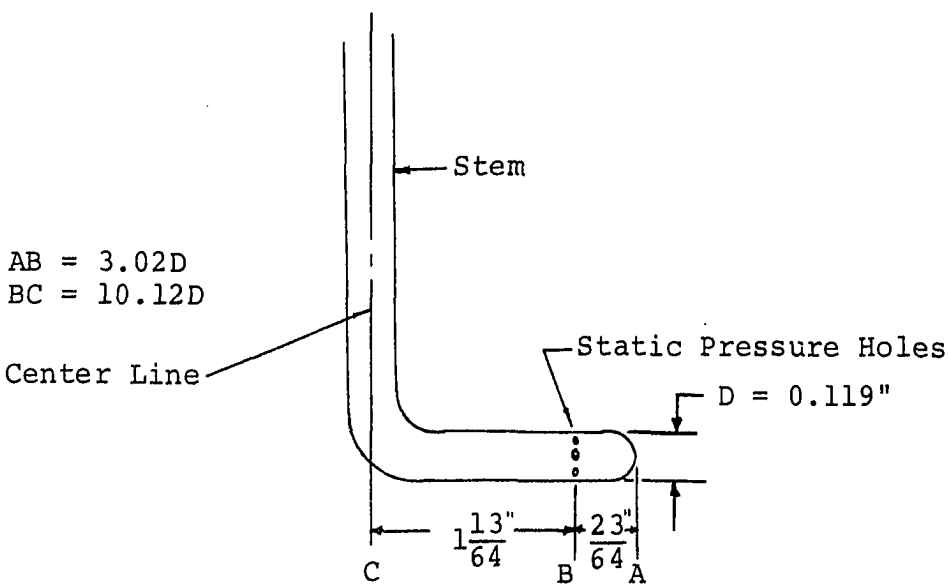

Figure (5.4) Pitot Tube Dimensions.

To compare the true head to the actual measured head the method outlined by Pope (44) was used. From the graphs in Pope's book the difference between the indicated and true dynamic pressure was 0.15 percent. Therefore the difference between the true velocity and the indicated velocity was also 0.15 percent. Since the correction factor is nearly equal to unity the true velocity was set equal to the indicated velocity.

The pitot tube was connected to an inclined manometer which could be read accurately to 0.005 inches of water. To calculate the velocity the following relationships were used:

$$P_t = P_s + \tfrac{1}{2}\rho V^2 \qquad (5.5)$$

$$P_t - P_s = \Delta P = \tfrac{1}{2}\rho V^2$$

$$V = \sqrt{\frac{2\Delta P}{\rho}} \qquad (5.6)$$

where $$\Delta P = \frac{62.4 \times \Delta h}{12}$$

and $$\rho = \left[\frac{P_1}{P_o}\right] \left[\frac{T_o}{T_1}\right] \rho_o$$

The standard pressure of 29.9 inches of mercury and the standard temperature of 519° R were used. Therefore by modifying Equation (5.6) one obtains,

$$V = 15.86 \sqrt{(\Delta h)(T_1)/(P_1)} \qquad (5.7)$$

where Δh is the dynamic head in inches of water.

The velocity as calculated from Equation (5.7) was plotted against the static pressure as shown in Figure (5.5).

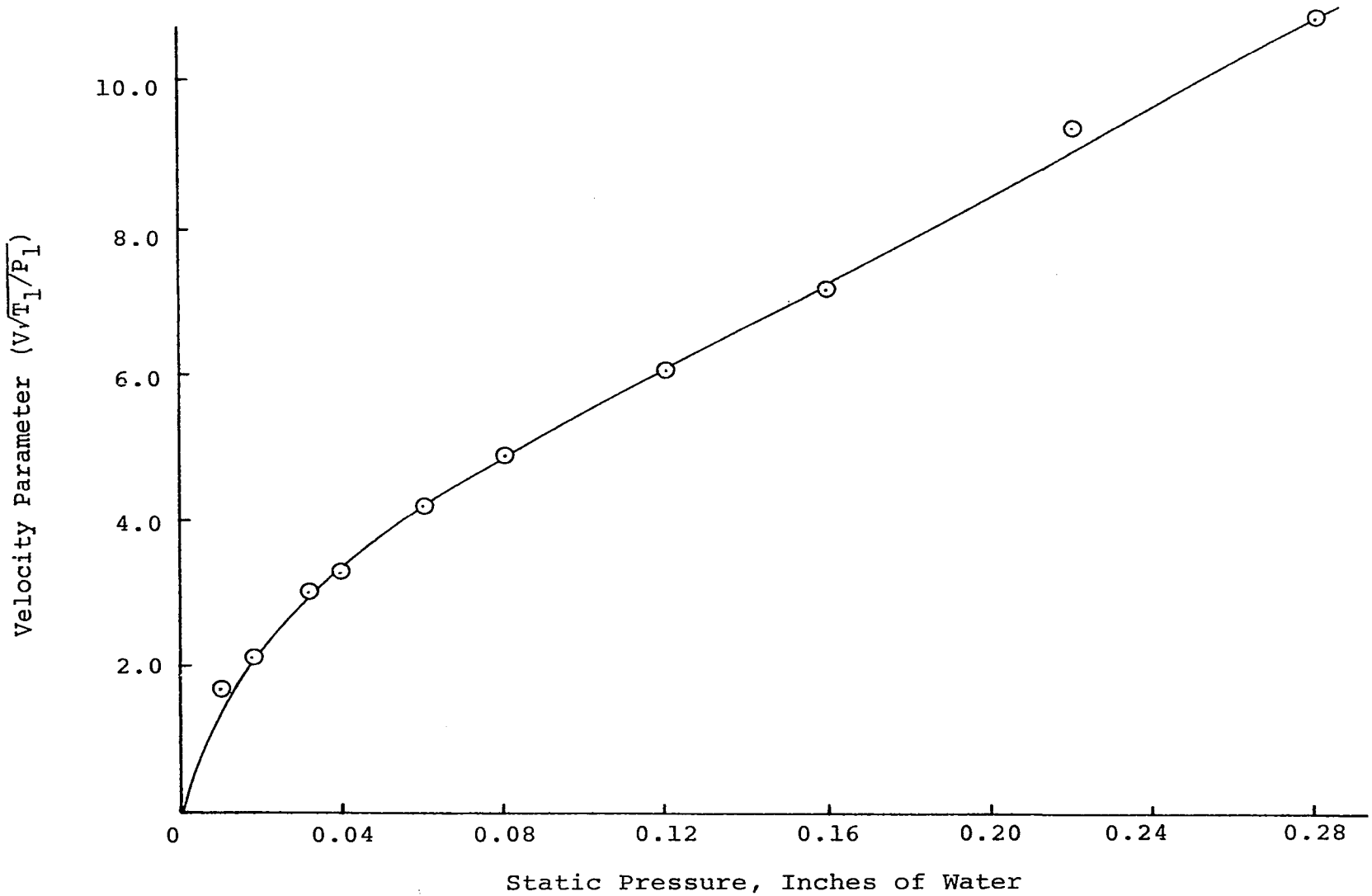

Figure (5.5) Velocity Correlated to Static Pressure for Circular Pipe Flow.

In this manner the velocity could be set without introducing the pitot-static probe.

Experimental Procedure

The pipe experiment was now ready to proceed. The first step in the experimental procedure was to observe the barometric pressure and the room temperature. The blower was then started and the flow valve was set at the position which would give the required velocity. This was done with the aid of Figure (5.5), which gave the static pressure setting at the test section. The pressure drop for the clean air was then recorded and compared to the results shown in Figure (5.3). Once this parameter was checked out the next step of the testing could proceed. The particles, which were previously weighed, were injected into the flow stream through the feeder system and the time of injection measured. In this manner the flow rate of the particles was determined. The injection time varied from 5 to 15 seconds depending on the flow rate of the particles. The static pressure drop across the test section of the circular pipe was noted. After each test run the pipe was cleaned by inserting a stick with a swab at one end. In this way the surface of the pipe was restored to the original smooth surface. The swabbing was an absolute necessity after the injection of the silica flour since the silica flour coated the inside surface of the pipe. The other particles did not coat the pipe but the process of swabbing was repeated

to insure that the surface was the same at the beginning of each test run.

Flat Plate Experiment

Calibration Prodedure

The calibration of the experiment was much more complicated and very sensitive as compared to the circular pipe experiment. The first step was the calibration of the drag measuring device. Next was the adjustment of the wind tunnel passage so as not to add a moment force to the flat plate. The accuracy of the entire system was once again checked by comparing the test results of the flat plate in clean air to the results previously obtained by other researchers.

Drag measuring device. The calibration of the system was accomplished by placing weights of 0.01, 0.02, 0.05, 0.10, and 0.20 pounds on the aft end of the plate. The moment caused by the weight can be related to the tangential force and thus the weight index is directly proportional to the skin-friction coefficient, which is given as:

$$C_f = \frac{F}{\frac{1}{2}\rho V_\infty^2 A} \qquad (5.8)$$

where the skin-friction force (F) is the tangential force. The moment caused by the weight put at the aft end of the plate, taken about point 0, as shown in Figure (5.6), is given by the

following:

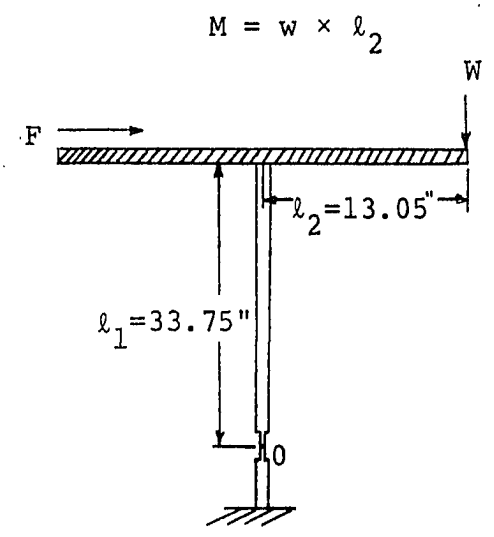

Figure (5.6) Schematic of Drag Measuring Device.

The skin-friction force which would give the same moment is given by:

$$F = \frac{M}{\ell_1}$$

Thus Equation (5.8) can be modified and rewritten as,

$$\rho V^2 C_f = \frac{2w\ell_2}{\ell_1 A} \qquad (5.9)$$

By means of Equation (5.9) a curve was plotted with apparent strain versus the skin-friction coefficient as shown in Figure (5.7). The value for the apparent strain is obtained by noting the deflection of the strain indicator for various weights placed at the aft end of the flat plate.

Adjustment of wind tunnel passage. The preliminary test runs indicated that there was a serious error in our set-up. The skin-friction coefficient was increasing with velocity instead ~~of~~ decreasing. It was postulated that this was

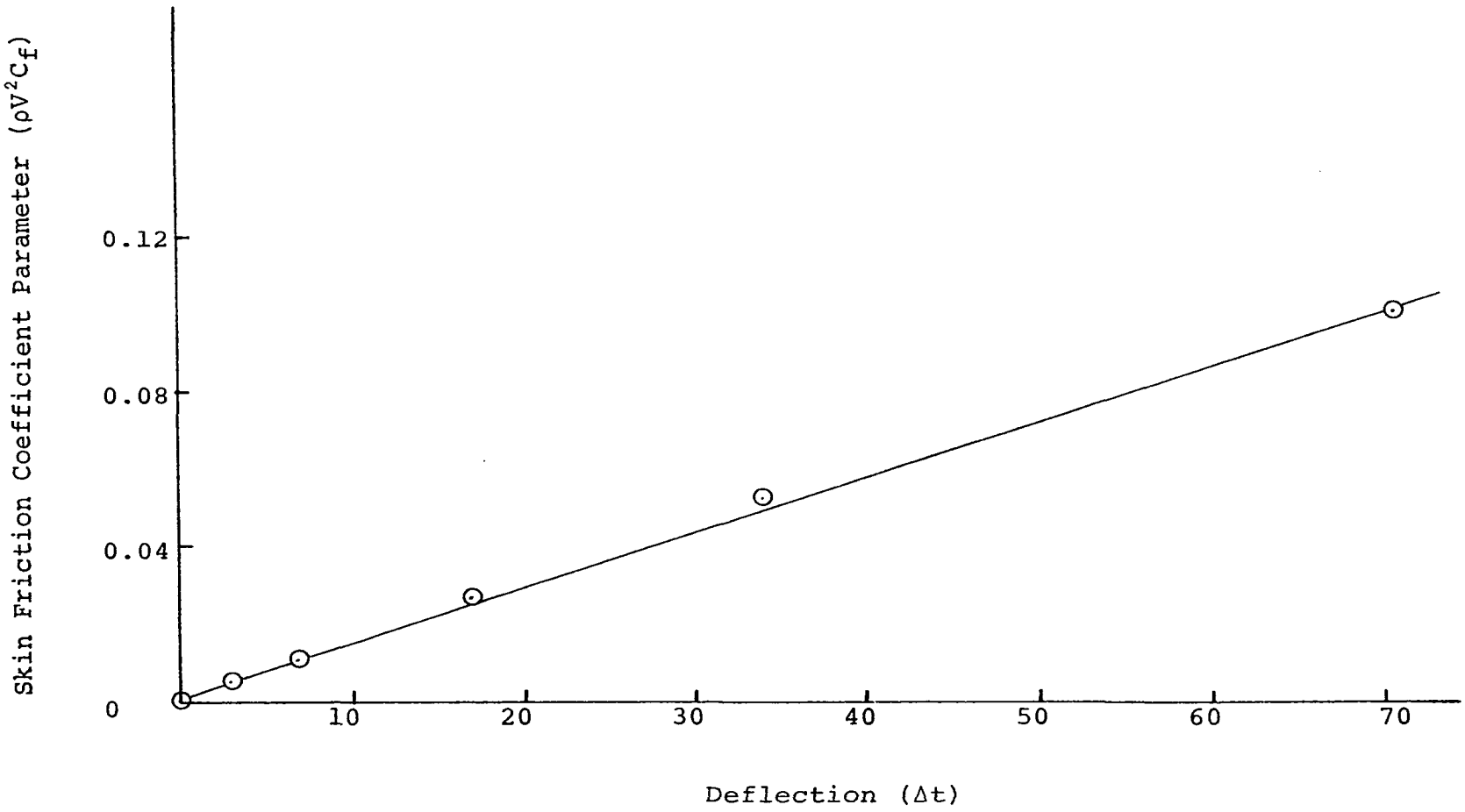

Figure (5.7) Skin Friction Coefficient Parameter as Indicated on the Strain Indicator.

due to an extraneous torque on the test plate introduced by the pressure gradient in the tunnel.

Previous work by Walters (39) on this same wind tunnel found, by the use of a hot-wire anemometer, that the turbulent boundary-layer displacement increased in depth 0.1095 inches from the front of the plate to the rear. Figure (5.8) shows the development of the boundary layer in the wind tunnel.

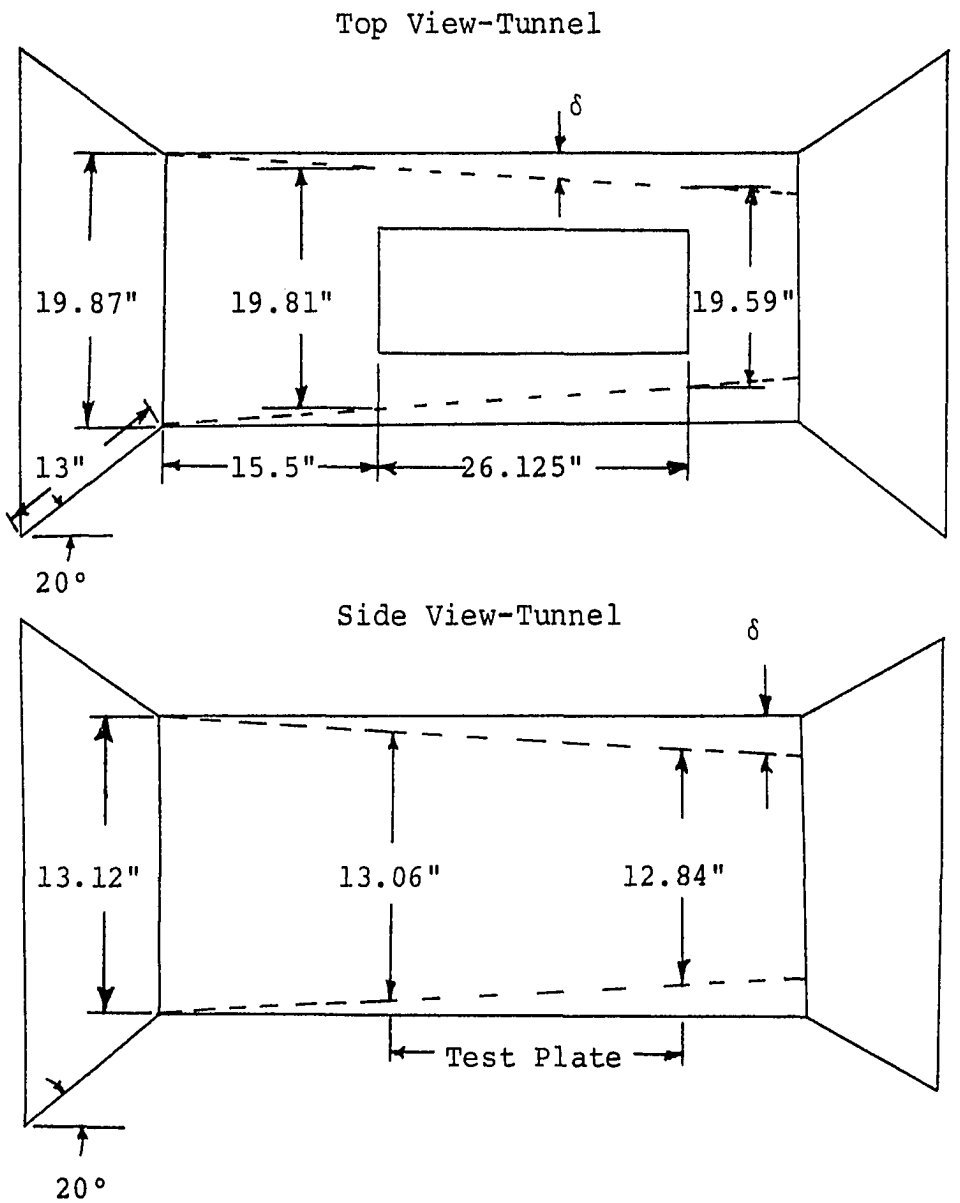

Figure (5.8) Boundary Layer in Tunnel.

This increase in the boundary layer decreases the effective area thus increasing the velocity and reducing the pressure. The pressure distribution on top of the test plate due to the boundary layer is shown in Figure (5.9). Owing to this pres-

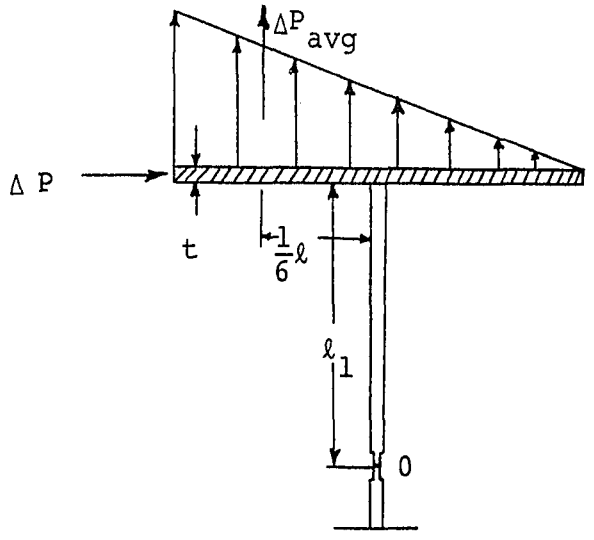

Figure (5.9) Plate Pressure Distribution.

sure gradient there are two forces which create a torque, the skin-friction force acting parallel to the plate and the pressure force acting perpendicular to the plate.

The change in area causes a change in velocity and consequently a change in pressure. The continuity equation for steady flow is:

$$\rho AV = \text{const.} \qquad (5.10)$$

By taking the logarithmic derivative of Equation (5.10) for constant density the following equation is obtained:

$$\frac{dA}{A} + \frac{dV}{V} = 0 \qquad (5.11)$$

Rearrangement gives,

$$dV = \frac{-VdA}{A} \tag{5.12}$$

The change in pressure can be given by the Euler equation:

$$dP = -\rho V dV \tag{5.13a}$$

Therefore,

$$dP = \rho V^2 \frac{dA}{A} \tag{5.13b}$$

From the above relationships it is obvious that owing to the decreasing area the pressure also decreases as indicated in Figure (5.9). To calculate the horizontal force the pressure is taken as acting on the end working area of the plate of width w_d and thickness t (see Figure (5.9)). Hence,

$$F_t = (\Delta P)(w_d)(t) \tag{5.14}$$

and the corresponding torque about 0 is:

$$T_{r1} = P_t \ell_1 = (\Delta P)(w_d)(t)(\ell_1) \tag{5.15}$$

This torque acts in the clockwise direction. The vertical force produces an even greater torque. Assuming that the pressure distribution on the top of the flat plate is linear, the average pressure is determined as,

$$\Delta P_{avg} = \tfrac{1}{2}\Delta P$$

and acts at a point 1/3 ℓ from the front edge of the plate. Thus the force acting perpendicular to the plate is given by,

$$F_p = \Delta P_{avg}(w_d)(\ell) \tag{5.16}$$

and the torque also acting in the clockwise direction is,

$$T_{rp} = (1/6)(F_p)(\ell) = (1/12)(\Delta P)(w_d)(\ell) \tag{5.17}$$

Thus the total torque acting on the flat plate due to the pressure gradient is the addition of the two torques. These torques act in the same direction as the skin-friction torque. Since the torques due to the pressure gradient vary directly as the velocity, the problem first encountered is the aparent increase in skin-friction coefficient as the velocity increases. Since this pressure torque can be 150 percent higher than the skin-friction coefficient, it predominates and should be eliminated.

To remove this large error it was decided to have a variable ramp roof as shown in Figure (4.11). This ceiling was made of a 1/4 inch plywood and could be easily molded at various places to give a zero pressure gradient across the plate. The four holes drilled along the plate were closely monitored by a micromanometer to see that there was no pressure gradient. The micromanometer has a capability of measuring air pressure changes with a 0.000006 psi. accuracy.

Secondary air and velocity profiles. Another problem encountered in the wind tunnel passage is the flow of secondary air jets coming through the slots around the plate and mixing with the main stream of flow in the region near the flow of the wind tunnel. To eliminate this problem the area below the test plate was enclosed in an air tight sheet-metal box. This box was specially constructed for this purpose and static pressure probes in the box and the wind tunnel passage were closely monitored to insure that no flow was being sucked into the wind tunnel.

Walters (39) and Looney (40), in their investigation of the flow in the same wind tunnel, found that owing to the flow through the gaps between the dummy floor and the test plate adverse curvatures were present in the velocity profiles near the plate. To remedy this problem they used a thick plastic bag to seal off the underside of the tunnel, thus stopping the flow of air. With the installation of the plastic bag the adverse curvature of the velocity profile was practically negligible.

Therefore, in this case, a more permanent fixture was installed from the beginning so that no such problem would be encountered. Figure (5.10) shows the velocity profile over the flat plate at different Reynolds numbers and indicates that no such problems existed here. Also once again the close agreement between the 1/7th power law velocity profile with the test data obtained in the fully turbulent region indicates that the flow is fully turbulent. At the lower Reynolds number the velocity profile tends towards the Blasius laminar profile. This good agreement of the velocity profiles indicates that the flow in the test section follows closely the expected flow patterns.

Skin-friction coefficient of the flat plate. To check out the accuracy of the system it was decided to compare measured skin-friction coefficient for the flat plate in clean air with the Prandtl-Schlichting Equation (6) for a smooth flat

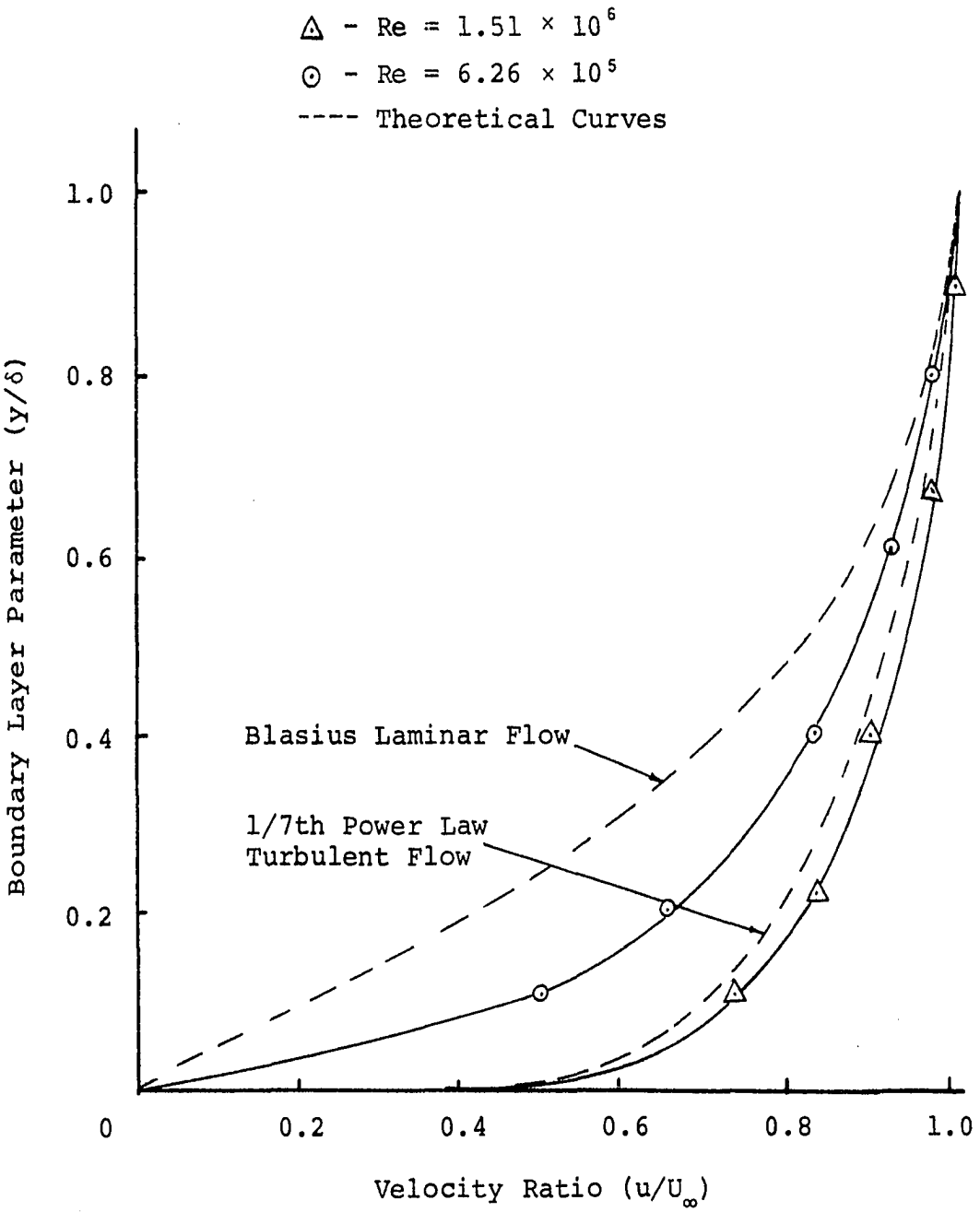

Figure (5.10) Velocity Profile Over a Flat Plate Varying With Reynolds Number.

plate at zero incidence,

$$C_f = 0.0576(V_\infty x/\nu)^{-1/5} \qquad (5.18)$$

To be able to compare the skin-friction coefficients, Equation (5.18) must be modified to obtain the average skin-friction coefficient. By integrating Equation (5.18) over the length of the test plate, L_2,

$$\overline{C_f} = \frac{1}{L}\int_{L_1}^{L_1+L_2} 0.0576(V_\infty x/\nu)^{-1/5}\, dx \qquad (5.19)$$

where L_1 is the distance from the leading edge of the wind tunnel floor. Integrating the above equation gives the total skin-friction coefficient as,

$$\overline{C_f} = 0.072(V_\infty L_2/\nu)^{-1/5}\{[(L_1 + L_2)/L_2]^{4/5} - [L_1/L_2]^{4/5}\} \qquad (5.20)$$

For the particular case in this report the equation reduces to:

$$\overline{C_f} = 0.00805\ V_\infty^{-1/5} \qquad (5.21)$$

where V_∞ is in feet per second. The skin-friction coefficient obtained by the test data is an average skin-friction coefficient and was based on the values obtained from Figure (5.7). Figure (5.11) shows the test data compared to the theoretical curve based on Equation (5.21). The good agreement between test data and the empirical curve based on Schlichting's equation gives confidence in the measuring system.

Experimental Procedure

With the systems calibration completed, the primary

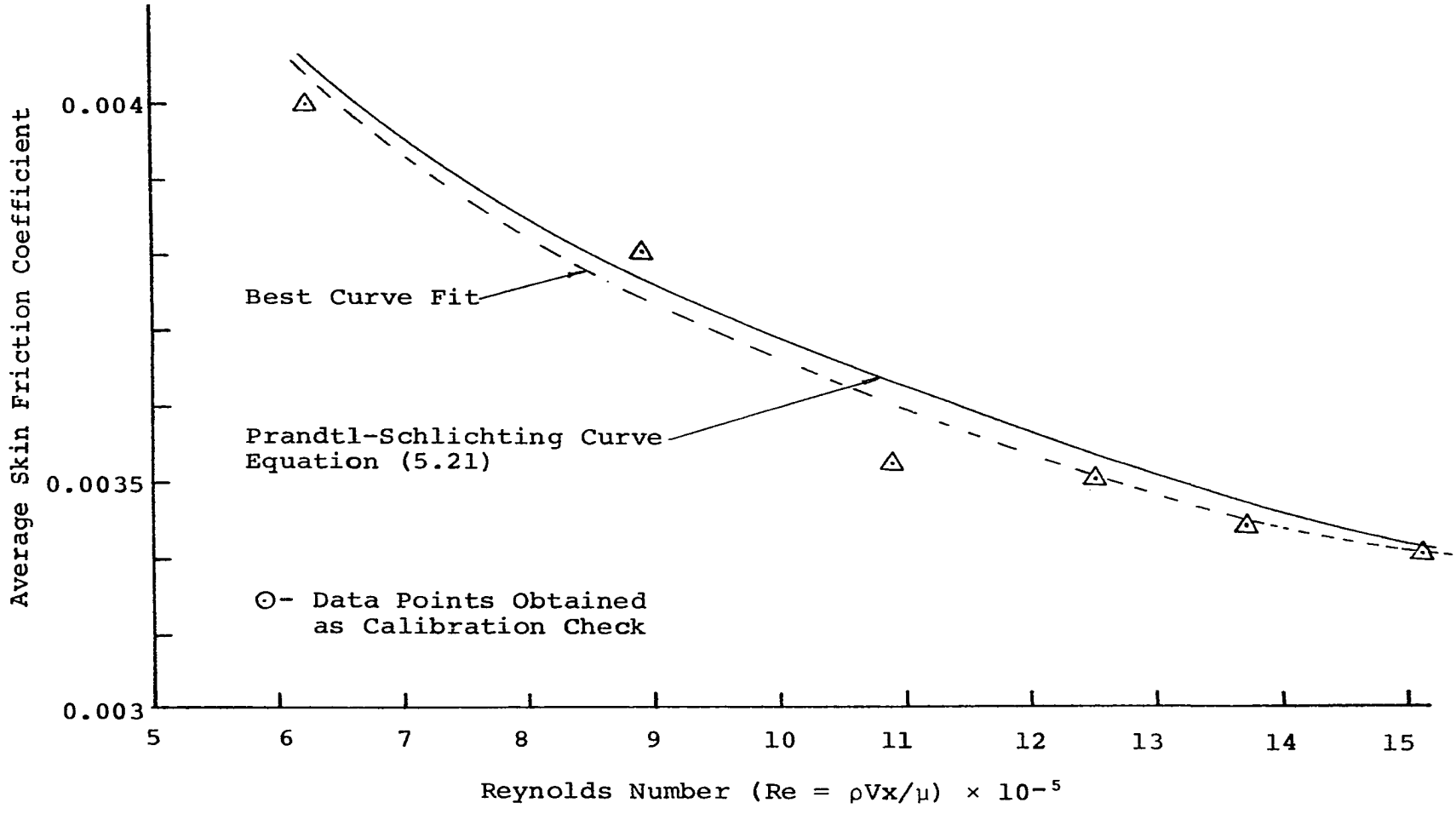

Figure (5.11) Skin Friction Factor for Smooth Flat Plate at Zero Incidence, Comparison Between Theory and Mesurement.

task of obtaining data was now ready to proceed. The clean air data had all been obtained in the calibration runs, thereby providing a good base line for comparison.

Before any data were taken the barometric pressure and room temperature were measured. The blower and the wind tunnel fan were then started. A careful investigation of the effect of the energizing of the boundary layer by the blower was undertaken. The results indicated no change in the deflection of the strain indicator with or without the blower on. The velocity of the air in the wind tunnel was adjusted by the vanes behind the wind tunnel fan. The static pressure taps were located on the side of the tunnel at the center line of the flat plate. Figure (5.12) shows the relationship between the static pressure and the free stream velocity. Another check on the velocity was made to compare it against the deflection of the strain indicator as was previously obtained for the skin-friction coefficient curve. Figure (5.13) shows the relationship between velocity and the deflection of the strain indicator. This curve was used mainly as a check since it was not entirely accurate from day to day because of changes in air density.

The flow rate now having been set, the particles were introduced into the blower and consequently entered the main flow upstream of the flat plate. The deflection of the strain indicator was noted. The duration of each test run varied from 10 to 25 seconds. After each test run the small

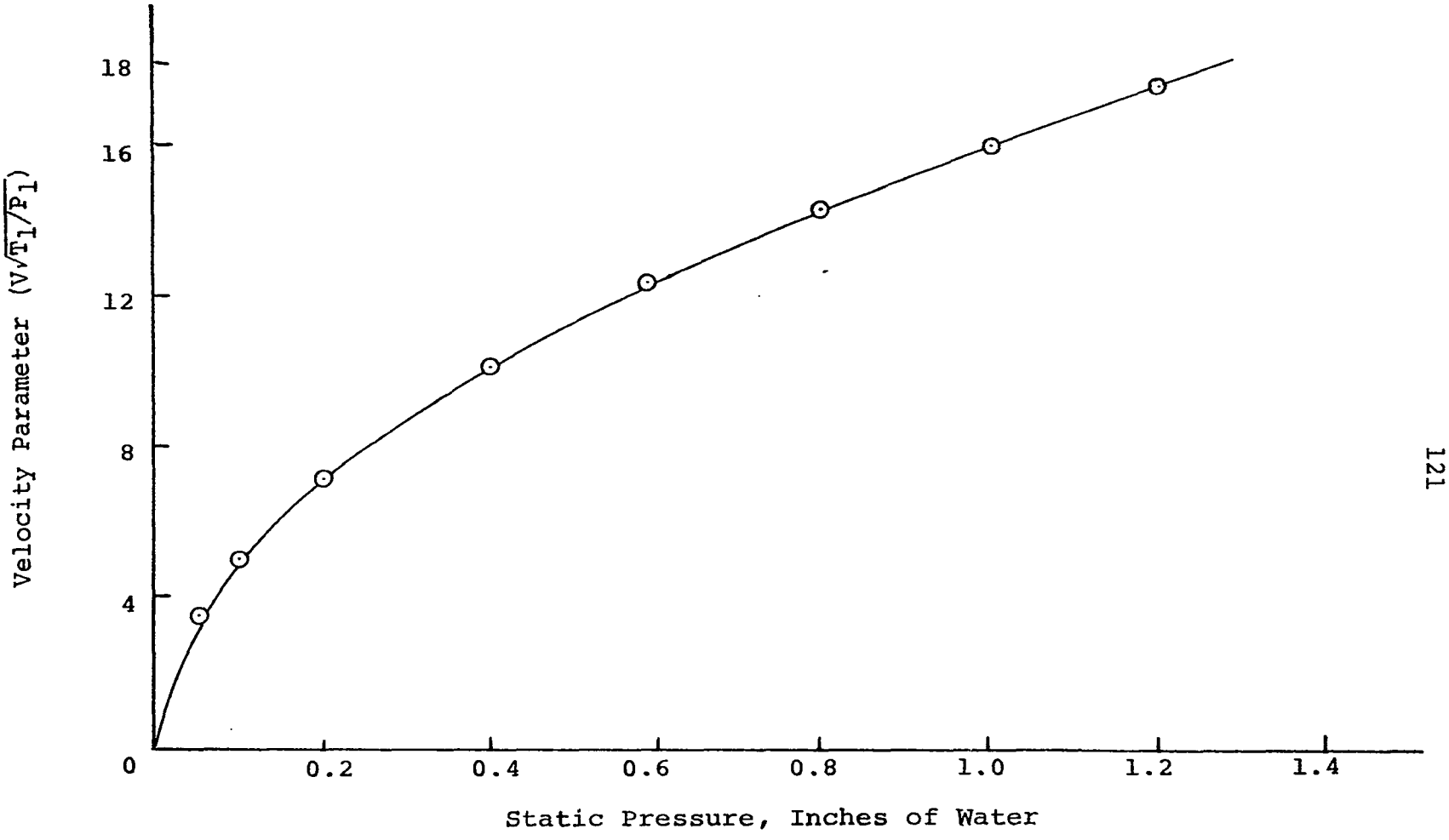

Figure (5.12) Velocity Correlated to Static Pressure For Wind Tunnel.

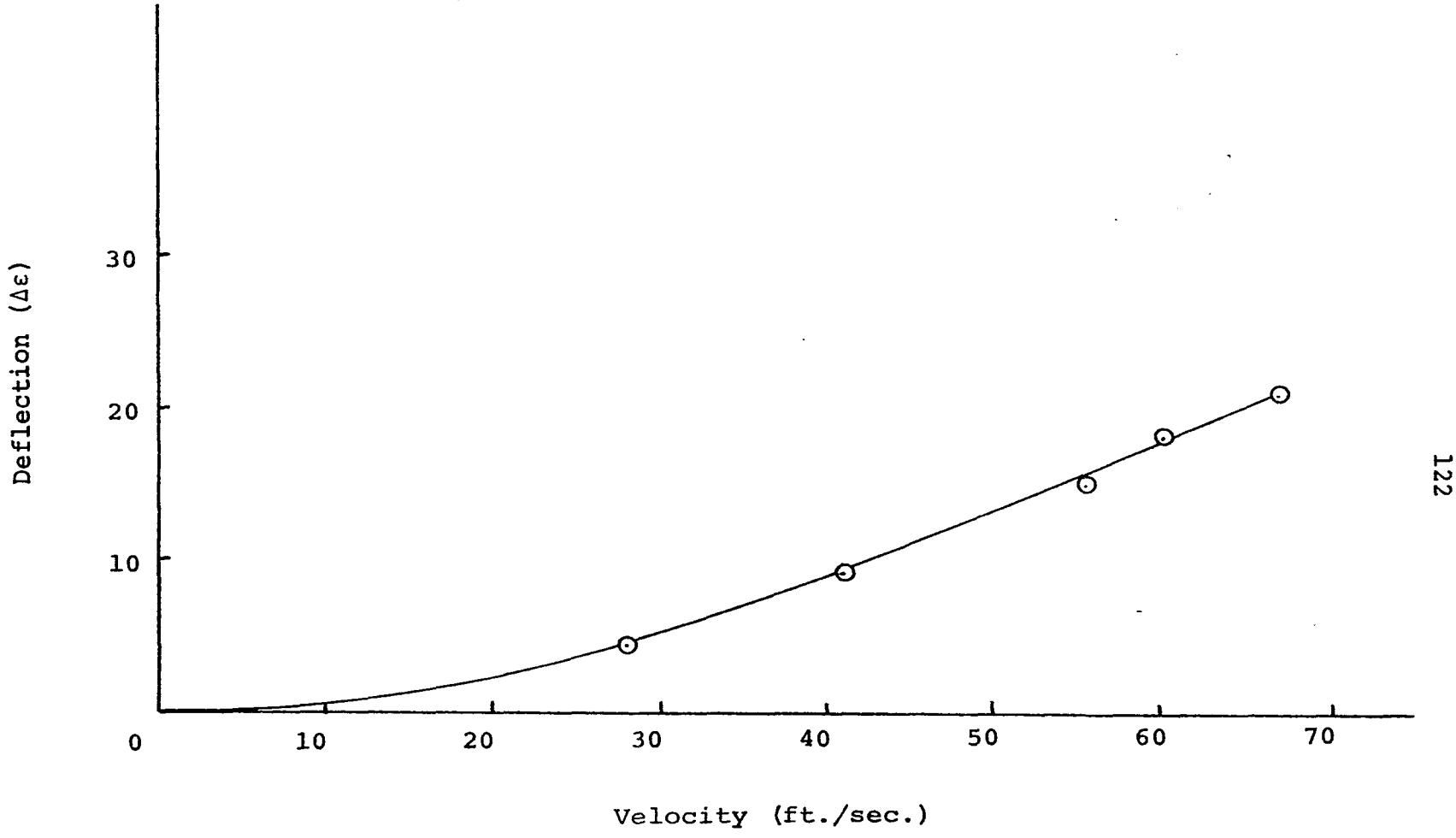

Figure (5.13) Deflection of Strain Indicator at Various Velocity Settings.

door in the transition piece was opened and any particles left were swept out and weighed. At the completion of tests for one size of particles the entire transition piece was dismantled and cleaned to be sure no particles were trapped in any crevices. This dismantling did not take too long (about 10 minutes) since the piece was specially designed for this purpose.

Throughout the tests the pressure along the flat plate was monitored to verify that there was no pressure gradient, with or without particles suspended in the flow. Also care was taken to see that the plate was always entirely free and did not bind in any place. At the start of each run the dust collector was sprayed with the chemical "Attract"; this prevented most of the particles from leaving the dust collector. Another precaution taken was the spreading of a large plastic sheet near the feed system so that any particles which did not enter the blower could, after each run, be collected and weighed to correct the particle weight flow measurements.

CHAPTER VI

PHOTOGRAPHIC TECHNIQUES

Flow visualization techniques have come of age very rapidly. The importance of being able to visualize the flow cannot be overrated. Flow visualization techniques have been used to design more efficient turbomachines, to check flow in bends, to describe flow around bodies, and for many other important problems. In this report the flow visualization techniques are used to calculate the velocity of the particles suspended in the air stream. The objective here was to obtain the velocity of the particles at different air stream velocities. The velocities were measured at selected points with the assumption that the ratio of the particle velocity to the air stream velocity remained constant. Thus no attempt was made to obtain a velocity profile of the particle flow.

Two different photographic setups had to be constructed, since the requirements of the two experiments were different. This necessitated the use of two different cameras to achieve the best resolution in each case. The basic system consisted of a specially constructed timer (Appendix I) and two strobe lights which were connected to the camera. By triggering the camera the time delay mechanism would be acti-

vated. This in turn would flash the first strobe light, and after the pre-set time delay the second strobe light would be flashed thus producing two images for each particle on the exposed film. The strobe lights had colored filters mounted on them thus giving flashes of different colors which would easily be distinguished. All the pictures were taken on high speed color film.

The velocity measurements were made at the center of the different test sections. By means of aperture settings that give a very small field of depth, particles only in the center of the test section were photographed. The particles photographed have a bright round image at the instant the strobe flashes and a tail for the duration of the flash. This is analogous to the head and tail of comets. The same type image for the second flash is also observed. The tail helps to tie together the images of the same particle. The velocity is calculated by measuring the distance between the two round points of the images when the slide is projected on the screen. This distance is then related to a known distance previously marked off on the test section which is projected on the screen, thereby enabling the calculation of magnification parameters. In this manner the actual distance traveled by the particle between flashes is known. Also, since the time delay setting is known, the velocity is easily calculated.

The general method has been outlined. The multifarious details are outlined in the following sections. Each test setup is described separately.

Circular Pipe Flow

To calculate the velocity of the particles in the circular pipe it was decided that the most suitable place to get an accurate picture of the velocity would be around the center of the test section. Attention was therefore concentrated on the flow at the center of the pipe at a position midway in the test section.

Many problems were encountered. On the first try, the two lights were placed about 1 foot from the pipe at right angles to the camera lens. The lens was about 8 inches from the pipe. The pictures were taken at aperture settings varying from f-2.8 to f-16.0, but the particles could not be seen due to excessive glare. To reduce this glare it was decided first to direct the light to a spot perpendicular to the lens at the top of the pipe. Then the pipe was covered with black paper that had two holes cut in it, one for the light and the other for viewing the flow. Again the whole range of aperture settings was tried, but only a very slight improvement in the reduction of the glare was obtained. It was felt that the light was being transmitted when the light beam struck the inner surface and hence the glare, although reduced, was still spread through the inner surface and obscured the particles. Even the use of "light polarization" techniques failed to substantially reduce this transmitted glare.

To correct this it was decided to retain the light directional mechanism, but make a more permanent device as

shown in Figure (6.1). This device was built from sheet-metal. It consisted of two rabbit ears which were connected to a 3-1/4 inch circular pipe. The lights were mounted on special

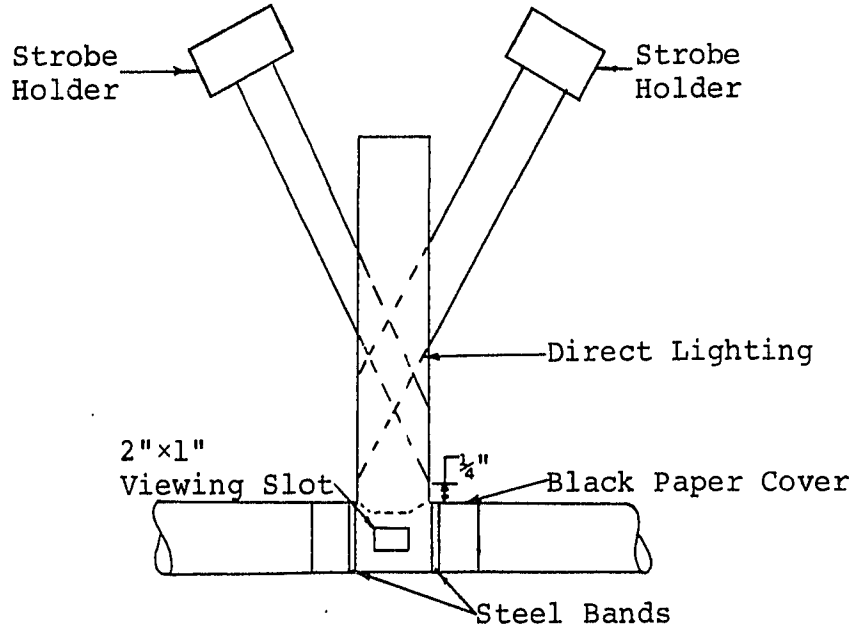

Figure (6.1) Rabbit Ears for Direction of Light.

mounts, each mount designed so that the two different strobe lights, with their filters, could be securely mounted. The inside of the apparatus was painted black so as to prevent any internal reflection. The rabbit ears were mounted so that a straight line traveled by the light would reach a point about 1/4 inch above the circular pipe, and in this manner a good diffused light reached the circular pipe. In addition an equal abount of light from each strobe would reach the circular pipe.

The second correction (to avoid the excessive glare) was to color the inside of the pipe black, leaving two windows perpendicular to each other so that light could enter through

one and the flow could be visualized through the other. This task was more difficult than one would initially expect. The reason for this was that the point in the test section where the photographs were to be taken was not easily accessible. To achieve the desired results, duct tape mounted on a six foot rod, with the sticky side facing out, was inserted into the pipe and the tape was then stuck to the glass at the desired position, part of the tape sticking out at one end. A second tape was also inserted in the same way and placed 90 degrees apart from the first. A roller attached to a long rod, dipped in flat black paint, was then inserted and the inside of the pipe was coated with black paint. This process was repeated twice to achieve an absolute black surface. When the paint was entirely dry, the ends of the tapes, which had been hanging out of the pipe, were connected to a rod, one at a time, and the rod was then rammed through, ripping the tape from the glass. Care had to be taken that the rod did not touch any of the inner pipe surfaces so as not to scratch them. The next step was to paint the clear strips inside the tubing (left by the removal of the tapes) with the paint roller. However just enough clear area was left unpainted for the light and viewing windows.

The outside of the circular pipe was covered with a black paper as previously described in the second run. Figure (6.2) shows a photograph of the entire setup. The viewing window was 2 inches by 1 inch.

Figure (6.2) Photographic Test Setup for Velocity Measurements in Circular Pipe.

The camera used was a Nikon 35 mm, which had a 50mm f-2.0 lens. Extension tubes were attached to the camera lens so that close-up pictures could be taken. The extension tubes enable close-up pictures because they shorten the focal length of the lens. The camera was focused to the center of the pipe on a thin rod positioned at that point. Care was taken to see that the entire outline of the viewing area was included on the picture since the frame was the reference point.

Two different model strobe lights were used. The reason for this was that they were the only ones available. It would have been better if the two lights were the same. To correct for the difference in intensities additional color filters were used. The two colors selected, blue and red, gave good separation of colors on the slides. This was done after considerable test runs using different combinations of color filters. The first strobe light to flash was an A. C. powered slave unit made by Honeywell which had a blue filter on it. It was used as the number one flash since it was very sensitive to any electrical impulse. The second strobe was a Honeywell battery powered strobe which had a red filter mounted on it. The lights were connected to the time delay system specially built for this experiment by Weather Service Incorporated of Norman, Oklahoma (Appendix II). The time delay was set at 4010 milliseconds.

The film used was High Speed Extrachrome Daylight Color Balance (5600°K), normal ASA 160. The aperture setting used was f-3.5.

Thirty-six pictures were taken at different air velocities, particle sizes, and weight-flow ratios. The air velocity was varied from about 20 feet per second to about 48 feet per second. The particle sizes were varied from 200 microns to 1640 microns. The reason that smaller sizes of particles were not considered was that at 200 microns the particle velocity was the same as that of the free stream; hence it was assumed that smaller particles would also travel at the free stream velocity. The weight-flow ratio was varied from 0.01 to 2.0. In this manner a variety of readings were possible.

Figure (6.3) shows the photographs of the particles in the circular pipe flow. The velocity was calculated by projecting the photograph on a screen. The observations from the velocity plots are given in detail in the next chapters. The significant points observed were that the increase in weight-flow did not seem to effect the measured velocity of the particles. Also the velocity ratio of the particle velocity to the average velocity of the air stream remained a constant for the particle size.

The films were "force" processed so as to increase the effective ASA number of the film. Appendix II shows, in detail, the steps that were followed to force process these films.

Flow Over a Flat Plate

The velocity of the particles suspended in the air

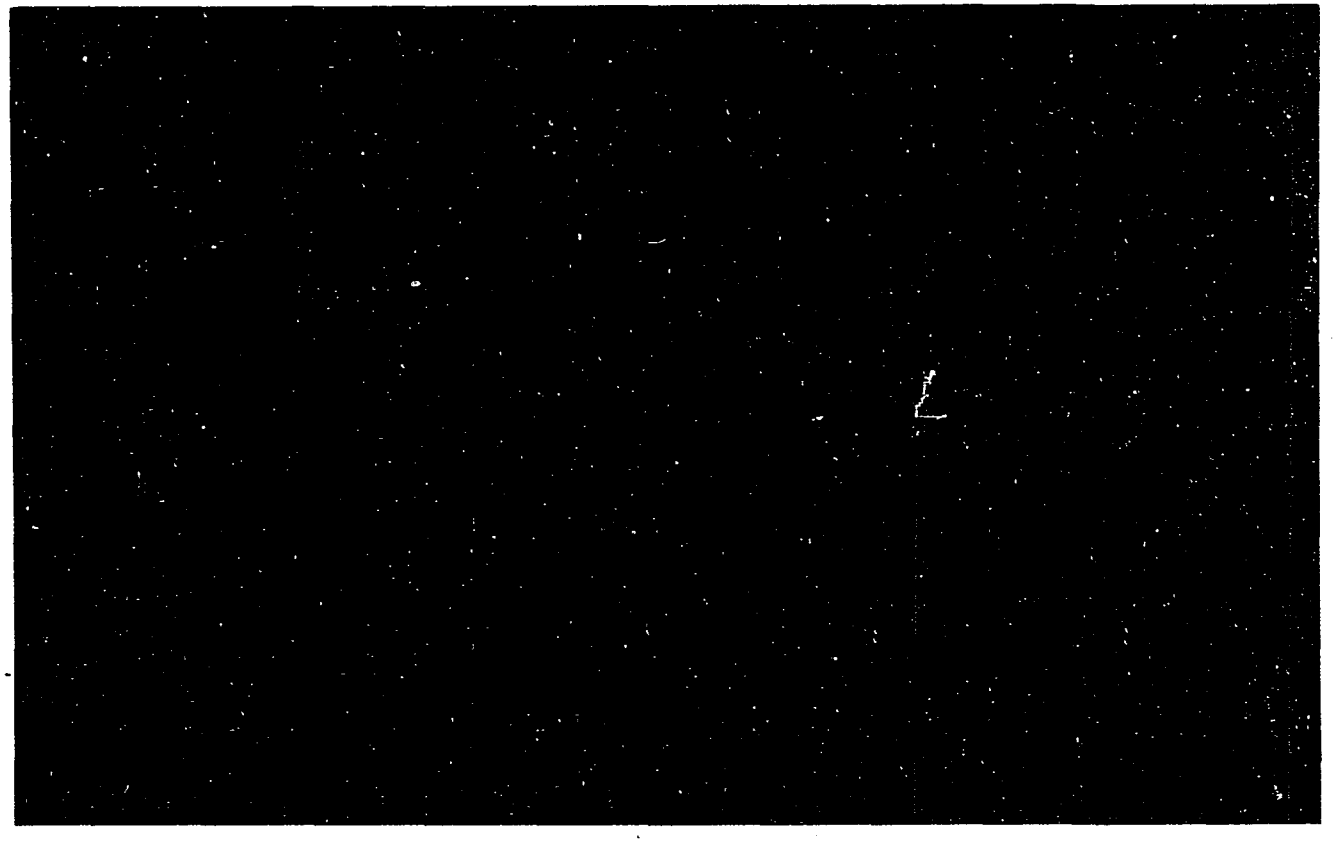

Figure (6.3) Particle Flow in Circular Pipe.

stream flowing over the smooth flat plate was computed by taking photographs over the leading half of the flat plate. The initial plans were to take the photographs at various different positions and then superimpose them to obtain an accurate picture of the flow over the entire plate. This plan was scrapped when it was ascertained that there was no axial velocity gradient of the particles over the first quarter of the plate. The reason that the entire plate or even a larger part of the plate was not photographed, was because any larger area than that which was photographed appreciably reduced the resolution obtained, making photographs of the small particles a practical impossibility.

The strobe lights were mounted on the roof of the wind tunnel. The light penetrated into the tunnel through the slot in the roof of the wind tunnel which was there for the traversing of the velocity probes through the entire length of the tunnel. This slot was covered for the data test runs by the use of duct tape which prevented any secondary flows that might otherwise have been introduced by the slot. Since the duct tape was not translucent it had to be replaced in the portion just underneath the lights. In that small section the tape was replaced by a strip of translucent plastic that allowed the lights to illuminate the test section of the wind tunnel. Figure (6.4) shows the schematic of the test section. The tape, with the black 1 inch squares in the figure, was attached onto one of the access doors of the wind tunnel. This tape, with its 1 inch squares, is used as the reference

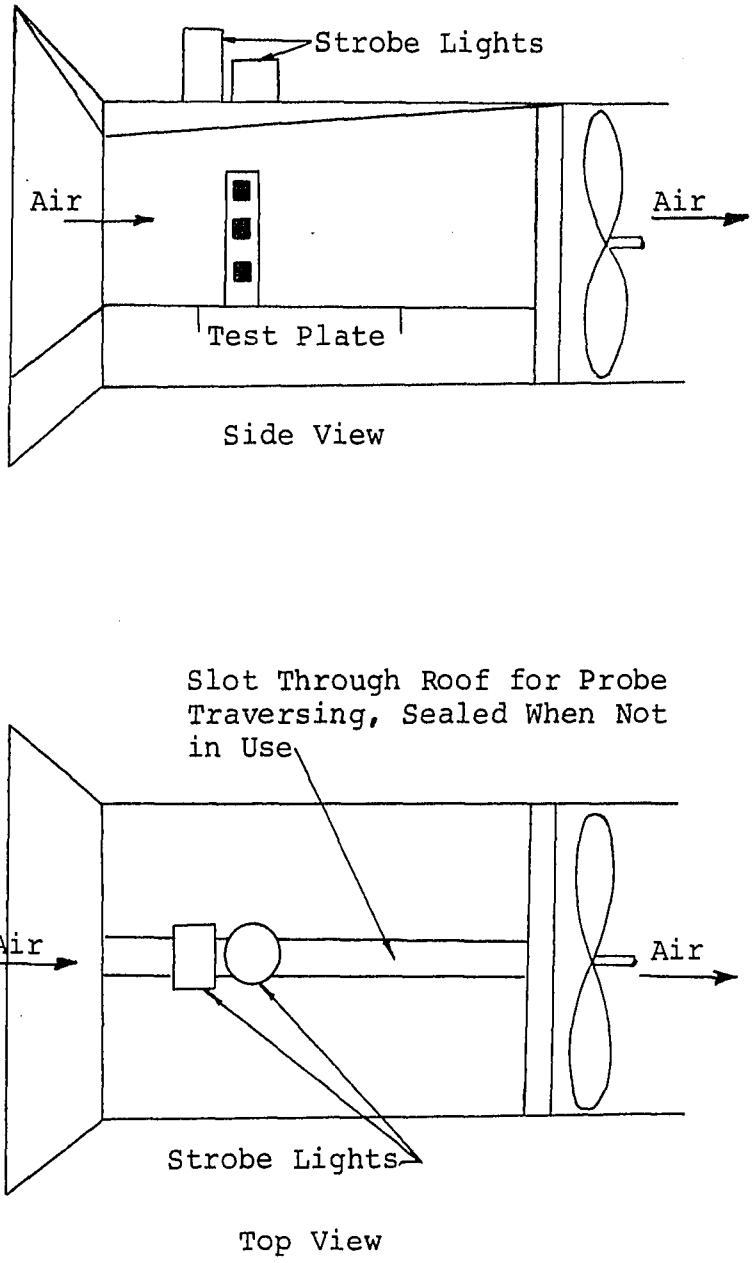

Figure (6.4) Photographic Setup for Flat Plate Experiment.

point providing the magnification scale on each photograph. Adjustments had to be made to the reference point to take into account the discrepancy arising because of the perspective of the lens, since it was focused at the center place of the tunnel and the reference point was at the wall of the tunnel.

The entire test section of the wind tunnel was painted with a flat black coat of paint to avoid any glare. The window through which the photographs were taken was entirely masked except for the portion through which the photographs were taken. The masking of the window reduced any glare that might have occurred from the light reflecting off the floor of the tunnel. The pictures were taken by turning off all lights in the hangar in which the wind tunnel was located. This prevented the camera image from being reflected in the glass. Another precaution was the masking of all shiny chrome parts of the camera.

The strobe lights used were the same as those used in the circular pipe experiment. They were used with the same color filters and were connected to the same time delay system. The time delay used was also the same, 4010 milliseconds. The black background used in this test was settled on after a number of tests were conducted on various backgrounds. The two colors that were acceptable were black and 18 percent grey.

The camera used was a Zenza Bronica, model S-2 with a Nikkor 75 mm f-2.8 lens. The Bronica was chosen because of its large negative size (2-1/4 inches by 2-1/4 inches) giving a very high degree of resolution. The 35 mm camera gave a much smaller negative and the resolution obtained was poor. The Ektachrome 35 mm negative area is 1.255 square inches whereas that of the Ektachrome 120 is 4.63 square inches. Since the same area is being photographed, more detail is possible on the larger slides. Figure (6.5) shows a photograph

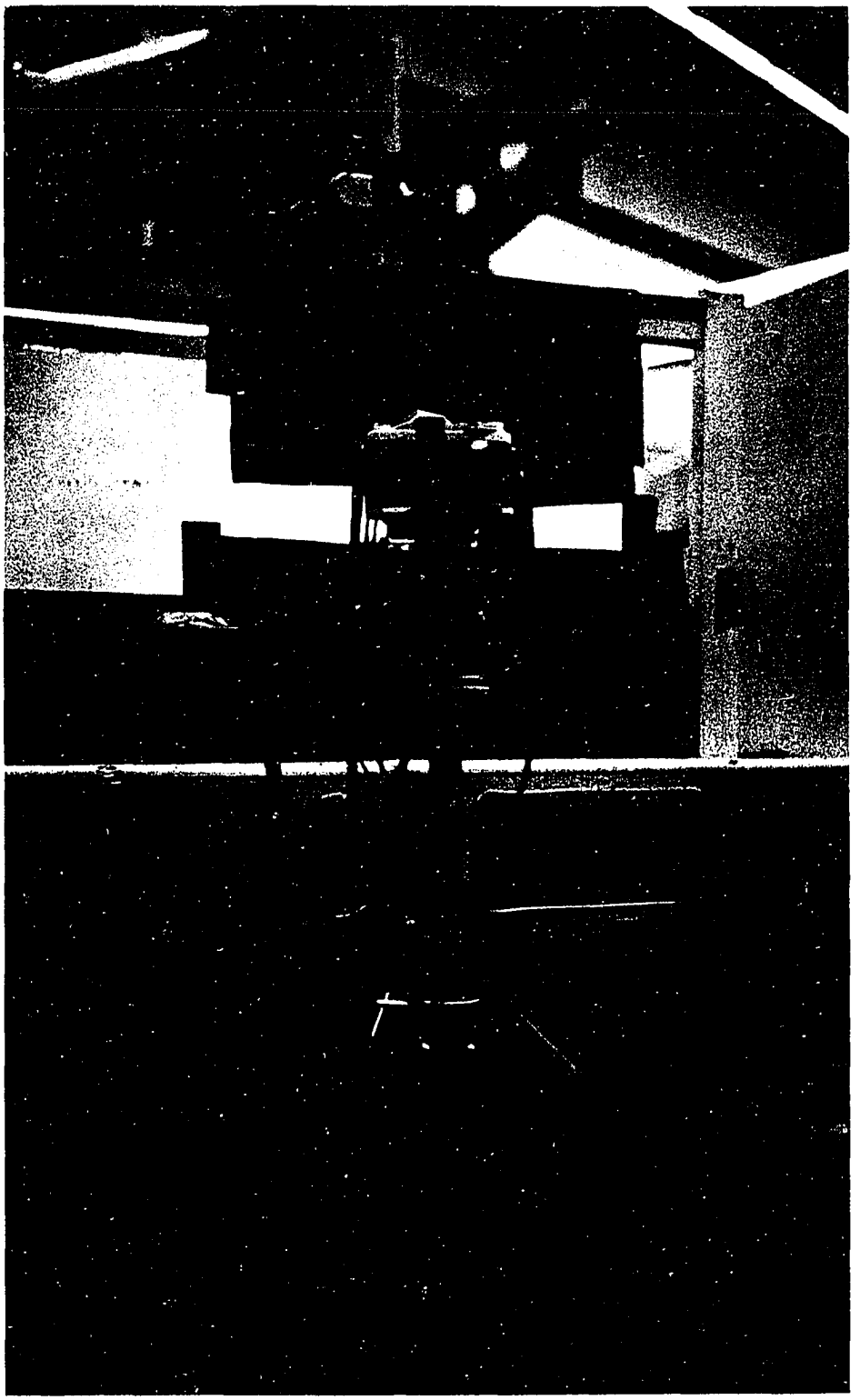

Figure (6.5) Photographic Test Setup for Velocity Measurements Over a Flat Plate.

of the entire test setup for the photographing of the particle velocities.

Thirty-six photographs were taken at various particle sizes, velocities, and weight-flow ratios. Figure (6.6) shows the photographs obtained. The results are explained in detail in the next chapter. The findings were similar to those found for the circular pipe flow, i.e., the weight-flow ratio did not effect particle velocity, and the velocity ratio for a fixed particle size remained constant.

The film used was a high speed "Ektachrome 120 Daylight Color Balance (5600°K) with a normal ASA rating of 160. The film was forced processed to an ASA rating of 320 using the technique outlined in Appendix II. The focal setting used was an f-2.8. This gave a very narrow depth of field. The camera was focused to a plane at the center of the wind tunnel.

The photographic techniques outlined in this chapter were perfected after a long trial and error period. It is hoped that this detailed description will aid other researchers in taking similar type pictures. This technique could be used in problems such as calculation of decay of particle size from a nozzle spray. The technique could also be used for particles suspended in liquids thus easily describing flow past bodies of different shapes.

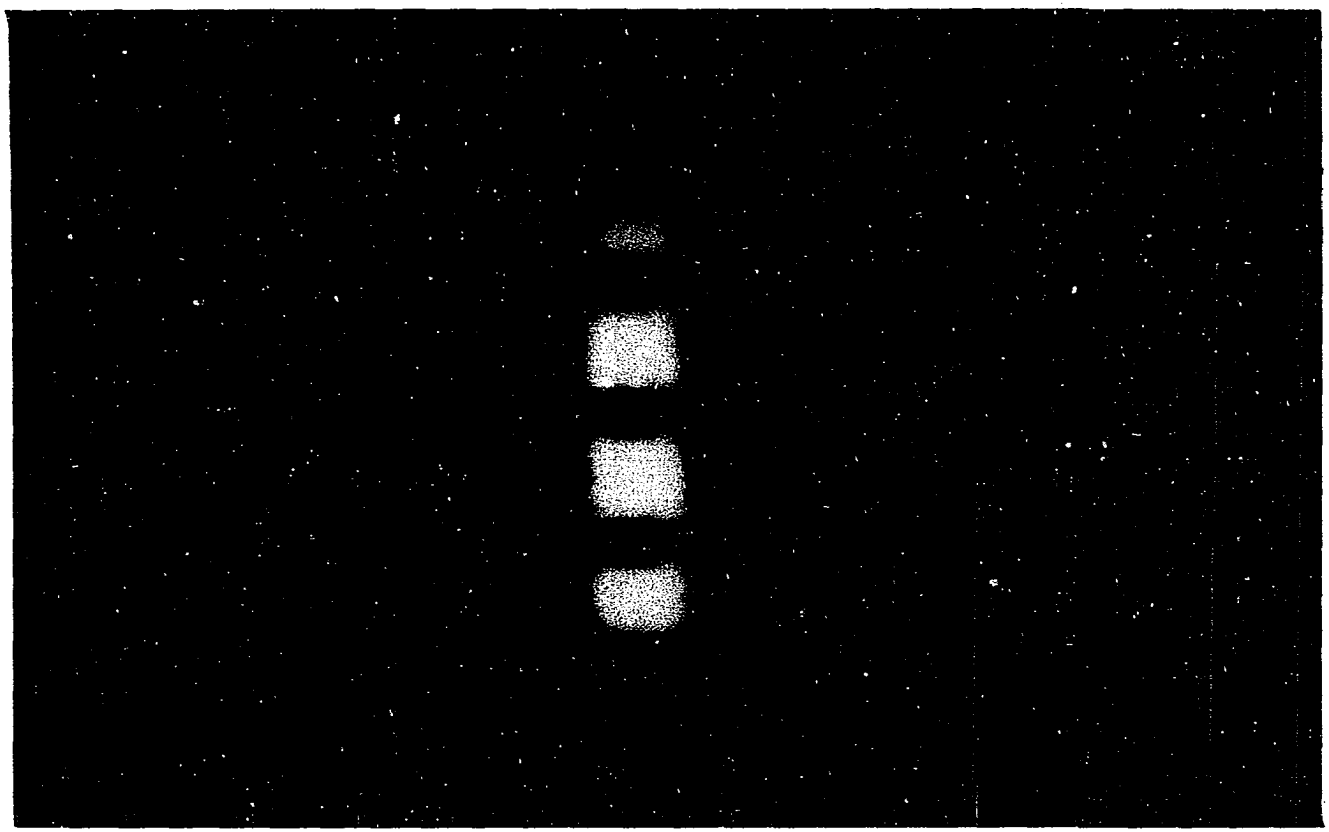

Figure (6.6) Particle Flow Over a Flat Plate.

CHAPTER VII

ANALYSIS OF RESULTS

In Chapter 5 it was shown that the data obtained by the author for clean air runs agreed well with that obtained by previous researchers, which indicated that the equipment's accuracy was very acceptable. The next step was the gathering of data by the method described in the same chapter. The data are presented here in graphical form rather than in tabular form thereby making evaluation much easier.

An attempt will also be made to explain most of the observations and some links to the theoretical background will be suggested. This will be in the form of explanations showing trends rather than quantative results. An attempt will also be made to explain some of the finer points observed in the test runs.

Data Observations

Flow Through a Circular Smooth Pipe

The tests indicate that when particles are suspended in the air stream they reduce the skin-friction coefficients as compared to the flow of clean air through the same circular

smooth pipe at the same flow rate. The effect of Reynolds number, particle diameter, and weight-flow ratio play a very important role in this phenomenon. Each of these parameters and their effect on the total picture will be investigated.

The Reynolds number was varied from close to the laminar region ($Re = 9.5 \times 10^3$) to high in the fully developed turbulent region ($Re = 6.3 \times 10^4$). The weight-flow ratio (W_p/W_g) of particles to air varies from about 0.025 to about 4.0. Figures (7.1) through (7.5) show the effect of dusty air through a smooth circular pipe on the pressure drop at the test section. This reduction in pressure drop is directly equivalent to the reduction of the skin-friction drag in this section. As can be seen from these results the maximum reduction of the skin-friction drag occurs in the low Reynolds number end of the turbulent flow region. This effect is very prominent for small particles suspended in the flow stream. Figures (7.6) through (7.8) show the effect of particle size at a constant weight flow of the particles. Also the effect of Reynolds number is very obvious in these Figures. The trends observed in the Figures agree well with those observed by Thomas (23) in his tests of aqueous solutions of thorium oxide, as described in Chapter 2.

Figure (7.9) shows the effect of particle size on the Reynolds number for maximum drag reduction. The Reynolds number range varies from $Re = 1.8 \times 10^4$ to $Re = 4.04 \times 10^4$ for particle sizes varying from 15 microns to 1680 microns.

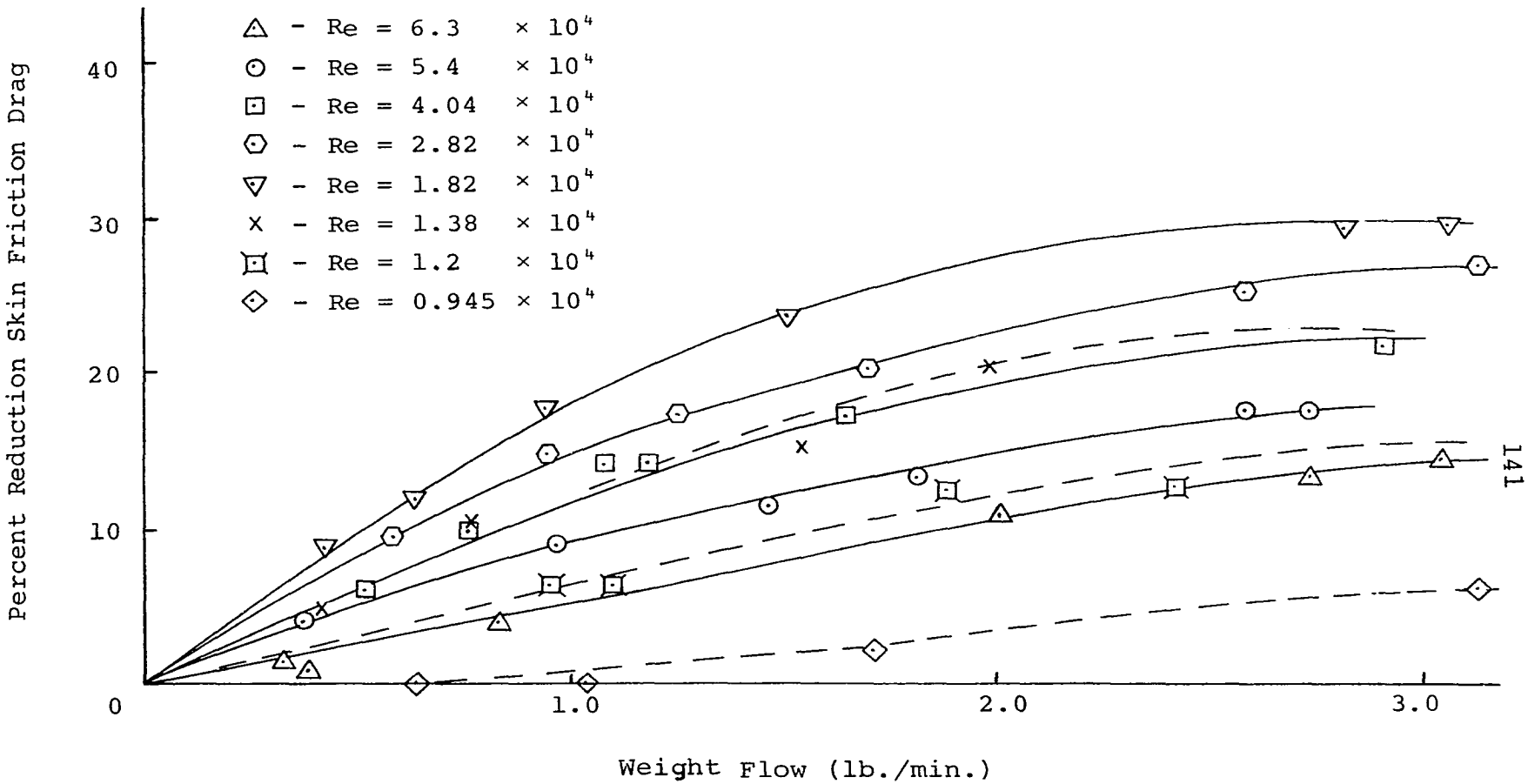

Figure (7.1) Reduction of Drag in a Circular Pipe (15μ).

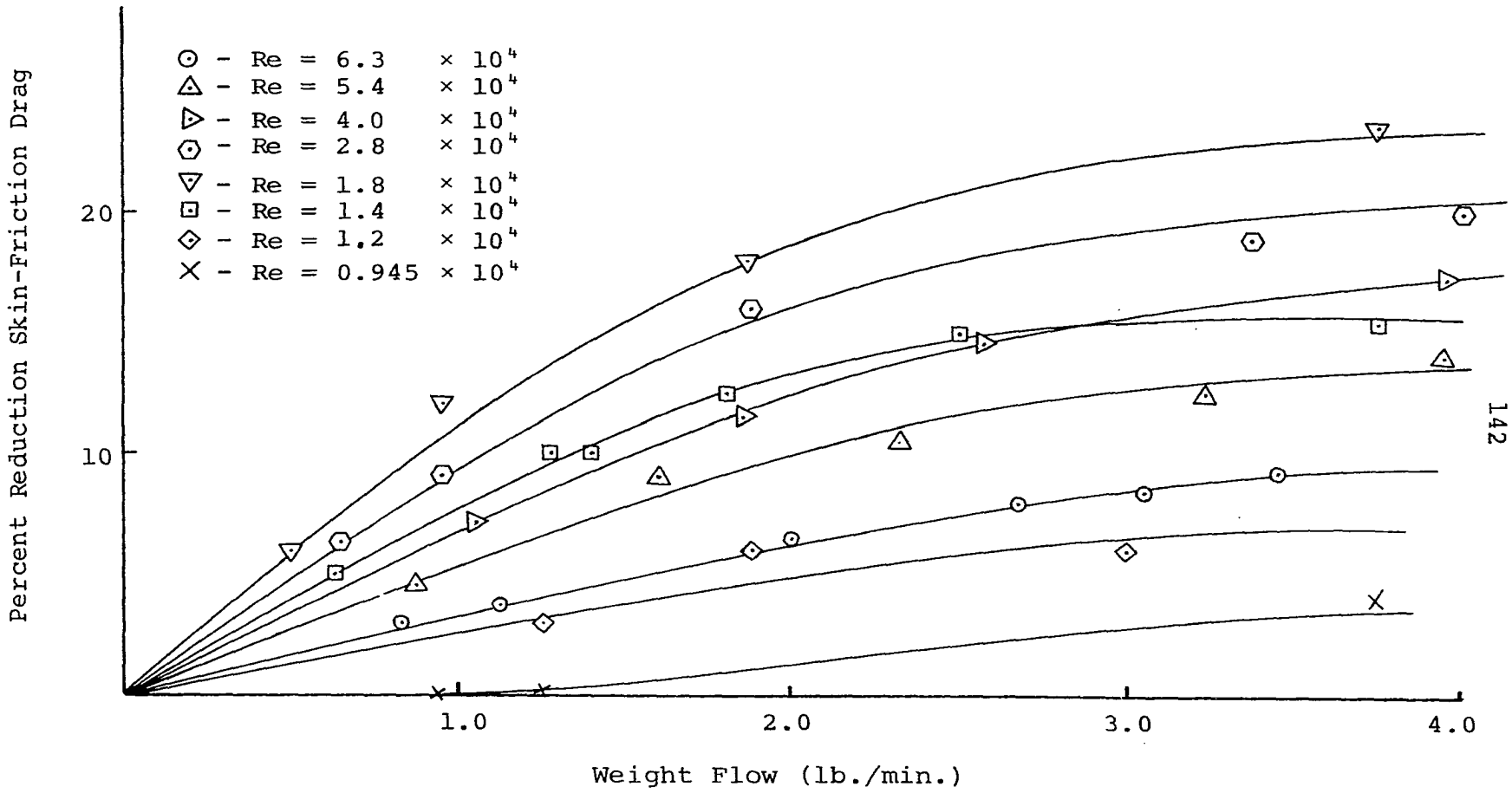

Figure (7.2) Reduction of Drag in a Circular Pipe (100μ)

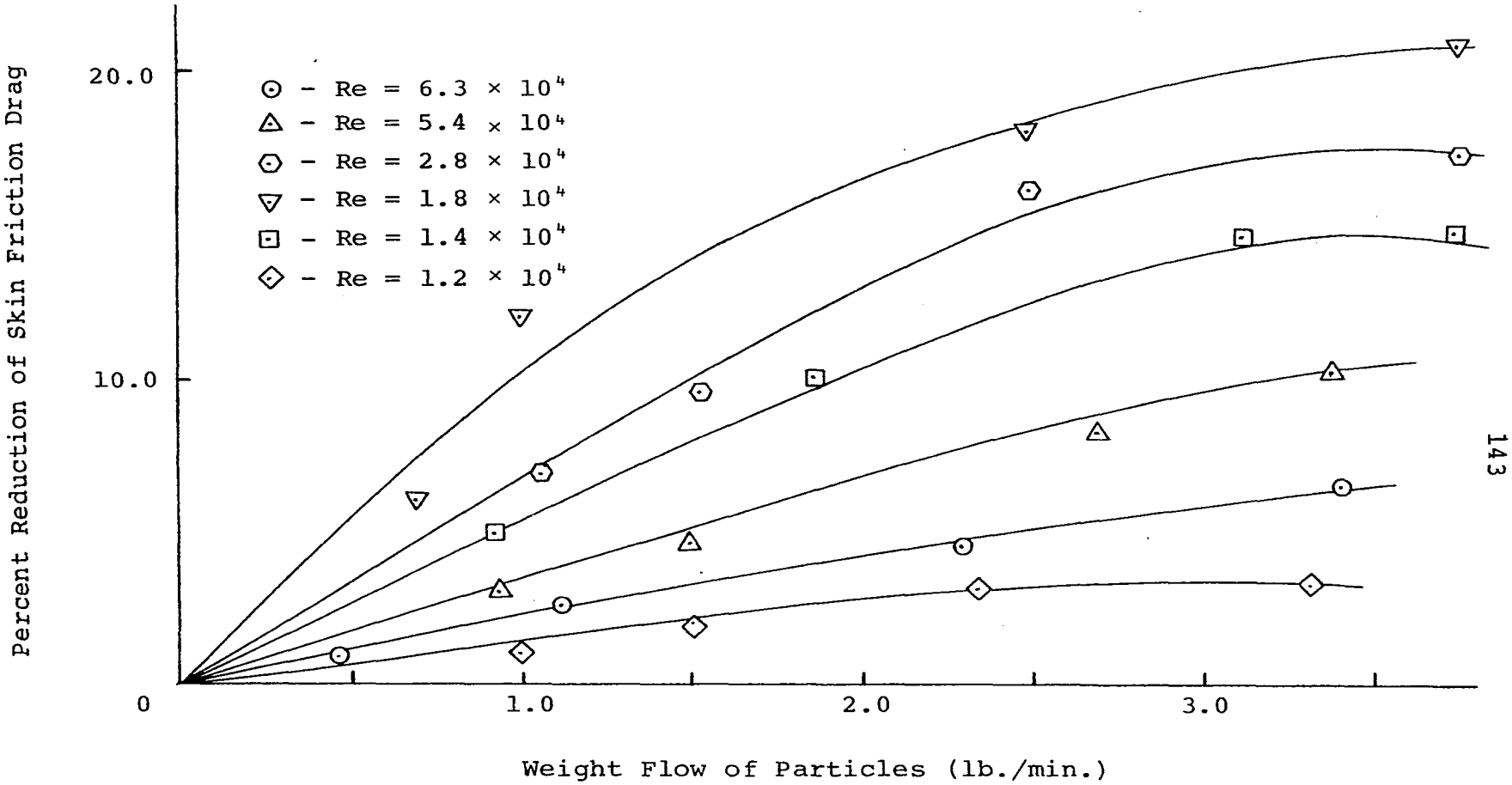

Figure (7.3) Reduction of Drag in a Circular Pipe (200μ).

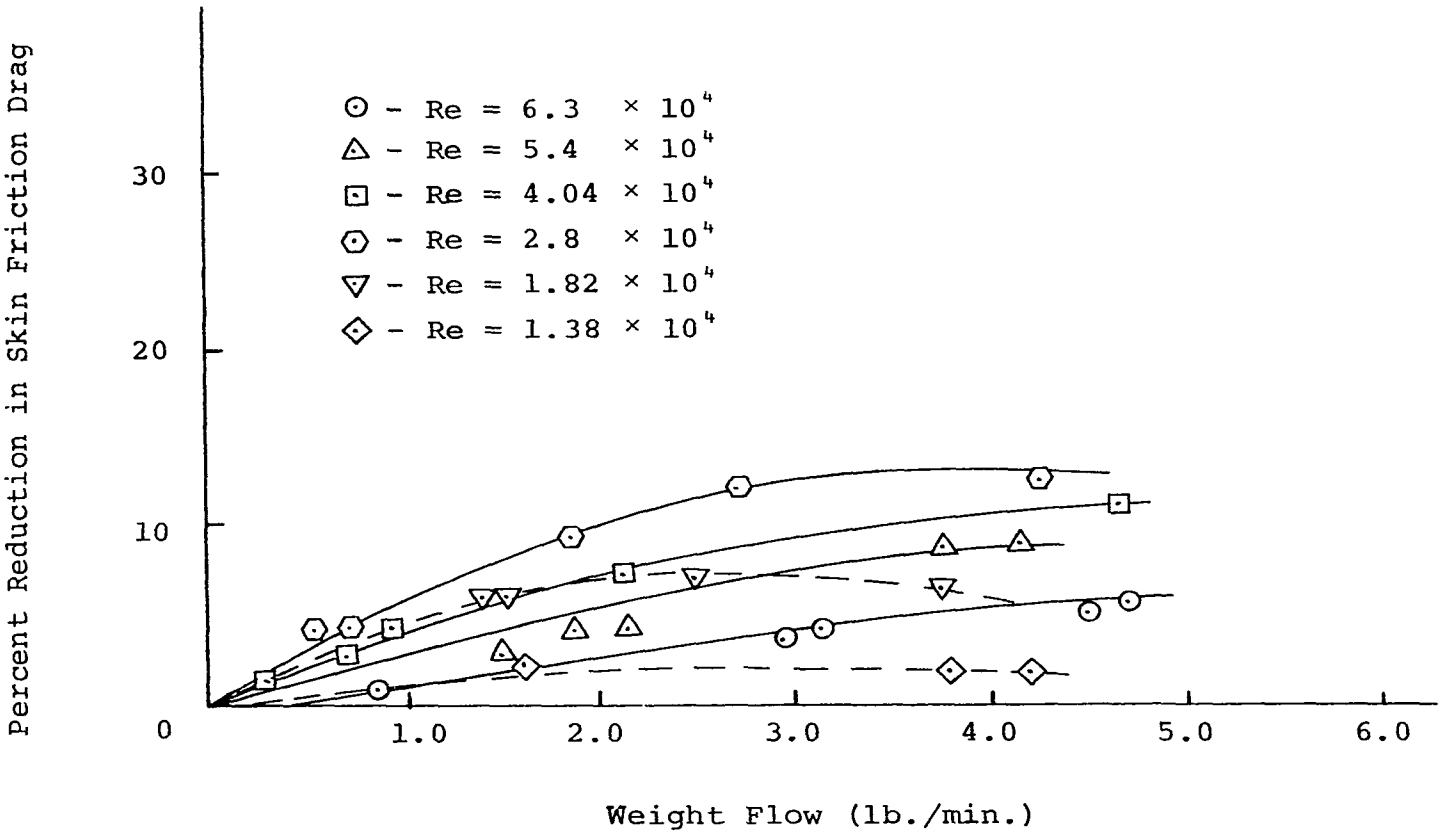

Figure (7.4) Reduction of Drag in Circular Pipe (840μ).

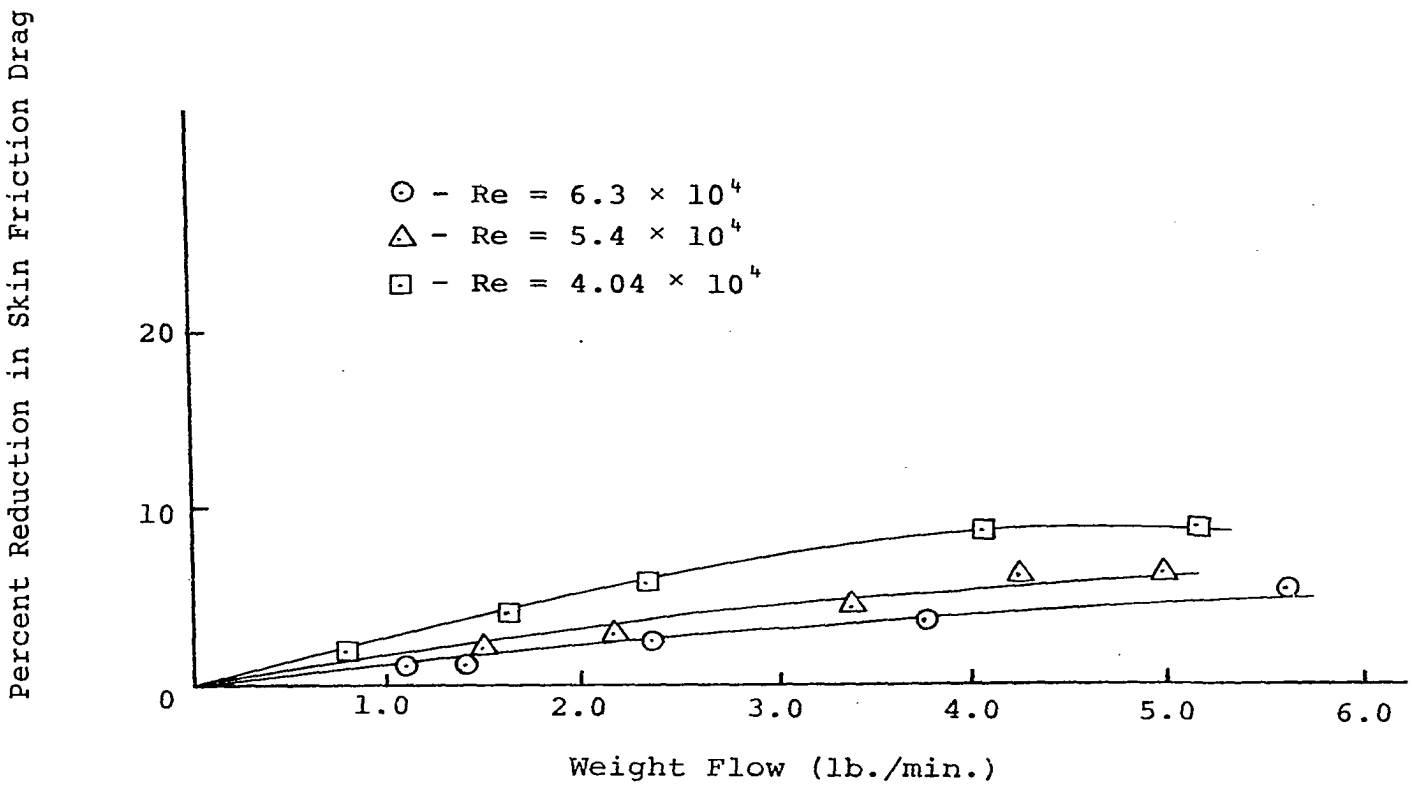

Figure (7.5) Reduction of Drag in Circular Pipe (1680μ)

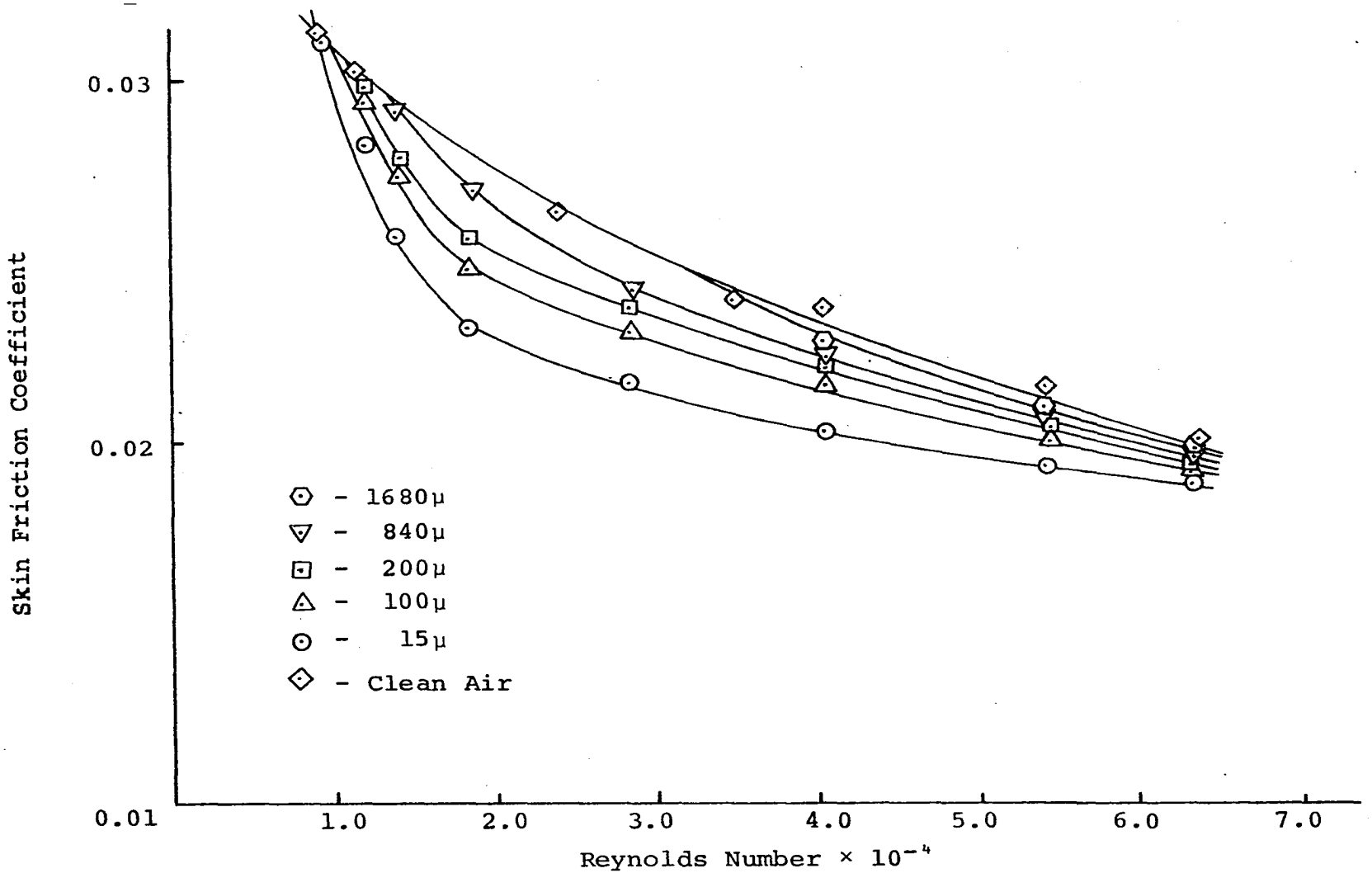

Figure (7.6) Friction Resistance of a Smooth Circular Pipe in Dusty Air (W = 1.0 lb./min.)

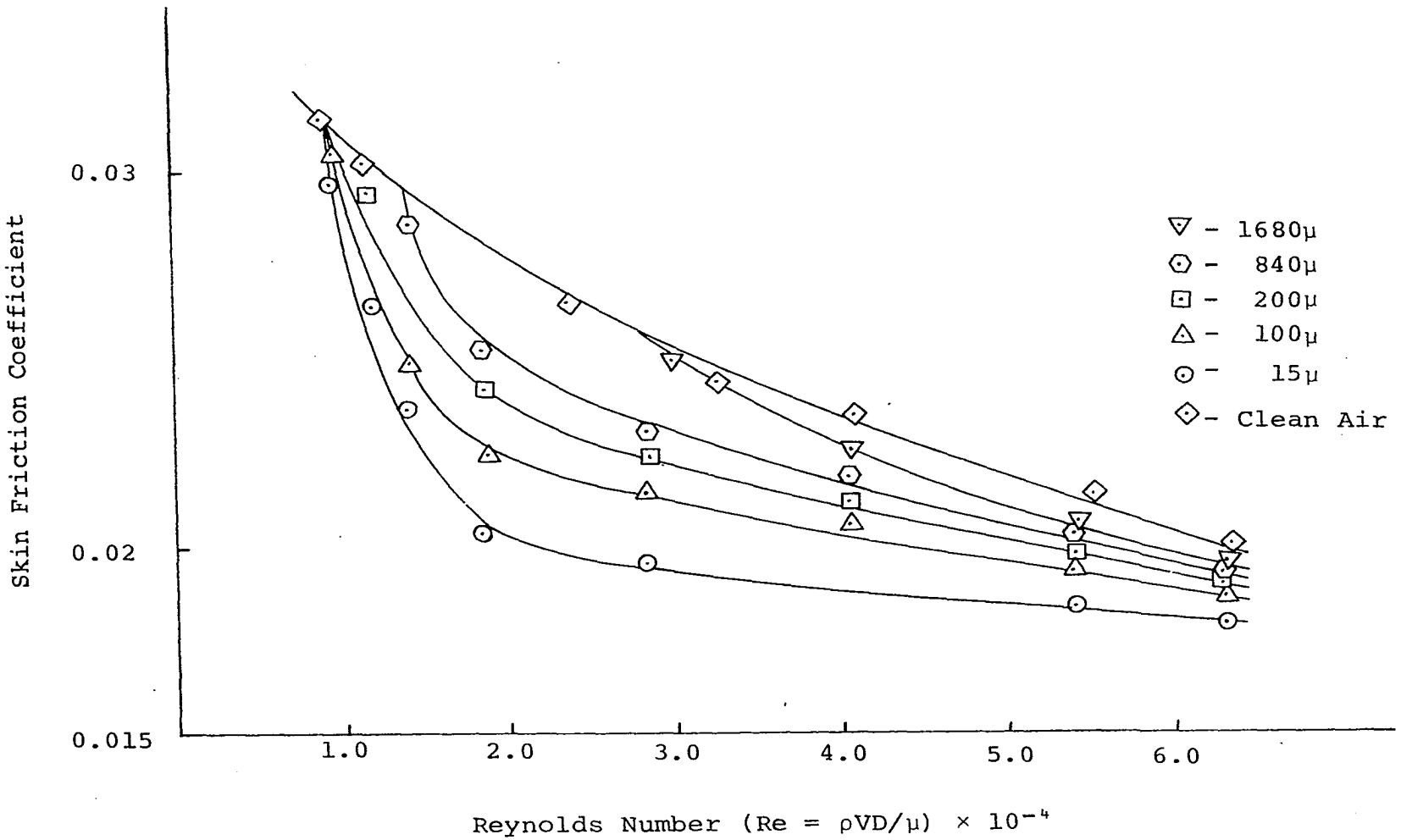

Figure (7.7) Friction Resistance of a Smooth Circular Pipe in Dusty Air Weight Flow (2 lb./min.).

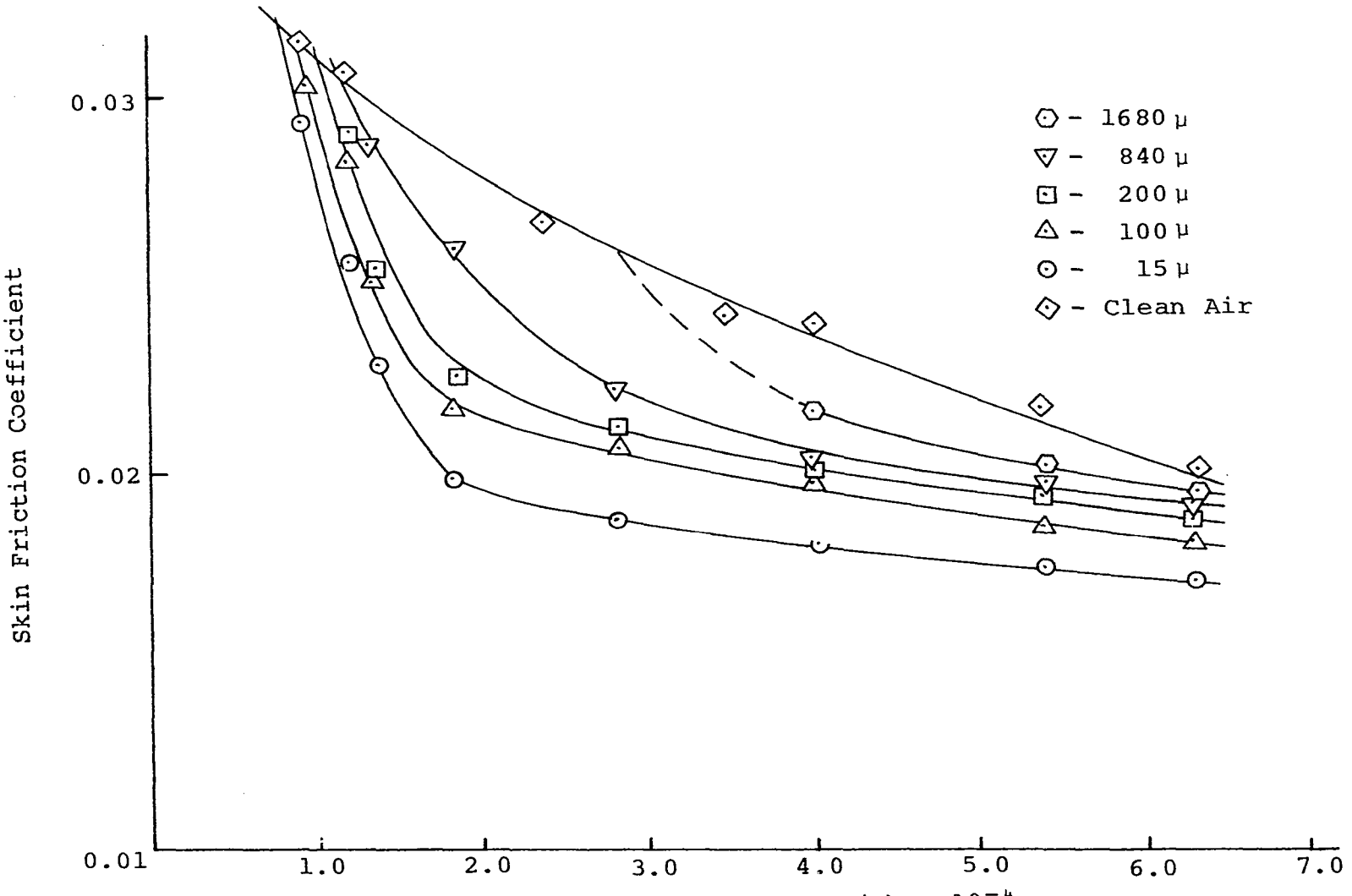

Figure (7.8) Friction Resistance of a Smooth Circular Pipe in Dusty Air (W = 3.0 lb./min.)

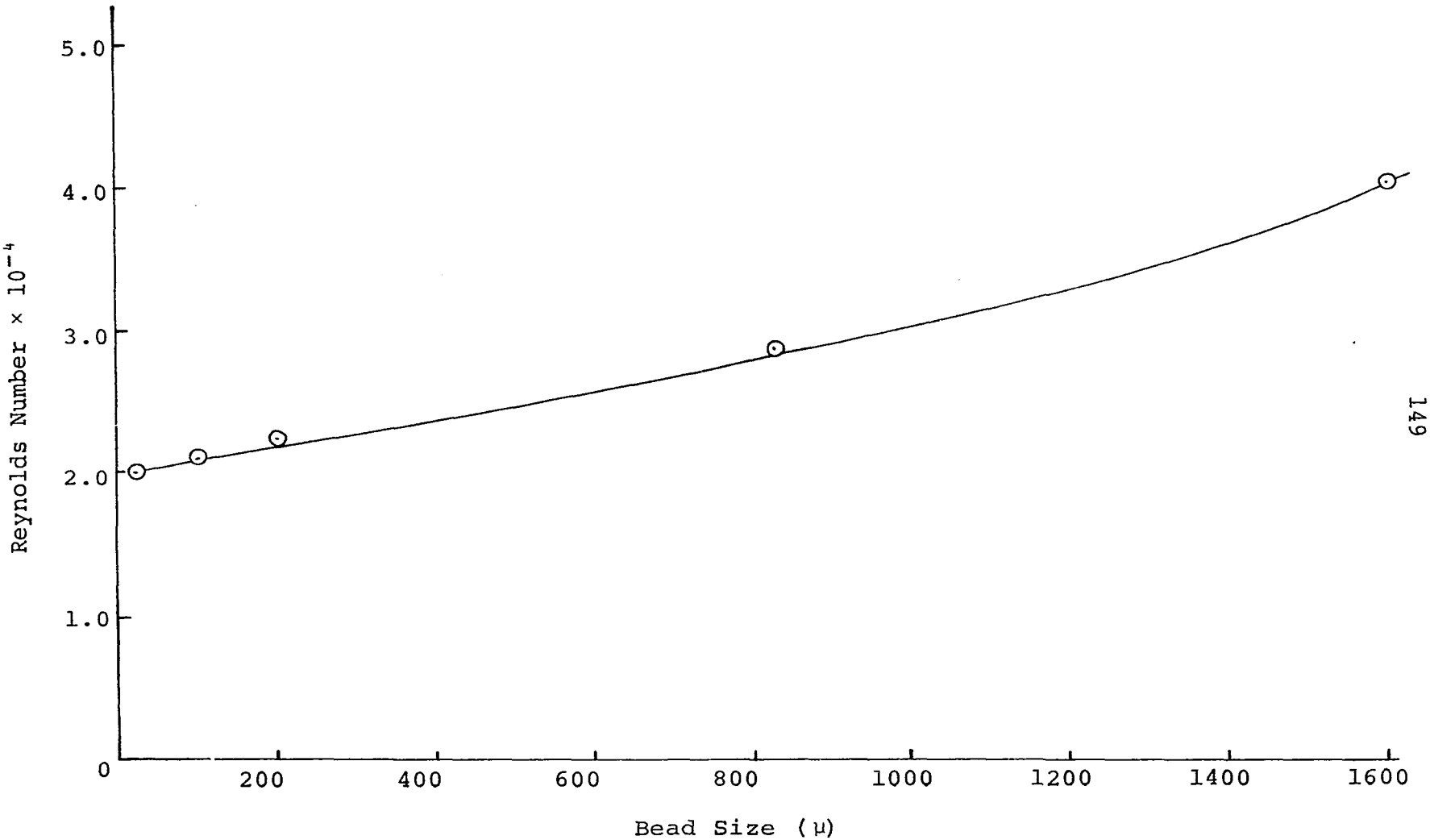

Figure (7.9) Reynolds Number For Maximum Drag Reduction For Circular Pipe Flow at Various Particle Sizes.

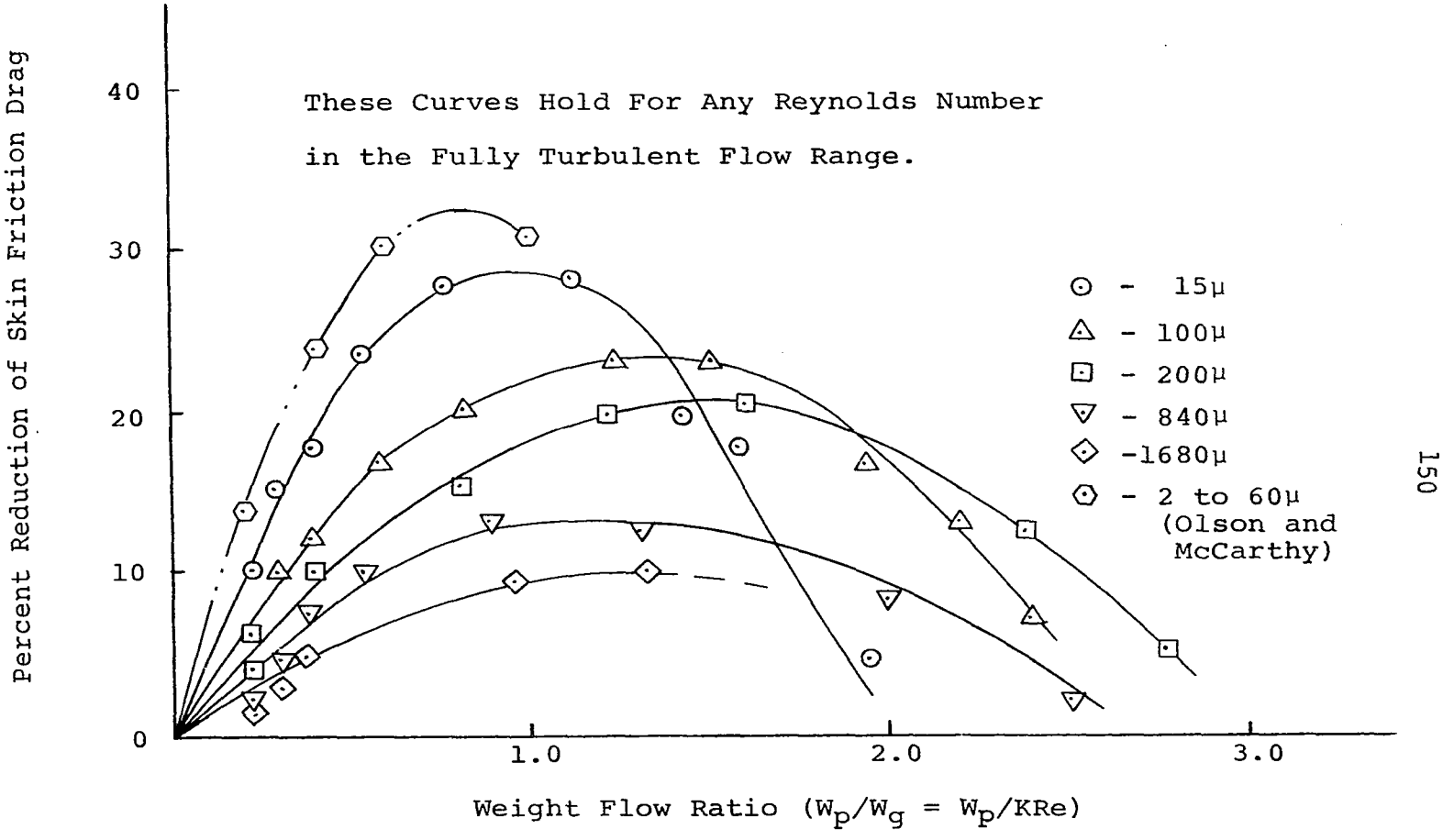

Figure (7.10) Reduction of Skin Friction Drag in Circular Pipe at Various Weight Flow Ratios.

Figure (7.10) shows the effect of the weight-flow ratio on percent reduction of the skin-friction drag. A comparison is also shown with the data of Olson and McCarthy (33) for 2 to 60 micron size particles. The weight-flow ratio giving maximum change in skin-friction drag is about 1.0 to 1.5 for all particles sizes. The weight-flow ratio may also be written in terms of Reynolds number. This relationship is obtained as shown:

$$\frac{W_p}{W_g} = \frac{W_p}{\frac{\rho AV}{\mu}\mu} \tag{7.1}$$

Therefore,

$$\frac{W_p}{W_g} = \frac{W_p}{KRe} \tag{7.2}$$

where $K = \mu\pi d/4$. In this manner Figure (7.10) can be used to calculate the percent reduction in drag for any pipe size and flow, thus making Figure (7.10) a very versatile and useful reference.

Flow Over a Flat Plate

The drag of the flat plate was first measured in clean air as described in Chapter 5. The close agreement achieved between these results and those obtained by other researchers indicated that the accuracy of the system was adequate. The next step was connecting the particle feed system. This system blew air and particles up from the floor of the tunnel into the main air stream. To be absolutely sure that the skin-friction variation on the flat plate was due to the particles suspended in the air stream and not due to the injected air,

the experiment was first conducted with the feed system blowing clean air through the slot in the floor of the wind tunnel. The tunnel was started and drag measurements on the flat plate were observed with the mixture of the two flow streams flowing over the plate. There was no significant change in the drag observed. Thus it was now possible to let the blower inject into the main stream a mixture of particles and air, and to evaluate the effect of the particles on the drag of the flat plate.

The particles suspended in the air stream reduced the skin-friction drag on the flat plate in a manner very similar to that experienced in the circular pipe flow. The weight flow of the particles was based on the amount of particles just above the plate and within the boundary layer. Therefore, to obtain the effective weight flow of the particles the actual weight flow measured was multiplied by the ratio of two areas. The first area was based on the flat plate width and the boundary layer of the plate and the second was based on the wind tunnel width and the particle layer, which varied from 2 to 4 inches. The factors which were prominent in the pipe flow study were also prominent in the case of the flat plate, i.e., Reynolds number, weight-flow ratio, and particle size.

Figures (7.11) through (7.16) show the effect of particle flow in reducing the skin-friction drag over a flat plate. The particle size was varied from 100 microns to 1680 microns. The silica flour was not used since there was no really adequate way of recovering the particles. The min-

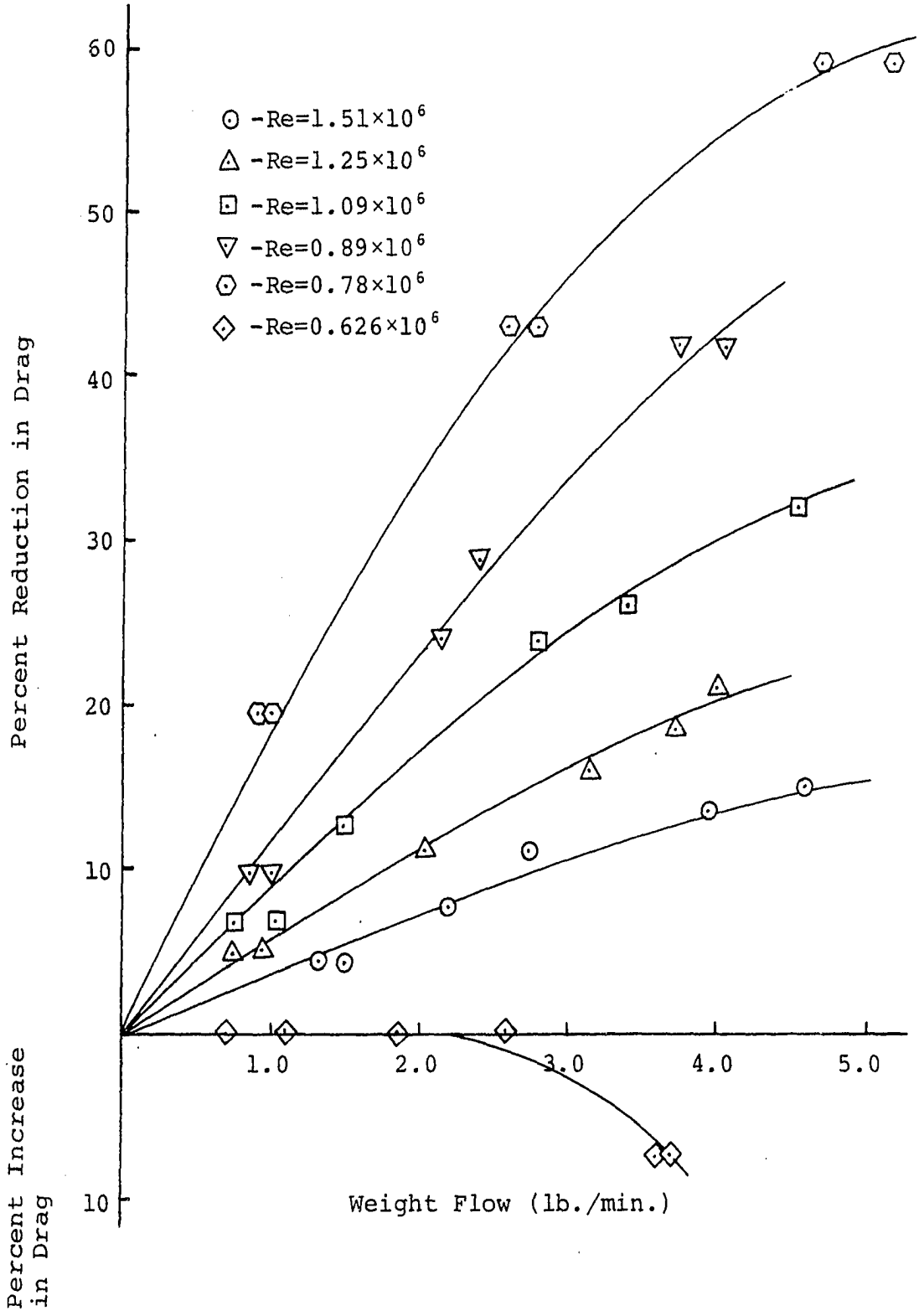

Figure (7.11) Reduction of Skin Friction Drag for a Smooth Flat Plate (100μ).

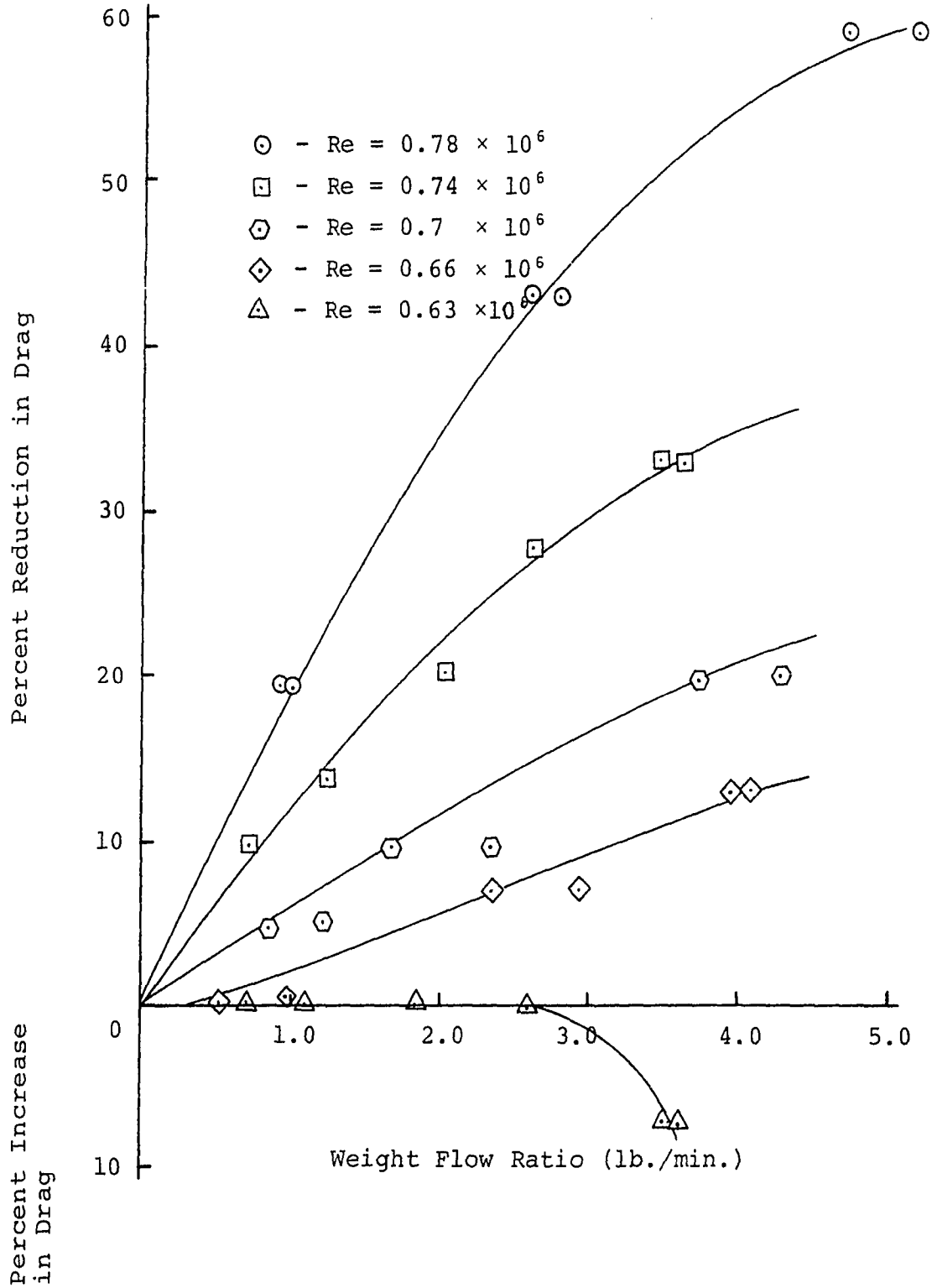

Figure (7.12) Reduction of Skin Friction Drag for a Smooth Flat Plate (100μ).

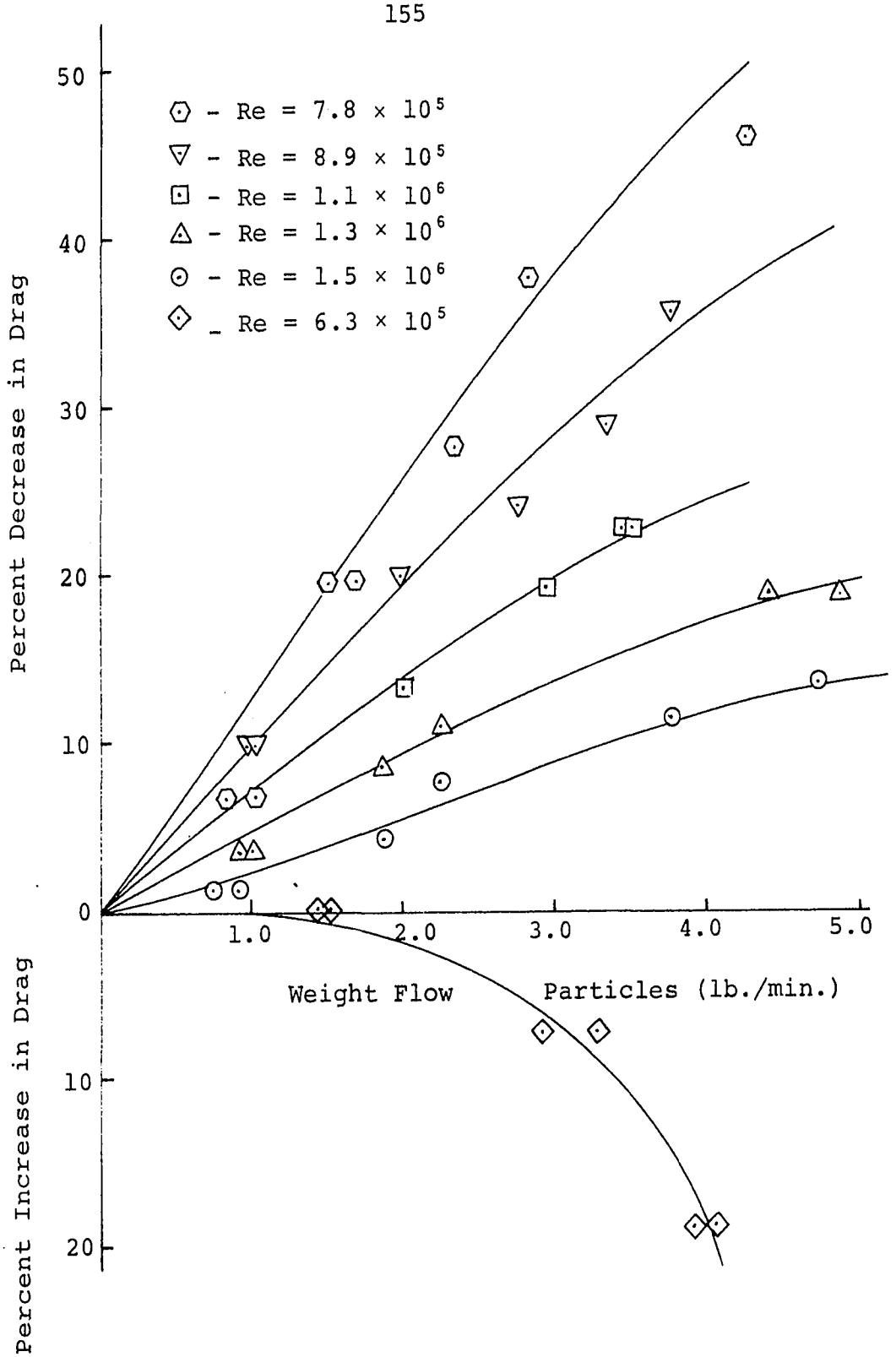

Figure (7.13) Reduction of Skin Friction Drag For a Smooth Flat Plate (200μ).

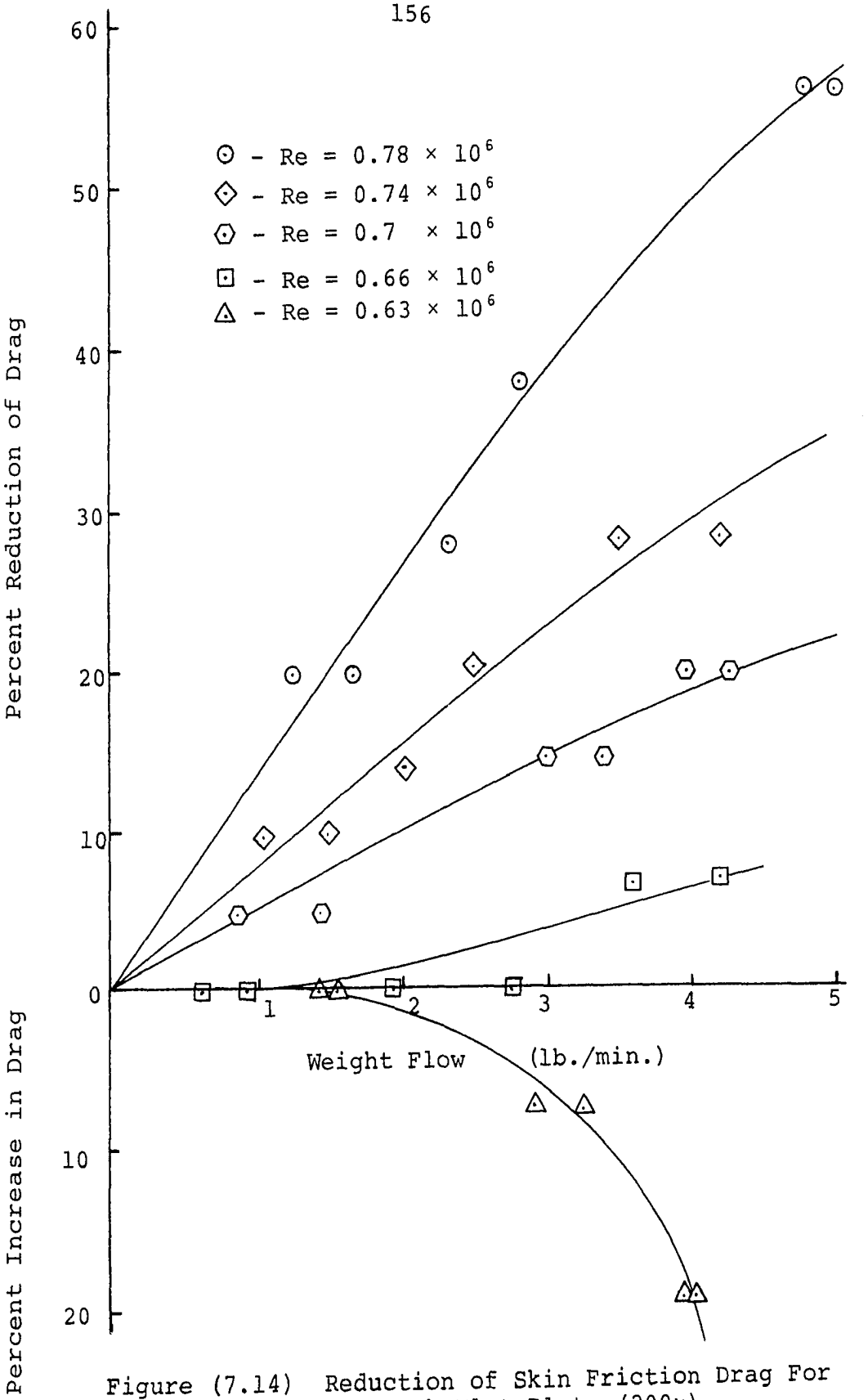

Figure (7.14) Reduction of Skin Friction Drag For a Smooth Flat Plate (200μ).

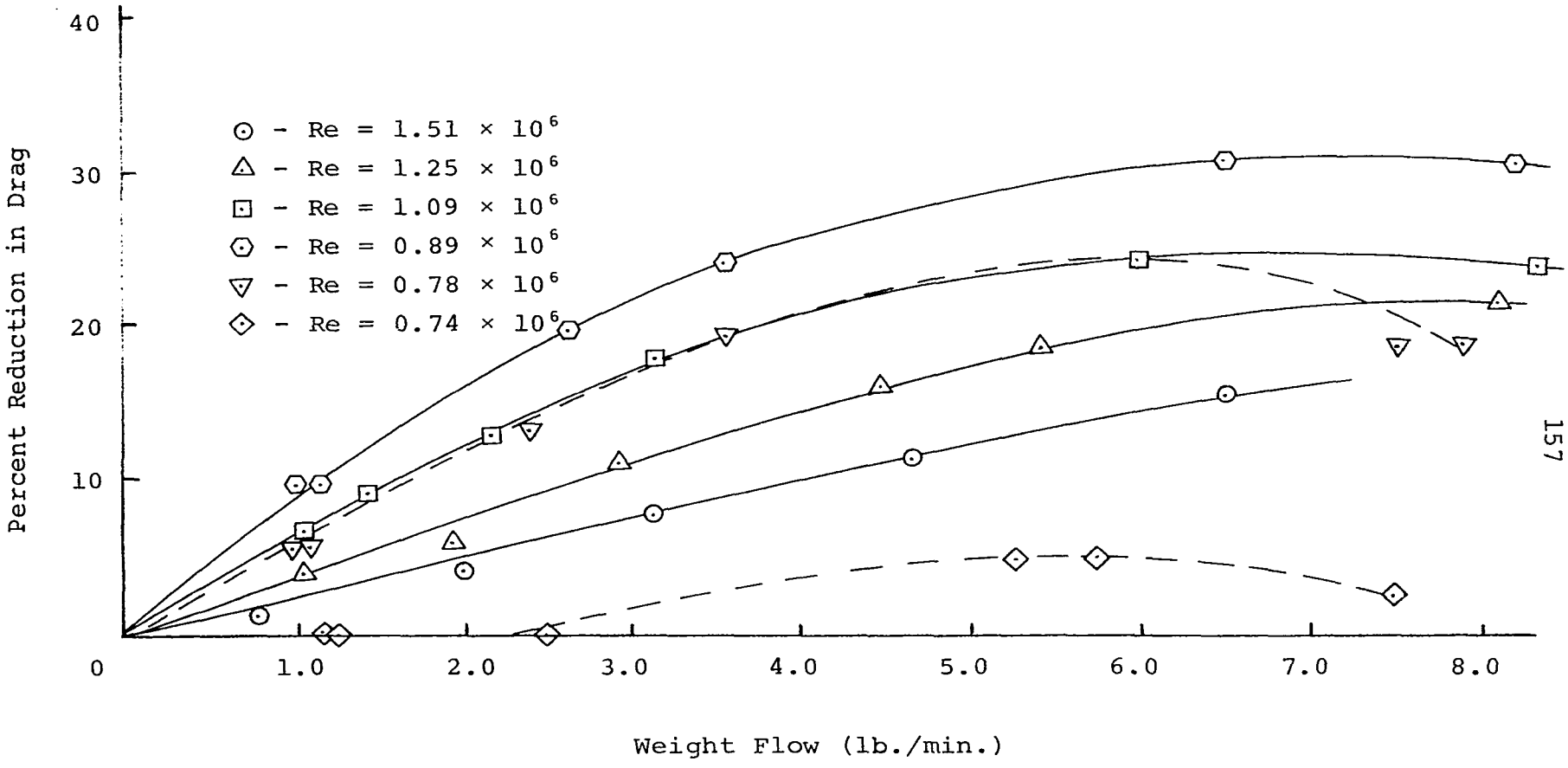

Figure (7.15) Reduction of Skin Friction Drag for a Smooth Flat Plate (840μ).

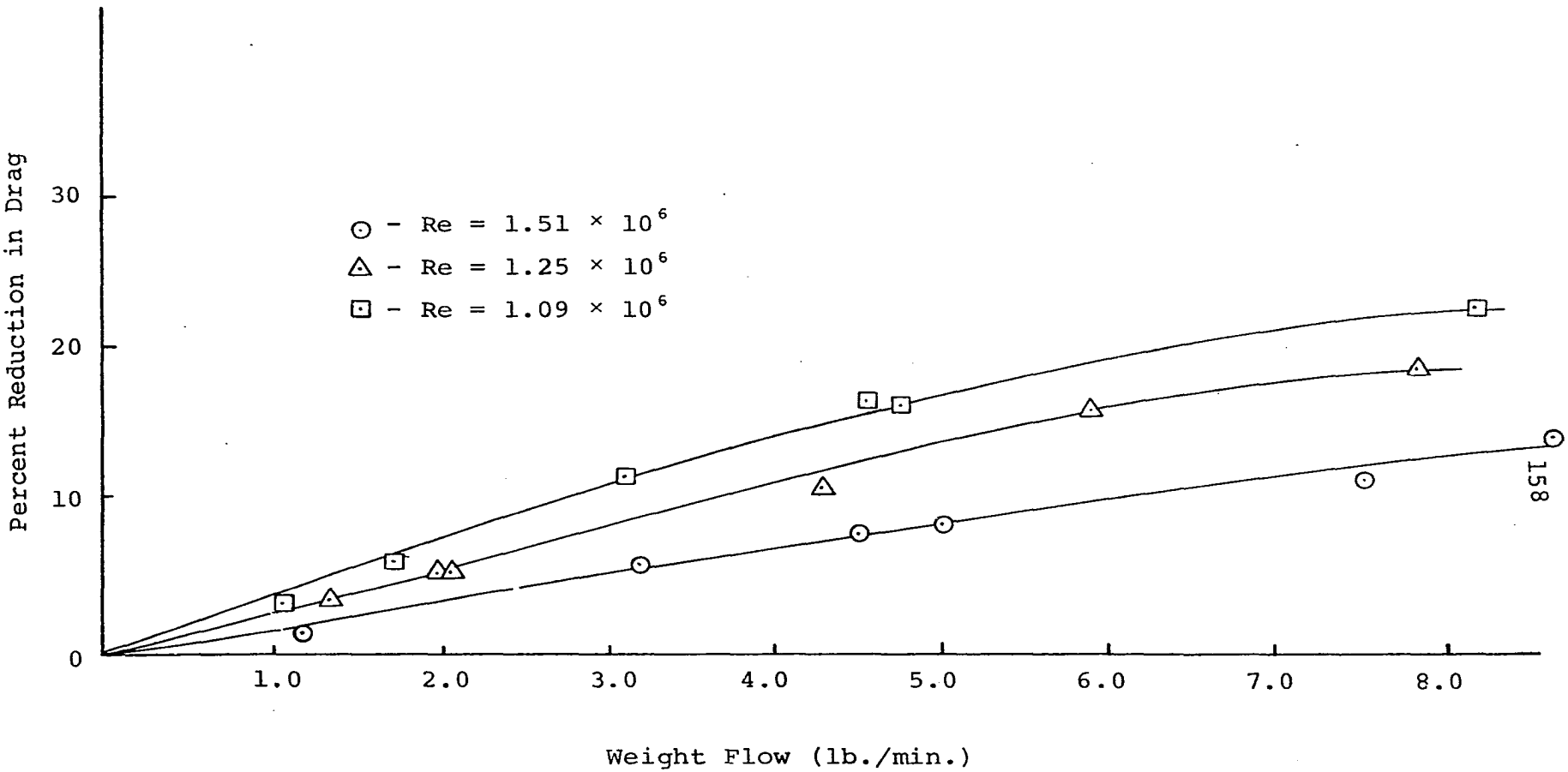

Figure (7.16) Reduction of Skin Friction Drag for a Smooth Flat Plate (1680μ).

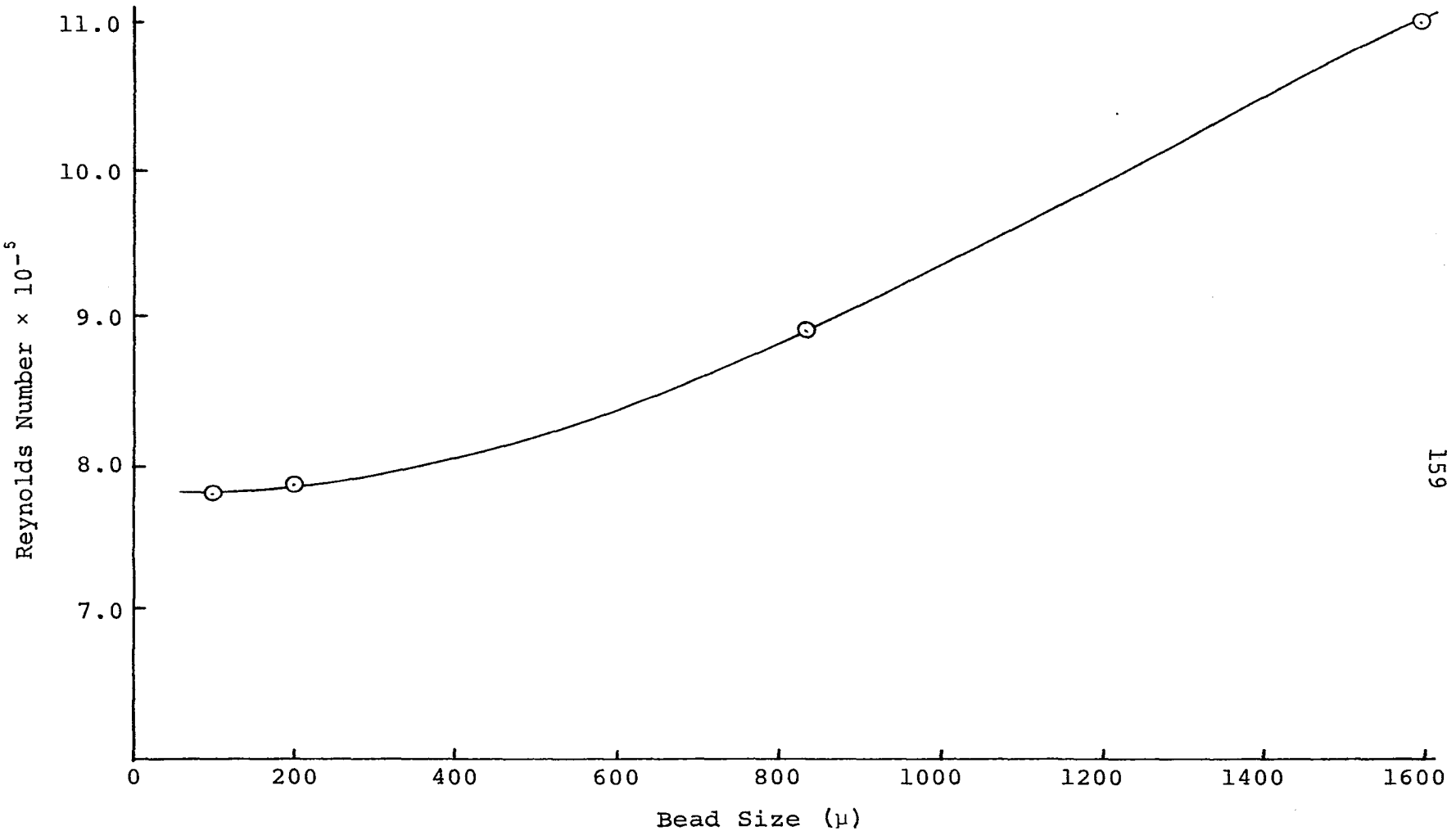

Figure (7.17) Reynolds Number For Maximum Drag Reduction For Flat Plate Flow at Various Particle Sizes.

imum reduction in skin-friction drag existed at Reynolds numbers at the low end of the turbulent flow region. Figure (7.17) shows the effect of particle size on the Reynolds number for maximum drag reduction. The effect of particle size was also similar to the pipe flow experiment, the smallest particle size giving the largest reduction in drag at the same weight-flow of the particles. Figures (7.18) through (7.20) show this effect. It should also be pointed out that at the high Reynolds number the change in skin-friction drag is not as significant. This agrees with the trend shown previously in the pipe flow experiment, both in this report and in the thorium oxide aqueous solution experiment carried out by Thomas (23).

The effect of weight-flow ratio on the skin-friction drag is shown in Figure (7.21). The weight-flow ratio may be modified, as in the case of the circular pipe flow, to be a function of Reynolds number and plate size as shown by the following relationships:

$$\frac{W_p}{W_g} = \frac{W_p}{\rho V A} \tag{7.3}$$

$$\frac{W_p}{W_g} = \frac{W_p}{(\rho V \delta)(w_d)(\frac{\mu}{\mu})(\frac{x}{x})}$$

$$\frac{W_p}{W_g} = \frac{W_p}{K(Re_x)} \tag{7.4}$$

where $K = \delta/x(w_d\mu)$. In this manner it is now possible to evaluate the effect of particle flow on any size plate in a flow stream at zero angle of incidence.

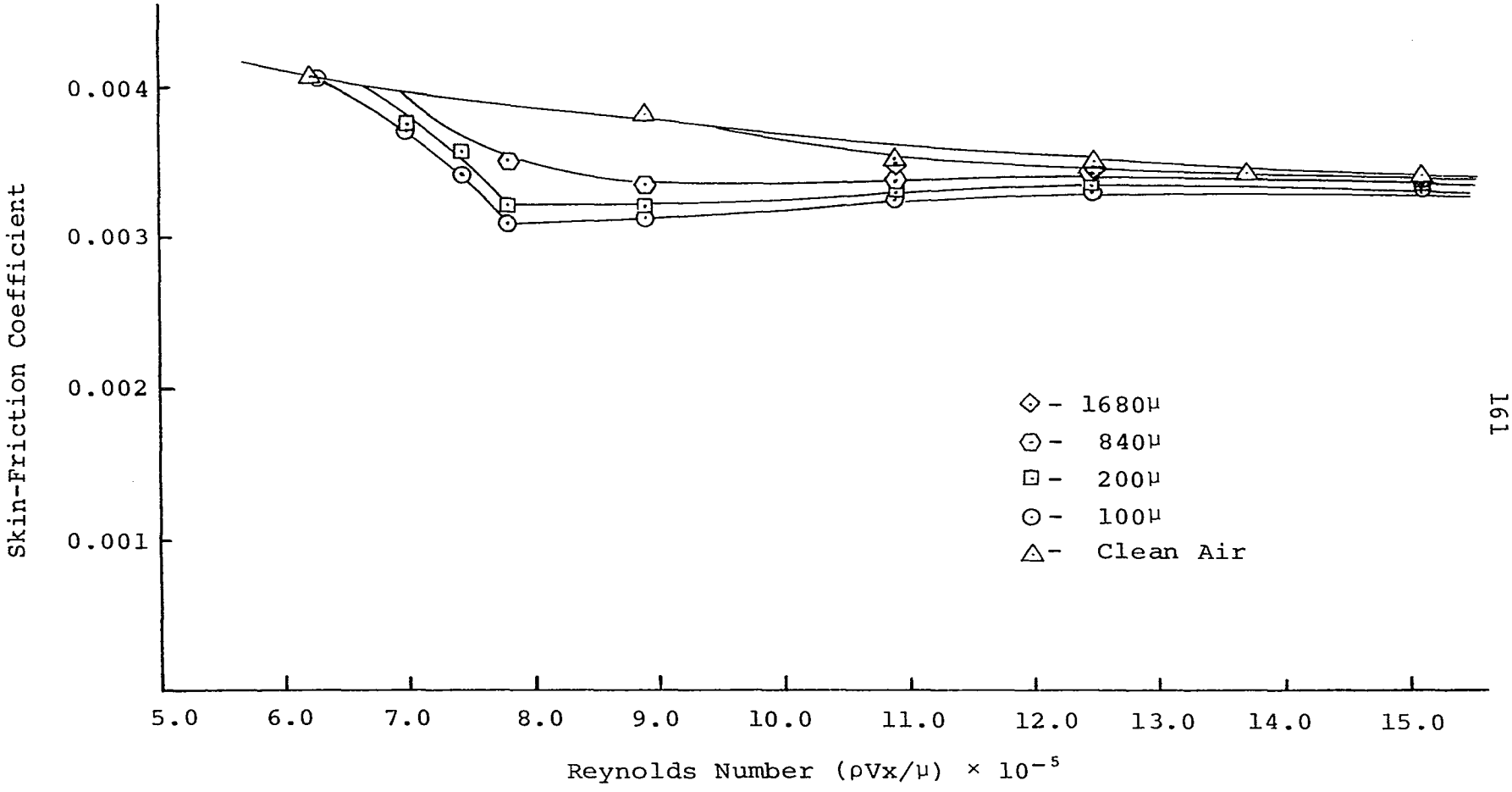

Figure (7.18) Friction Resistance for a Smooth Flat Plate in Dusty Air (W_p = 1-lb./min.)

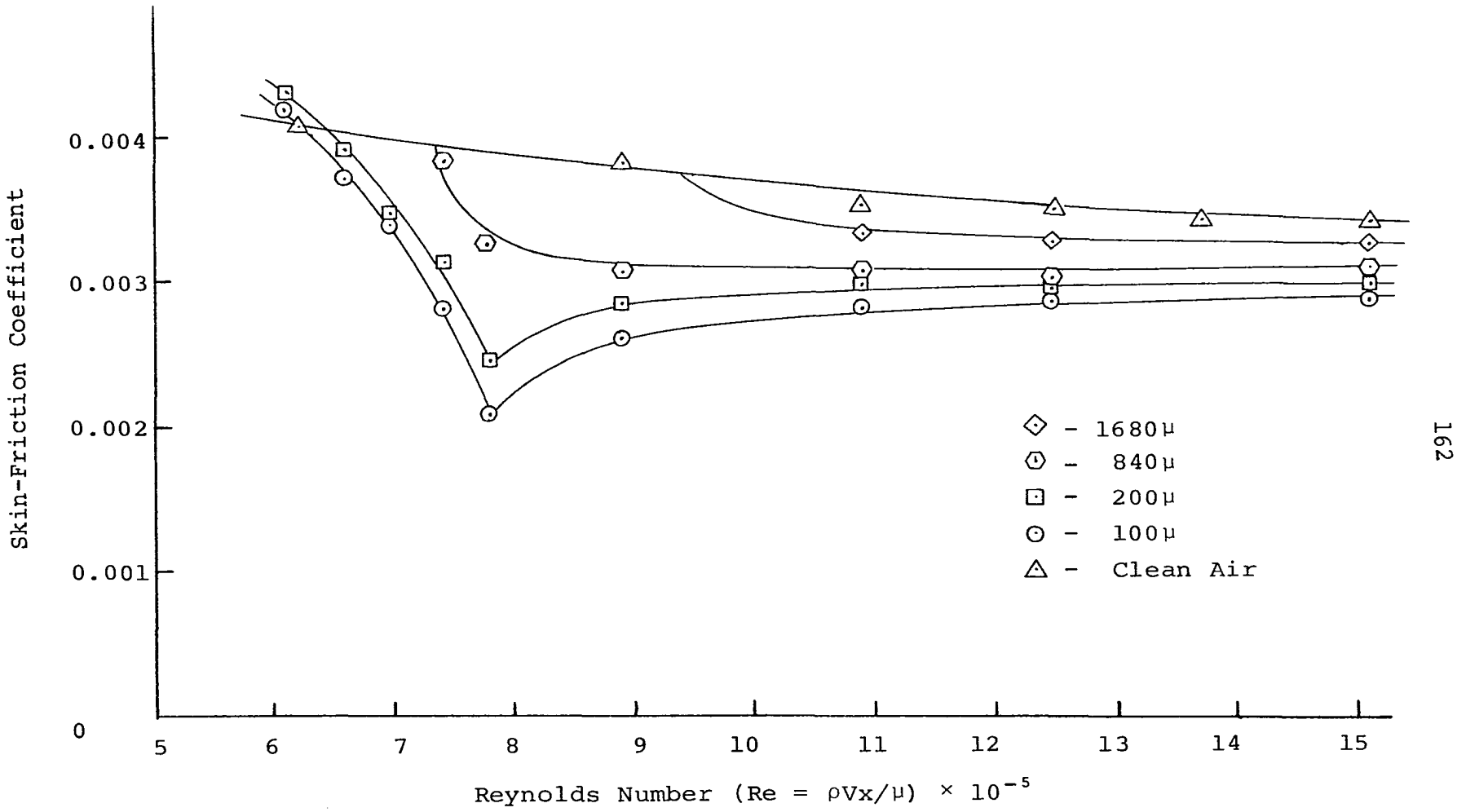

Figure (7.19) Friction Resistance for a Smooth Flat Plate in Dusty Air (W_p = 3-lb./min.).

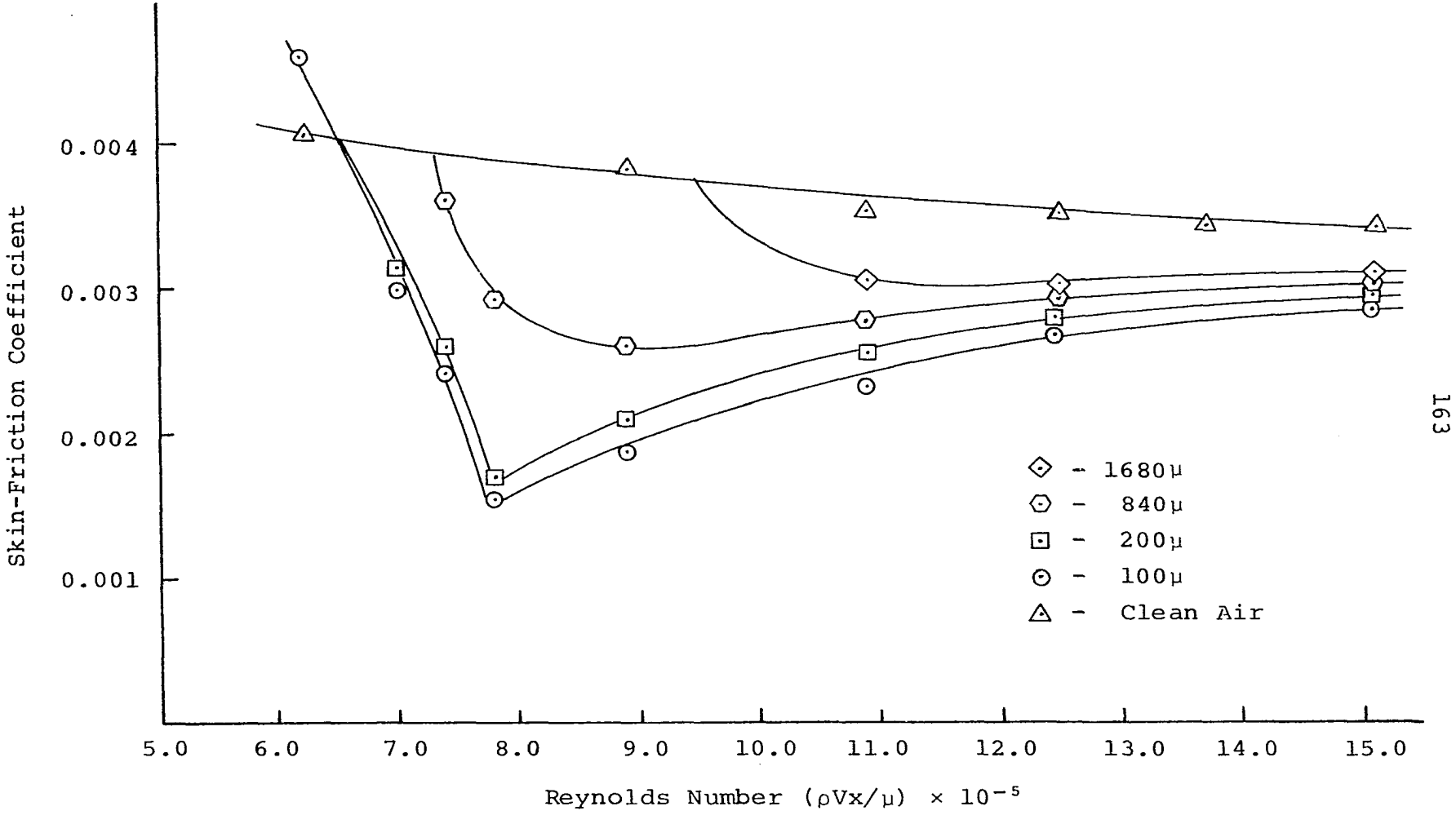

Figure (7.20) Friction Resistance for a Smooth Flat Plate in Dusty Air (W_p = 5-lb./min.)

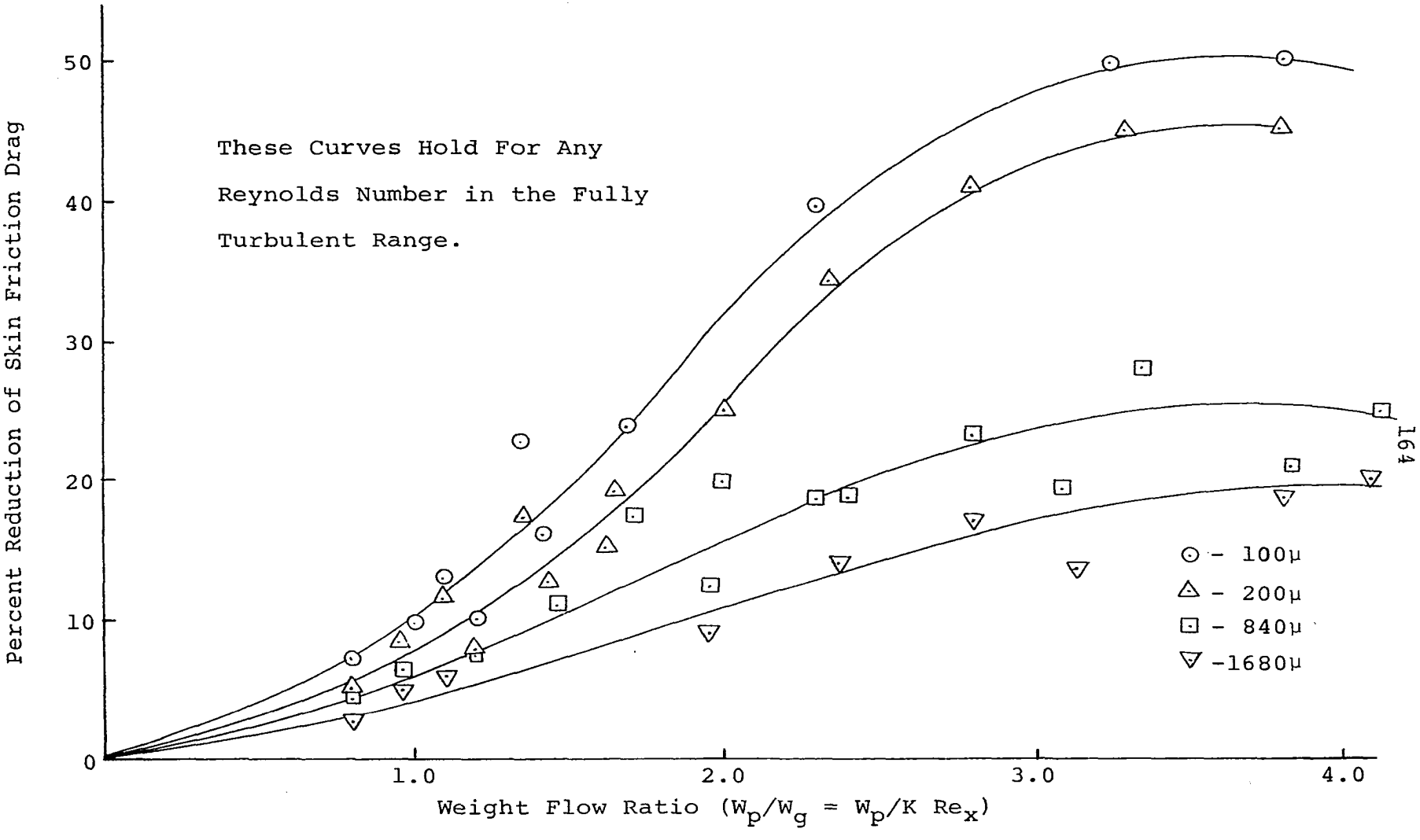

Figure (7.21) Reduction of Skin Friction Drag For a Flat Plate at Various Weight Flow Ratios

Velocity of Particles

The velocity of particles in the air stream in the majority of previous investigations was assumed to be the same as the air stream. The assumption in most cases was quite accurate since the particle sizes under investigation were under 200 microns in diameter. The particle sizes under investigation in this report vary from 15 microns through 1680 microns in diameter, and therefore in this case the particles velocity plays an important role. Since, in this report, W_p/W_g was varied from 0.0 to 3.0 in the circular pipe experiments, it was important to investigate whether or not at the high weight-flow ratio there was an interaction between the particles, thus effecting their velocity.

Velocity of particles in the circular pipe. The photographs of the flow in the circular pipe were taken in the center of the channel. Thirty photographs were taken at various air velocities and different particle sizes. Figure (7.22) shows the velocity of the particles at various particle sizes.

As one may have observed in both these Figures no values are given for the weight-flow ratio. This is due to the fact that no variation was found to exist between the particle-air velocity ratio and the particle-air weight-flow ratio. This indicated that there was very little interaction between the particles. Also from the Figures (7.22) and (7.23) it is obvious that the velocity ratio is only a function of particle size.

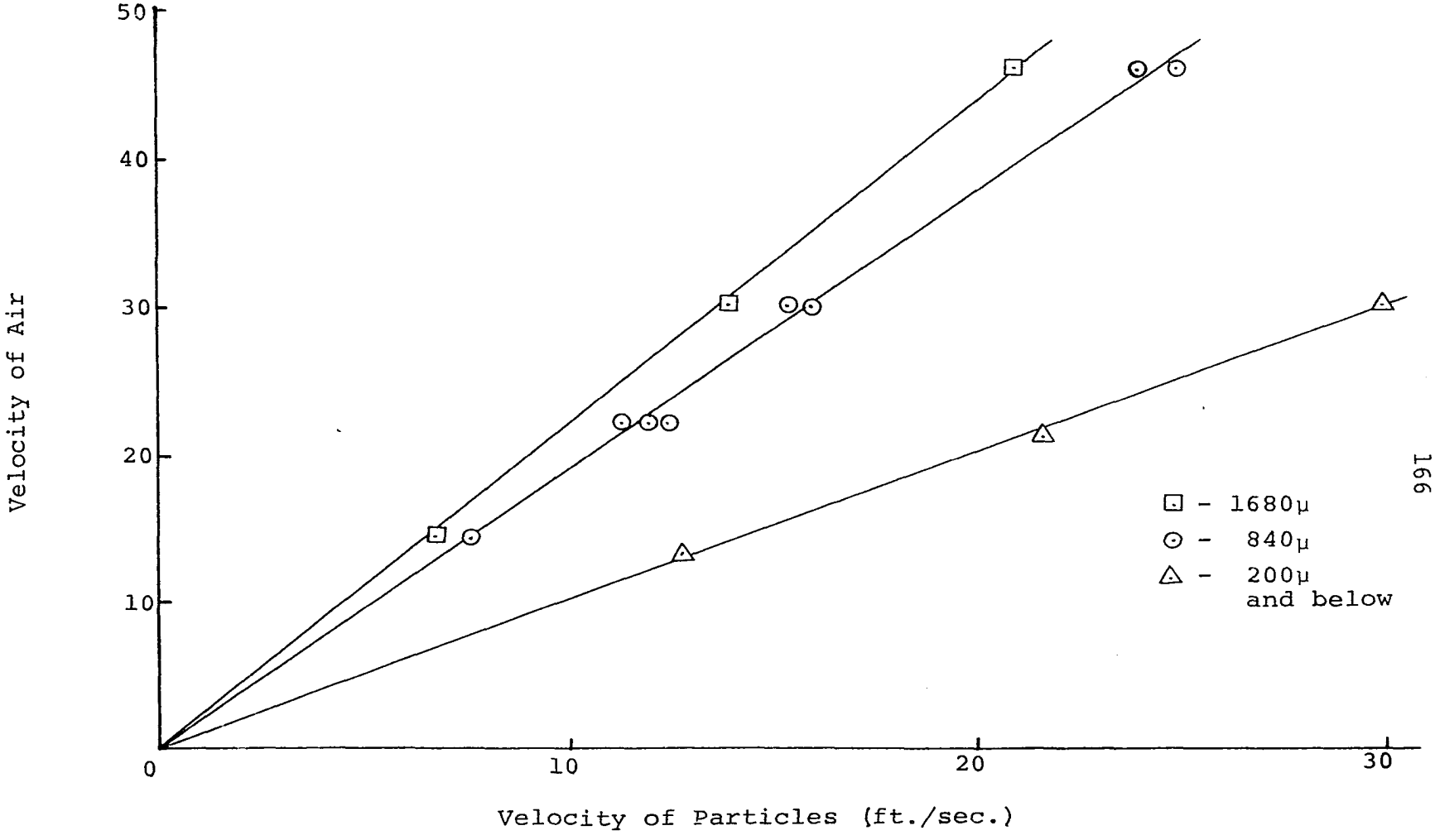

Figure (7.22) Velocity of Particles in a Circular Pipe.

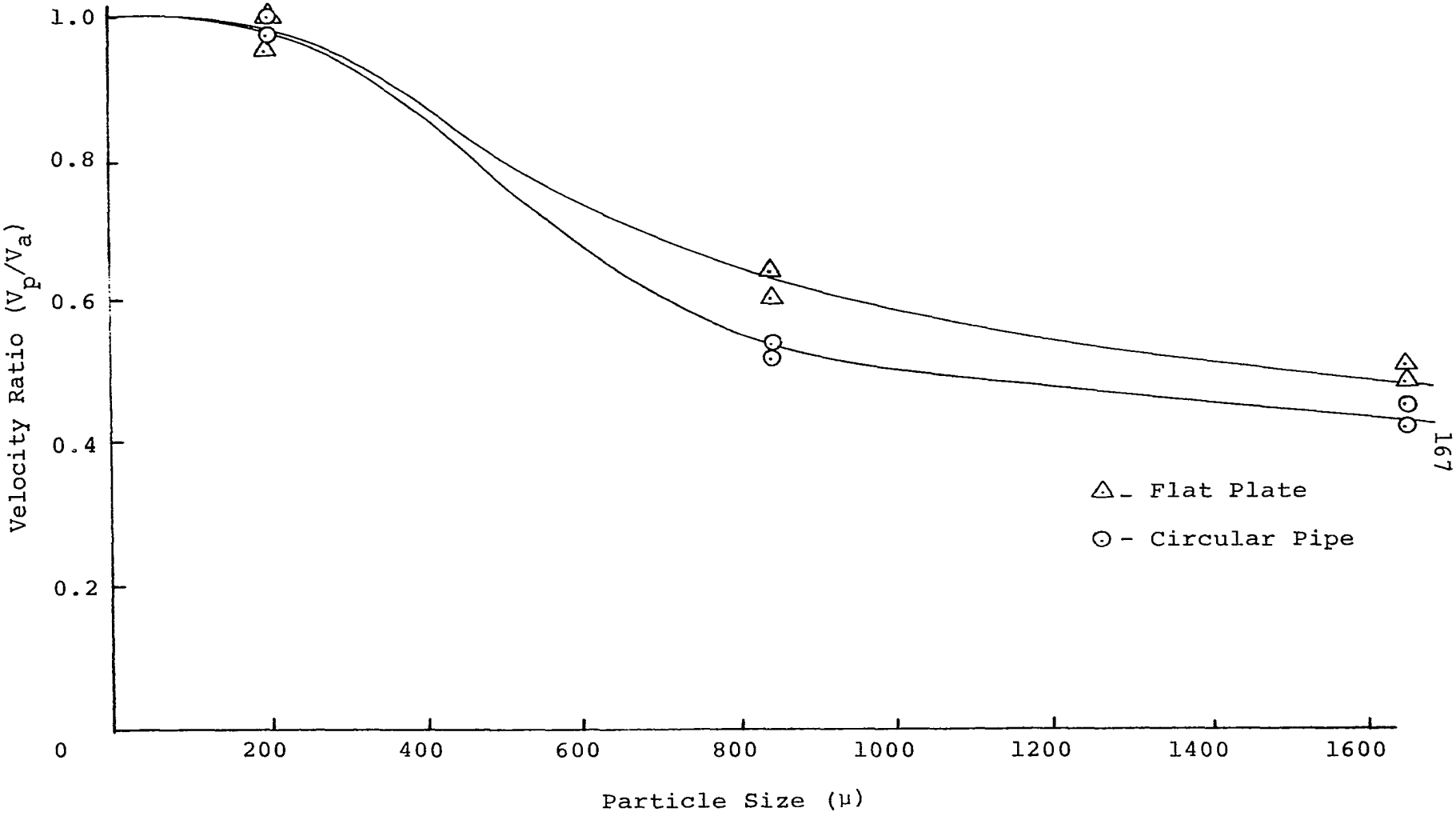

Figure (7.23) Velocity of Particles With Varying Particle Sizes.

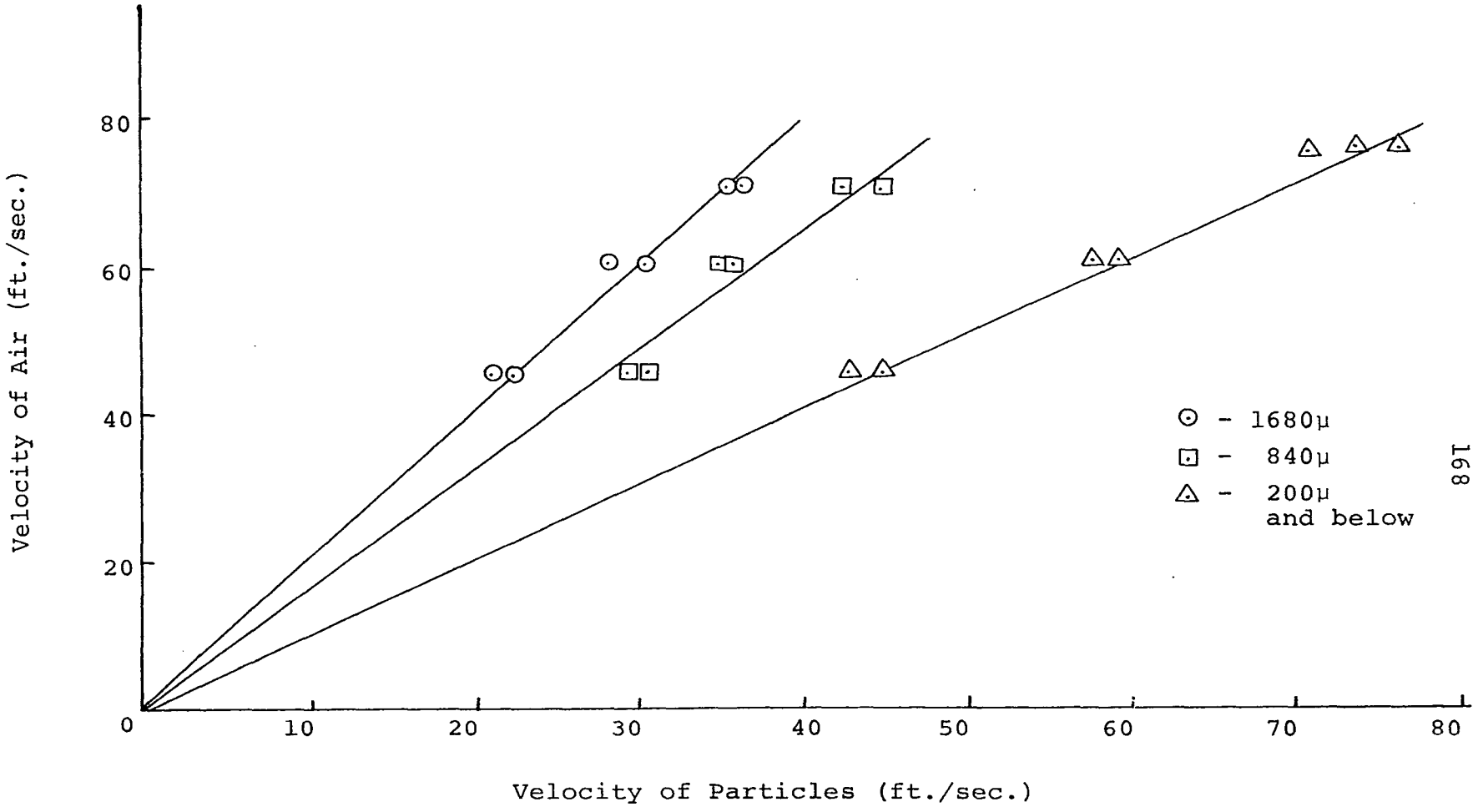

Figure (7.24) Velocity of Particles Over a Flat Plate.

Velocity of particles over a flat plate. The particles flowing over the flat plate were photographed at 4 inches above the plate in the center vertical plane of the wind tunnel. Figures (7.23) and (7.24) show the velocity of the particles as compared to the air stream. The velocity ratio is only a function of particle size as was the case in the circular pipe. The velocity ratio for the case of the flat plate was slightly greater for the same particle size than in the case of the circular pipe flow. This may be attributed to the fact that in the case of the flat plate the particles are injected into the flow stream with a finite forward velocity, while in the case of the circular pipe the initial injection velocity was zero in the forward direction. If the particle-air mixture did not have enough time to come into equilibrium on the flat plate, then the particle-air velocity ratio might read higher than for an equilibrium flow. Another possible reason for the higher particle-air mixture velocity ratio on the flat plate is that at a fixed elevation above the floor in the boundary layer, a deceleration of the flow exists in the downstream direction. The inertia effects of the heavy particles would tend to maintain a higher speed.

Discussion and Theory

The effect of adding dust to clean air flowing in a turbulent motion is the reduction of skin-friction coefficient of the surface in contact with it. Particle size, weight-flow ratio, and Reynolds number are the most important.

After examining the theory proposed by other researchers in this area, notably Lumley (36) and Saffman (28 and 29), it was felt that the Reynolds similarity parameter could be used to describe the flow phenomena in dusty air. Saffman (29), in his theoretical investigation of small size particle flow in dusty air, concluded that the change in density was a major factor contributing to the change in Reynolds number. Since his analysis was based on the fact that there was no slip velocity and no change in viscosity of the mixture, its application was rather limited.

The analysis outlined in this report assumes that, if an effective Reynolds number can be defined appropriately, the plot of skin-friction coefficient against effective Reynolds number would form a single curve regardless of particle size. The first step was the investigation of the effect of density change on Reynolds number. After calculating the Reynolds number based on the density of the mixture,

$$Re = \frac{(\rho_p + \rho_g) V_g L}{\mu},$$

and plotting it against the skin-friction coefficient, it was found that for the 100 micron and 200 micron particles a single curve could be drawn. However, for the smallest particle size the points fell below this curve, and for the larger particle sizes the points fell above the curve. Because there exists a slip velocity for the larger particles, the Reynolds number was further modified by taking into account the average velocity of the medium. This definition of the effective Reynolds

number,

$$Re = \frac{(\rho_p V_p + \rho_g V_g)\ L}{\mu},$$

tended to bring in line the points of the larger particle sizes. However this change did not account for the smallest particle size because for these particles no slip velocity exists. A check was made to see if the results obtained for the smallest particle size were correct. Figure (7.10) shows that the results compared favorably with that obtained by McCarthy and Olson. Also further checks with other published data indicated that the results were accurate. Therefore, if the assumption that the effective Reynolds number describes this flow phenomenon was to be correct then the viscosity of the gas had to be modified. From the graph it was noted that the viscosity was reduced for the dust cloud (smallest size particles) and was increased for the large size particles suspended in the air stream.

The calculation of the viscosity of the particle-air mixture varies considerably with the particle size. In the experiments conducted here there were basically two types of flow. The first type of flow consisted of a "cloud of particles" suspended in an air stream. The second type of flow consisted of a dilute system of large sized spheres suspended in an air stream. The two systems will be treated differently since no single equation adequately gives the viscosity of the mixture.

The case of the dilute system of spheres has been examined in detail by many researchers. The best known of the numerous viscosity formulae is the Einstein formula (48). The Einstein Equation is based on the Stokes Equation, which holds for small Reynolds numbers. This equation is obtained by modifying the general Navier-Stokes Equation for a steady flow of an incompressible fluid. The steady Navier-Stokes Equation is:

$$\vec{V} \cdot \nabla\vec{V} = -1/\rho \nabla P + \eta/\rho \Delta\vec{V}. \qquad (7.5)$$

The term, $\vec{V} \cdot \nabla\vec{V}$ may be neglected if the Reynolds number is small, and the equation of motion reduces to a linear equation,

$$\eta\Delta\vec{V} - \nabla\vec{P} = 0 \qquad (7.6)$$

The effect on a single sphere immersed in a fluid having a constant velocity gradient, was then considered. The unperturbed flow was described by a linear velocity profile. With these conditions Stokes Equation was solved for the velocity and pressure. To calculate the effective viscosity the next step was the calculation of the mean value of the momentum. The calculation is based on a single particle fully immersed in the fluid. Since the concentration of the suspension is small the results can be multiplied by the concentration of the suspension. The following equation is obtained for the effective viscosity as shown in Landau and Lifshitz (45):

$$\mu_{pg} = \mu[1 + (5/2)\phi] \qquad (7.7)$$

where $\phi = (1/6)a^3N_p$, the ratio of the total volume of the sphere to the total volume of the suspension.

The Einstein formula, as shown above, is restricted to a dilute system of large spheres, thus holding only for Knudsen numbers tending to zero,

$$Kn = \lambda/a \rightarrow 0 \qquad (7.8)$$

which also indicates that the flow is considered to be physically continuous.

For the flow consisting of a cloud of particles the Einstein formula does not hold since in this case the sphere sizes are very small and the concentration of the suspension large. Also examining the Knudsen number for these particles (Kn = 0.03) it is observed that the flow of gases in this range is called the slip flow. The Einstein formula holds in the continum flow range (Kn → 0) where the gas adjacent to the solid surface is at rest with respect to the surface, while for the dust cloud (Kn = 0.03) the phenomenon of slip occurs. This signifies that the gas adjacent to the solid surface is no longer at rest but has a tangential velocity. Thus it is obvious that the Einstein relationship does not hold in this range. It may be deduced from the above arguments that the viscosity of the mixture should be a function of the Knudsen number and the ratio of the total volume of the spheres to the total volume of the suspension:

$$\mu_{pg} = f\ (Kn, \phi) \qquad (7.9)$$

The results obtained by Sproull (20) and Soo (31) indicate that for the dust cloud a reduction in viscosity was observed. The results obtained by the experiments in this

project also indicate a similar trend for the smallest particles tested. The explanation of this phenomenon is not entirely understood.

To explain this phenomenon various attempts have been made to extend the results of single particles to a cloud of small sized particles with no success. Even the use of Oseen's (31) Equation which included inertia terms in the field away from the body, or the Proudman and Pearson (49) Equation which treated the problem by matching different series expansions in the flow regions near and away from the spherical body, do not hold when extended to a cloud of particles. One of the reasons forwarded to explain why the extension of single particles does not hold has been given by Soo (31). He shows that for a high volume of particles "the interaction of the boundary layer of adjacent particles plays an important part and the wakes may actually disappear, thus altering the drag coefficient."

The treatment of the dust cloud as a true continuum is also subject to much controversy since in a true continuum flow not only would the gas impart its momentum to the particles but the dust cloud would in turn transfer its momentum to the gas. Soo (31) points out that if this were true then in a diffusion process, as the particles were slowed down, they would contribute to the pressure rise. However, as shown by many researchers in the field, this does not always happen.

The above reasons, together with the fact that the results for the dust cloud indicated that a reduction in viscosity took place, led other researchers and the author to examine and extend the kinetic theory of gases to this phenomenon. It was apparent that the determination of the viscosity based on this theory without the knowledge of the motion of the other components is not completely valid and that its extension to gas-solid suspensions of particles larger than the mean free path length of the gas cannot be theoretically justified. Nevertheless, the results obtained by using it verify the data obtained by the author and various other researchers.

The kinetic theory of gases is usually only applicable for the case of gas molecules of one gas colliding with molecules of another gas. However, as pointed out previously, by extending this to gas molecules colliding with very small dust particles, the change in viscosity of the gas-particle mixture can be determined. The kinetic theory (46) states that viscosity, μ, is given by:

$$\mu = (1/3)\rho\bar{C}\lambda \qquad (7.10)$$

where ρ is the gas density, $\bar{C}$ the average molecular velocity, and λ the mean free path. The mean free path in simple kinetic theory is given by:

$$\lambda = 1/(\sqrt{2}\pi N a^2) \qquad (7.11)$$

where N is the particle number density and a is the particle diameter.

Assuming that the dust cloud is regarded as a second gas mixing with the true gas in which it is suspended, one can

compute the mean free path length, λ_g, of the gas molecules in the dust-laden gas by (46):

$$\lambda_g = \frac{1}{\sqrt{2}\pi(N_g a_g^2 + N_p a_p^2 \sqrt{1 + m_g/m_p})} \qquad (7.12)$$

By examining the above equation it can be noted that, since m_g is much smaller than m_p, the value under the radical reduces to 1.0. Thus the change in mean free path length depends on the magnitude of the term $N_p a_p^2$ which varies in magnitude from about 5 to 15 percent of the term, $N_g a_g^2$. Calculating the viscosity of the suspension based on this new mean free path length of the gas a reduction in the viscosity of the gas flowing over the plate is observed. The above method was used by Sproull (20) with the difference that he assumed a very large boundary layer around each particle thereby obtaining a reduction in viscosity of about 50 percent. Soo (31) suggests the use of the following equation:

$$\frac{1}{\mu_m} \simeq \left[\frac{(x_1)^2}{\mu_{11}} + \frac{2x_1x_2}{\mu_{12}} + \frac{(x_2)^2}{\mu_{22}} \right] [1 + f(x_1, x_2, \mu_1, \mu_2, m_1, m_2)] \qquad (7.13)$$

where x_1, x_2 are the mole fractions based on number densities of components; m_1, m_2 are the molecular or particle masses, and μ_{11} is the viscosity of interaction between particles of the same species. This equation was obtained by Hirschfelder, Curtiss, and Bird (50) for a binary mixture. The equations hold for species of particles whose size is smaller or of the same order of magnitude as the mean free path length, thus placing on it the same restrictions that hold for the kinetic

theory of gases. Equation (7.13) also points to a reduction in viscosity. The reason this equation was not used was that there was not enough data to fully explain all the terms in it.

The Reynolds number for clean air is as follows:

$$Re = \frac{\rho V L}{\mu} \tag{7.14}$$

Modifying it for the change in density and viscosity as outlined previously, the following relationship is obtained:

$$Re = \frac{(\rho_p + \rho_g) V_g L}{\frac{1}{3}\rho_g \bar{C}[\sqrt{2}\pi(N_g a_g^2 + N_p a_p^2)]^{-1}} \tag{7.15}$$

Based on this Reynolds number the new value of the skin-friction coefficient was calculated with the use of the Blasius Equation (5.4) or the Prandtl-Schlichting Equation (5.20) for turbulent flows, depending on whether the investigation was for the circular pipe flow or the flat plate flow respectively. Equation (7.15) works well for the fine dust particles whose motion follows the air motion closely. To show this the term σ is introduced. This term may be called the relaxation time of the dust, i.e., the time for the velocity of a particle to become adjusted to changes in the velocity of the air. Using Stoke's law for drag on the particles the value of σ is ascertained:

$$D = -3\pi\mu a V \tag{7.16}$$

Newton's law gives,

$$m \frac{dV}{dt} = -3\pi\mu a V$$

Integration gives,

$$\frac{V_2}{V_1} = e^{-3\pi\mu at/m} = e^{-t/\sigma}$$

where the value of σ is:

$$\sigma = \frac{m}{3\pi\mu a} = \frac{\rho(1/6)\pi a^3}{3\pi\mu a}$$

or finally:

$$\sigma = \frac{1}{18}\frac{\rho a^2}{\mu} \qquad (7.17)$$

For small sized particles the value of σ is much smaller than the turbulent time scale, and thus the dust follows the air motion closely. For the larger sized particles the relaxation time, " σ", will be comparable with or greater than the time scale of turbulent fluctuations and hence the dust particles do not follow the air motion but lag behind. This has been shown by the particle velocity pictures taken in both the circular pipe and the wind tunnel. This relative velocity of the particles and air causes an extra dissipation of the energy.

The change in viscosity of the larger particle sizes has to be accounted for differently, as shown earlier. There no longer exists a "fine dust cloud" which can be treated as another gas. Thus in this type of flow the Einstein formula for the viscosity of a suspension is used since the particle size is large and the volume ratio small. Therefore for the large sized particles (840 microns and 1680 microns) the Reynolds number is modified by three factors; one, the velocity of the air stream which is modified by the effect of the large relaxation time scale, two, the increase in density,

and three, the increase of the viscosity based on the Einstein formula. The new effective Reynolds number is therefore given by:

$$Re = \frac{(\rho_p V_p + \rho_g V_g)\ L}{\mu(1 + 5/12\ a^3 N_p)} \qquad (7.18)$$

where L is the length parameter suitable for each of the different apparatus.

If one assumes a priori that Reynolds similarity still holds for dusty gas, and if the effective Reynolds number is used, then it becomes possible to predict the skin-friction coefficient. Figures (7.25) and (7.26) show the results based on the assumption of Reynolds similarity and effective Reynolds number. The "theory" points on these curves were obtained from a Prandtl-Schlichting curve or a Blasius curve using the effective Reynolds number and then replotted using the clean air Reynolds number. The Kinetic theory of gases applies to only the smallest particle size (15 microns). At a particle size of 100 to 200 microns no effects of viscosity were observed from applying either system. For particle sizes over 200 microns the Einstein formula was used and this gave an increase in viscosity. The encouraging part of this correlation is the excellent trend that it shows as all three principal parameters (weight-flow ratio, Reynolds number, and particle size) are varied. There was found no other theory that could show any agreement with the results.

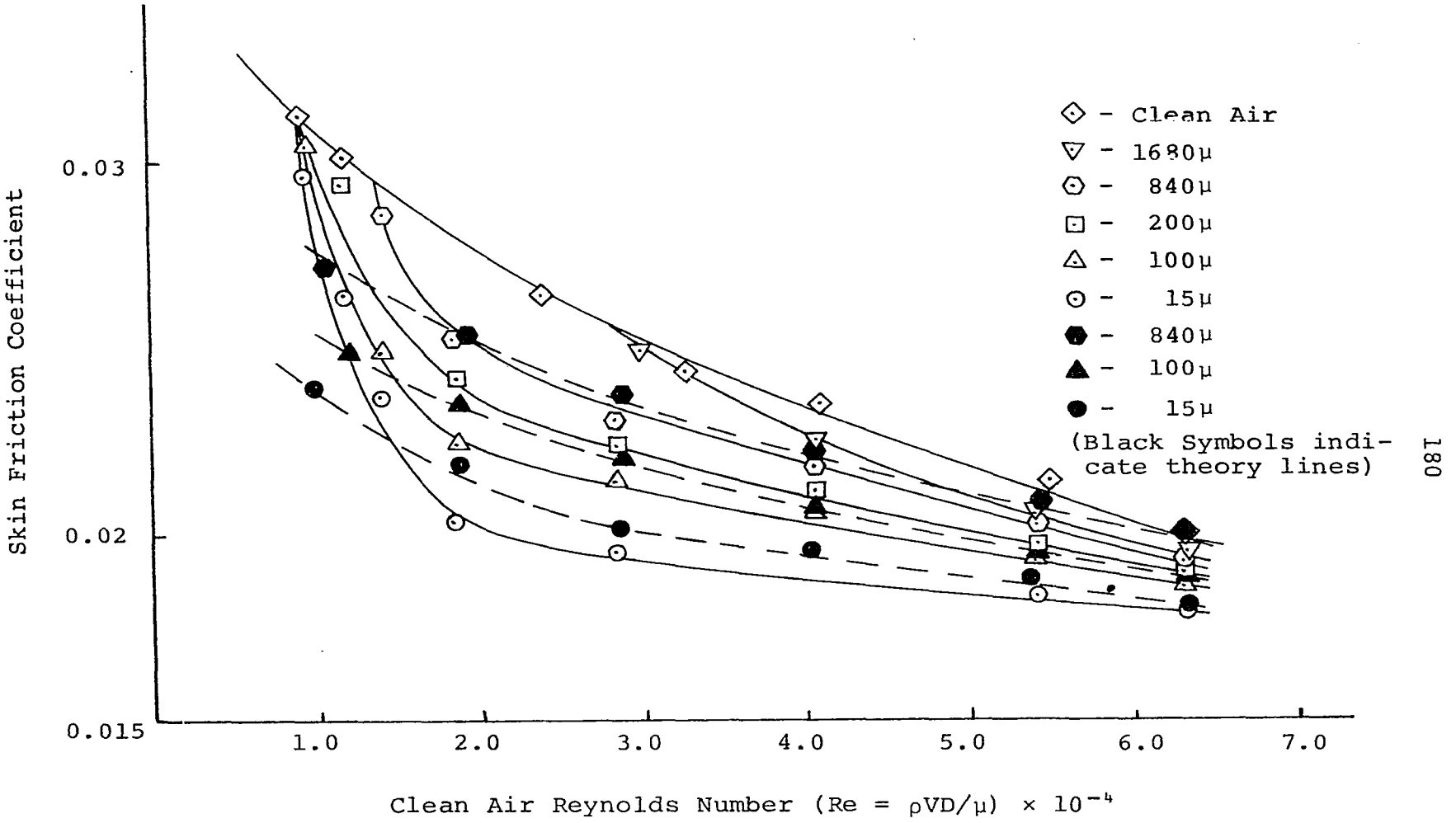

Figure (7.25) Theoretical Predictions of Dusty Gas in a Circular Pipe.

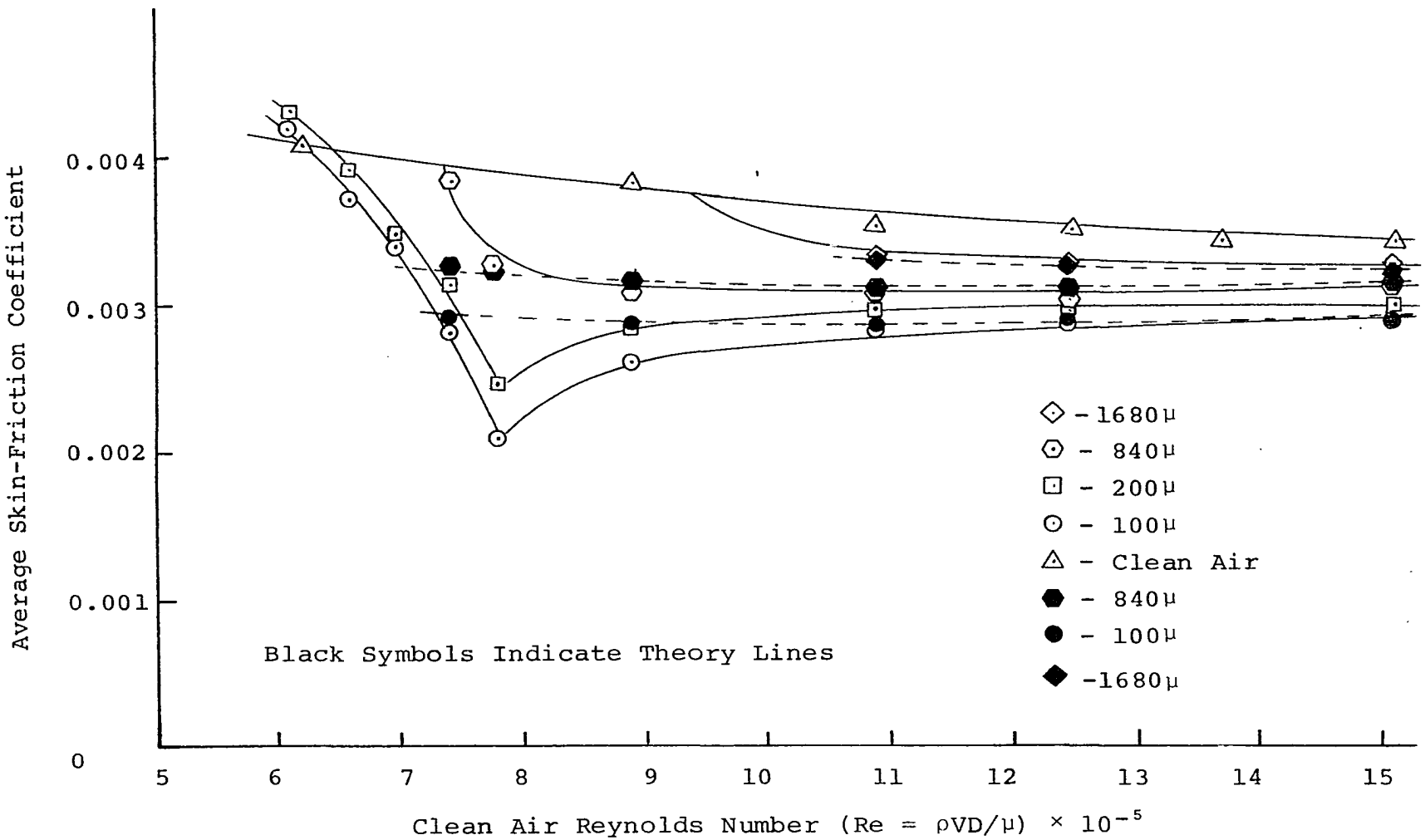

Figure (7.26) Theoretical Prediction of Dusty Gas Over a Flat Plate (W_p = 3-lb./min.).

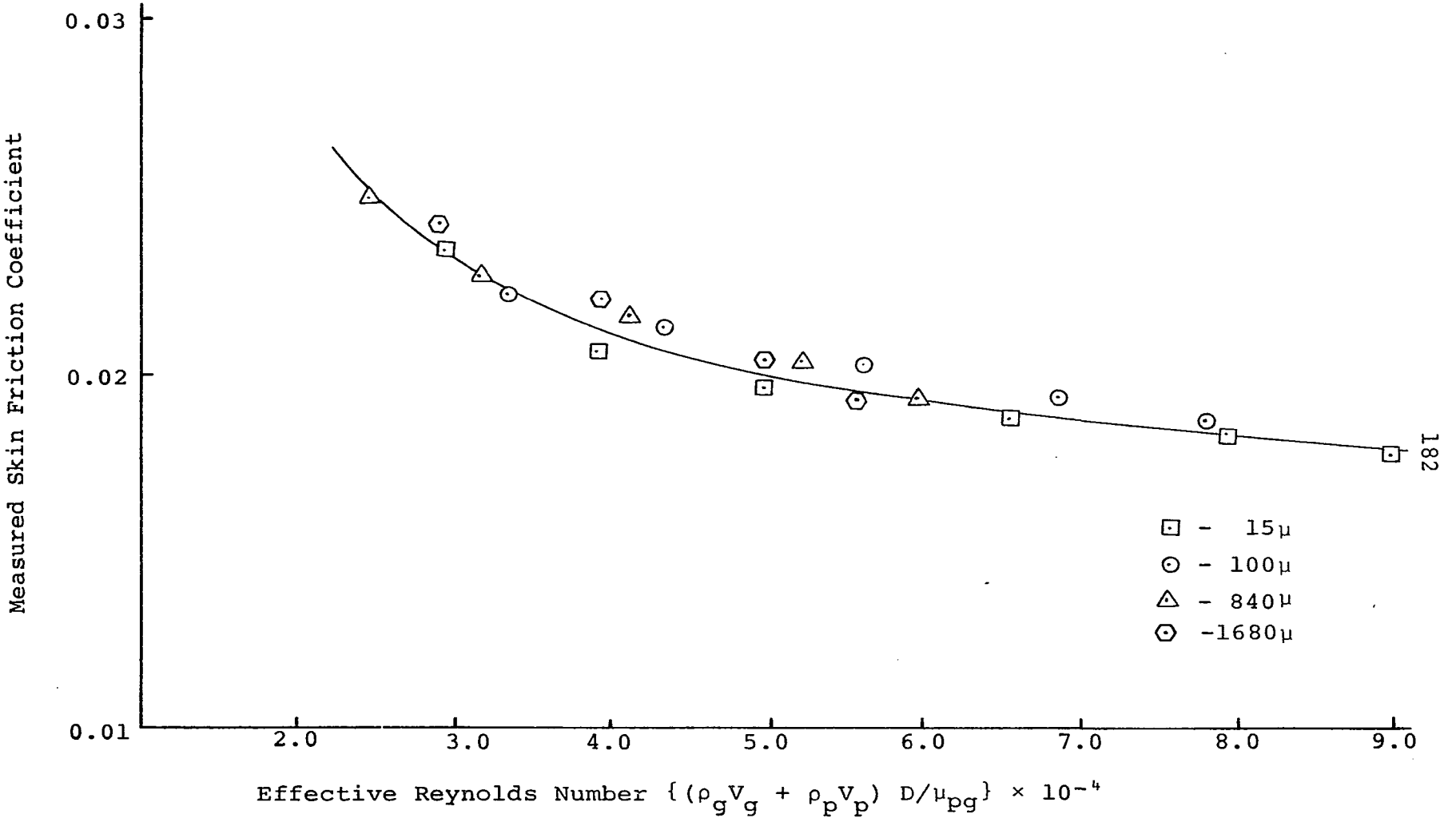

Figure (7.27) Parametric Study For Flow of Dusty Gas Through a Circular Pipe

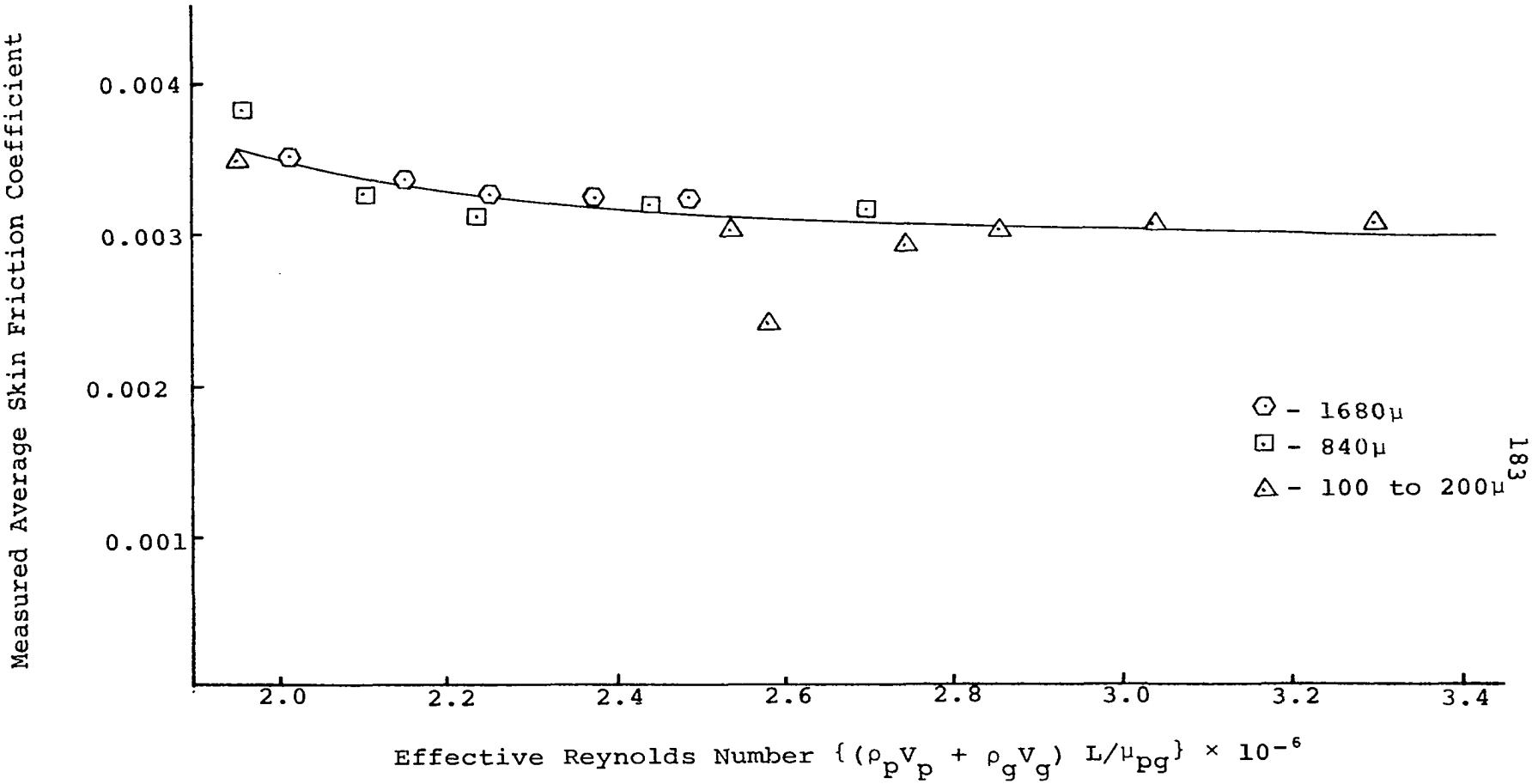

Figure (7.28) Parametric Study For Flow of Dusty Gas Over a Flat Plate

Figures (7.27) and (7.28) show that the skin-friction coefficient, based on the effective Reynolds number, falls on one line regardless of the weight-flow ratio or the particle size, thereby indicating that Reynolds similarity is valid for a dusty gas.

Mixing Length Effect

Prandtl's mixing length theory, with systematic experiments, helped in theoretically explaining turbulent flows with the air of the boundary-layer theory. Using Karman's hypothesis for the Prandtl mixing length (47) we have

$$\ell_m = -\kappa \frac{\partial \bar{u}/\partial y}{\partial^2 \bar{u}/\partial y^2} \qquad (7.19)$$

where κ is the universal constant. Figures (7.29) and (7.30) show the effect on "κ" with the suspension of particles in the air stream. The Figures indicate that the mixing length is reduced for values of $Re\sqrt{C_f} < 3 \times 10^3$ and increases for values greater than $Re\sqrt{C_f} > 3 \times 10^3$. This seems to indicate that the reduction of the mixing length is an important parameter in the reduction of the skin-friction coefficient; however, it is not the sole parameter inducing skin-friction reduction.

Physical Description

The introduction of particles into the turbulent flow stream tends to break up the large eddies into smaller ones, thereby reducing the Reynolds stresses and with it the skin-friction drag. This is one of the explanations put for-

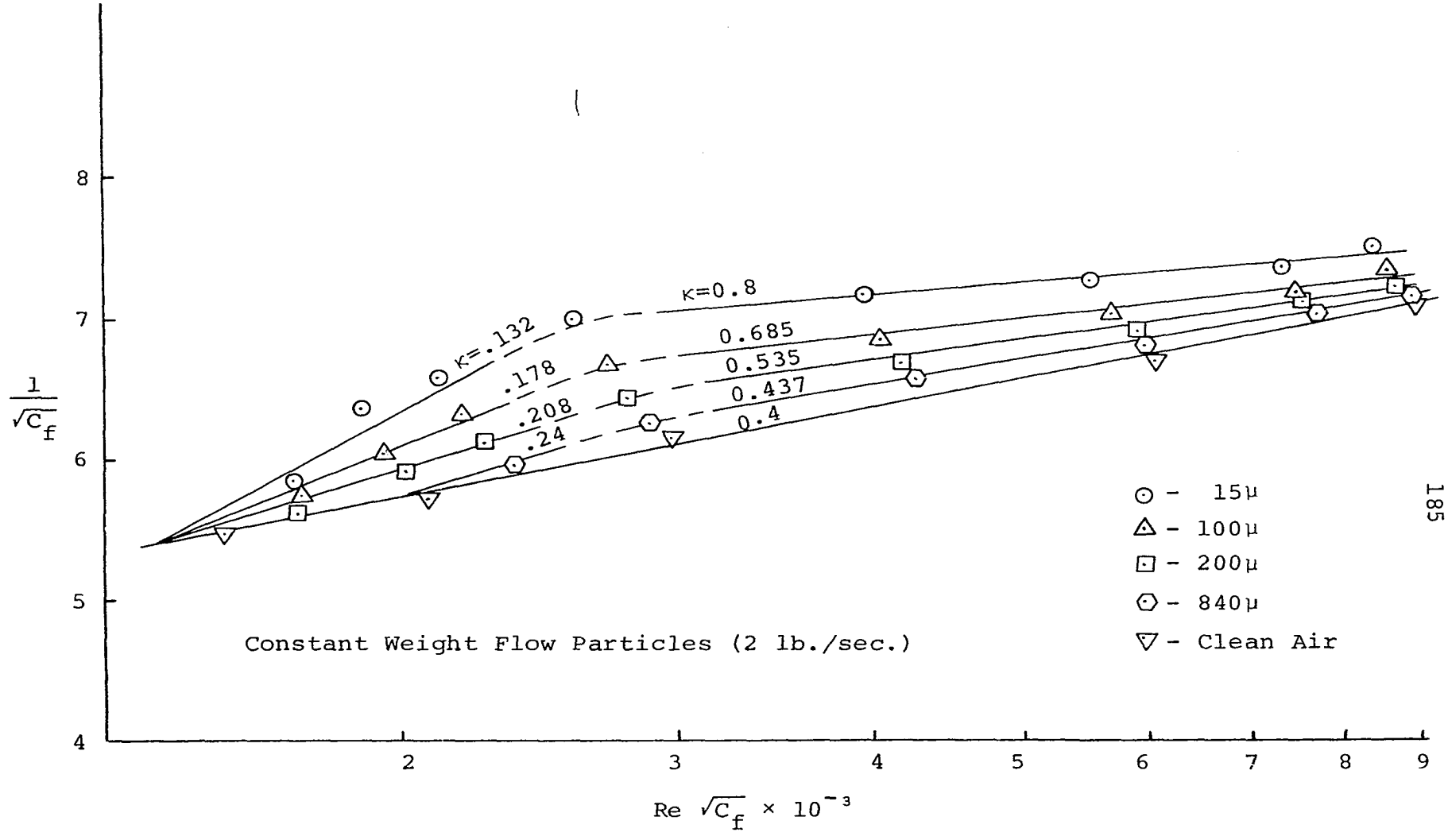

Figure (7.29) The Effect on the "Universal Constant", "K", for Dusty Air in a Circular Pipe.

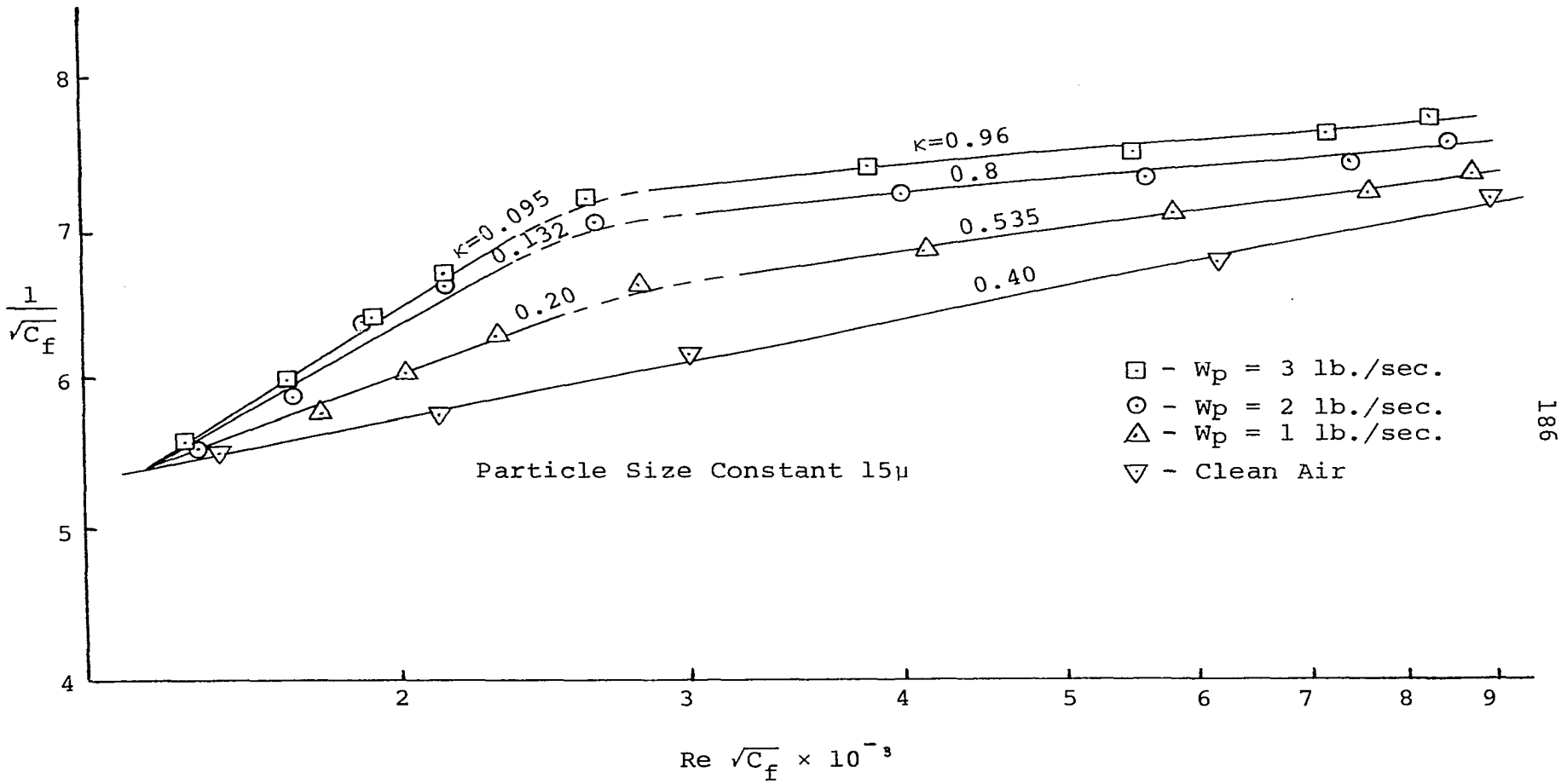

Figure (7.30) The Effect on the "Universal Constant", "K", for Dusty Air in a Circular Pipe.

ward to try and describe this phenomena.

Increasing the concentration of particles tends to decrease even further the skin-friction coefficients until an optimum concentration is achieved. The increase in the number of particles present increases the number of eddies decayed until the optimum condition is reached. The reason for the loss of effectiveness at very high concentrations is not too clear. It may be that there is, at these high concentrations, a large amount of collisions between the particles themselves thereby reducing their eddy-decaying effect.

The smallest sized particle was found to be most effective in reducing the skin-friction drag for a constant particle flow rate. This may be explained by the same phenomenon, since at a constant flow rate there would be many more of the smaller sized particles. It may also be noted that the point of maximum drag reduction for the small particles occurs at smaller weight-flow rates than for the larger particles. This may be due to the fact that the number of particles have reached the point where interaction between particles takes place, thus reducing their eddy-decaying effects.

CHAPTER VIII

CONCLUSIONS

Reduction of skin-friction coefficient to a greater or lesser degree was observed for all sizes of particles investigated. The two experiments conducted were dissimilar in their test setups and yet the results followed a very similar pattern. The results on the whole followed trends observed by other researchers in different fluid mediums.

The tests conducted covered a very wide range of parameters. The important parameters such as Reynolds number, weight-flow ratio, particle size were varied widely. This enabled a complete and thorough investigation of the effect of solid suspension on the flow phenomena. The calculation of relative velocity parameters and the photographic techniques developed should be very useful for future researchers in many related areas. The correlation developed here indicated clearly the trends that can be expected when solids are suspended in turbulent air streams. The equations show the effect of weight-flow ratio on percent reduction of turbulent skin friction for various particle sizes. The following sums up the important points concluded from the research:

1. Skin-friction reduction was observed for solids suspended in an air stream.

2. The maximum reduction in skin-friction coefficient was observed for the smallest particle sizes tested in each of the two flow loops.

3. The maximum reduction in skin-friction coefficient is observed in the low Reynolds number range of the turbulent flow region.

4. For constant particle sizes the weight-flow ratio plays a very important role. For small values of weight-flow ratio the skin-friction reduction increases linearly with weight-flow ratio. At higher values of weight-flow ratio the skin-friction reduction decreases with weight-flow ratio.

5. The skin-friction data exhibited Reynolds similarity in that all of the data fell on a single line when plotted against the effective Reynolds number.

6. The viscosity of the solid-gas mixture decreased for the fine dust particles (based on the kinetic theory of gases) but increased for the larger sized particles (based on the Einstein viscosity formula).

7. The velocity ratio (V_p/V_g) remains unchanged for variation in Reynolds number and weight-flow ratio for constant particle size.

8. The photographic techniques (see Chapter 6 and Appendix 2) developed are based on a double color exposure and should be very useful for many flow study problems.

BIBLIOGRAPHY

1. Newton, I. Philosphiae Naturalis Principia Mathematica. London (1686): Translated into English by A. Motte (1729), edited by F. Cajor, Berkley: University of California Press, Book II, p. 245.

2. Robbins, B. "New Principles of Gunnery", as shown in reference 3.

3. Sutton, O. G. The Science of Flight. Baltimore: Penguin Books, 1955, p. 32.

4. Prandtl, L. "Über Flüssigkeitsbewegung bei sehr kleiner Reibung," Verhandlung III. International Mathematic Kongress, Heidelberg, 1904, represented in Vier Abhandlungen zur Hydrodynamik und Aerodynamik, Göttingen, 1927.

5. Reynolds, O. "An Experimental Investigation of the Circumstances Which Determine Whether the Motion of Water Shall be Direct or Sinuous, and the Laws of Resistance in Parallel Channels." Philosophical Transactions Royal Society-London (1883), Vol. 174, p. 273.

6. Schlichting, H. Boundary-Layer Theory. New York: McGraw-Hill Book Co., 1960, p. 420.

7. Kuethe, A. M., and Schetzer, J. D. Foundations of Aerodynamics. New York: John Wiley and Sons, Inc., 1961 p. 355.

8. Antonatos, P. P. "Laminar Flow Control Concepts and Applications," Astronautics and Aeronautics, Vol. 4, No. 7, July, 1966, p. 34.

9. Bacon, J. W., Tucker, V. L., and Pfenninger, W. "Experiments on a 30° Swept 12 Percent Thick Symmetrical Laminar Suction Wing in the 5 Feet by 7 Feet University Of Michigan Tunnel," Northrop Corp, Norair Div., Report NOR 59-328 (BLC-119), Aug., 1959.

10. Pfenninger, W. "Untersuchungen über Reibungsverminderung an Tragflügeln, insbesondere mit Hilfe von Grenzschichtabsaugung." Reports of Aero. Inst., ETH, Zurich, No. 13 (1946); see also Jour. Aero. Sci. 16, 227 (1949) NACA TM NO. 1181 (1947).

11. Gasich, W. E. "Application of Laminar Flow Control to Transport Aircraft." Aerospace Engineering, Vol. 20, No. 10, Oct., 1961, p. 48.

12. Boyce, M. P. "A Practical Three-Dimensional Flow Visualization Approach to the Complex flow Characteristics in a Centrifugal Impeller," A.S.M.E. Paper No. 66-GT-83.

13. Kramer, M. O. "Boundary-Layer Stabilization by Distributed Damping," J. Aeronautic Sciences, Vol. 24, No 6, (1957)

14. Kramer, M. O. "Boundary-Layer Stabilization by Distributed Damping," J. American Soc. Nav. Engrs., Vol. 72 (1960), p. 25.

15. Kramer, M. O. "The Dolphin's Secret," J. American Soc. Nav. Engrs., Vol. 73, Feb., 1961.

16. Blick, E. F., Walters, R. R., Smith, R., and Chu, H. "Compliant Coating Skin-Friction Experiments," A.I.A.A. Paper No. 69-165.

17. Toms, B. A. "Some Observations on the Flow of Linear Polymer Solutions Through Straight Tubes at Large Reynolds Numbers," Proceedings of the International Rheological Congress, Scheveningen, Holland (1948), pp. 11-135-141.

18. Hoyt, J. W., and Fabula, A. G. "The Effect of Additives on Fluid Friction", NAVWEPS Report 8636 (Dec., 1964), U. S. Naval Ordinance Test Station, Pasadena, Calif.

19. Pruitt, G. T., Rosen, B., and Crawford, H. R. "Effect of Polymer Coiling on Drag Reduction", Report No. DMT B-2 The Western Col, Research Division, Aug., 1966.

20. Sproull, W. T. "Viscosity of Dusty Gases", Nature 190, (1961), p. 976.

21. Oldroyd, J. G. "A Suggested Method of Detecting Wall Effects in Turbulent Flow Through Tubes", Proceedings of the International Rheological Congress, Scheveningen, Holland (1948), pp. 11-130-134.

22. Goldstein, S., ef alia. Modern Developments in Fluid Dynamics, Clarendon: Oxford, 1938, p. 338.

23. Thomas, D. G. "Heat and Momentum Transport Characteristics of Non-Newtonian Aqueous Thorium Oxide Suspensions", A.I.Ch.E. Journal, Vol. 6, No. 4, p. 631.

24. Thomas, D. G. "Transport Characteristics of Suspensions II. Minimum Transport Velocity for Flocculated Suspensions in Horizontal Pipes", A.I.Ch.E. Journal, Vol. 7, No. 3, p. 423.

25. Thomas, D. G. "Transport Characteristics of Suspensions III. Laminar Flow--Properties of Flocculated Suspensions", A.I.Ch.E. Journal, Vol. 7, No. 3, p. 431.

26. Thomas, D. G. "Transport Characteristics of Suspensions IV. Friction Loss of Concentrated Flocculated Suspensions in Turbulent Flow", A.I.Ch.E. Journal, Vol. 8, No. 2, P. 266.

27. Knudsen, J. G., and Katz, D. L. Fluid Dynamics and Heat Transfer. New York: McGraw Hill, 1958.

28. Saffman, P. G. "Flow of Dusty Gas Between Rotating Cylinders", Nature 193, P. 463.

29. Saffman, P. G. "On the Stability of Laminar Flow of a Dusty gas", Journal of Fluid Mechanics (1962), Vol. 13, Part 1, pp. 120-128.

30. Soo, S. L., and Trezek, G. J. "Turbulent Pipe Flow of Magnesia Particles in Air", I & EC Fundamentals, Vol. 5, No. 3, Aug., 1966, p. 388.

31. Soo, S. L. Fluid Dynamics of Multiphase Systems. Waltham, Mass: Blaisdell Publishing Col, 1967.

32. Hinze, J. O. Turbulence. New York: McGraw-Hill Book Co., 1959, p. 281.

33. McCarthy, H. E., and Olson, J. H. "Turbulent Flow of Gas-Solids Suspensions", I & EC Fundamentals, Vol. 7, No. 3, Aug., 1968, p. 471.

34. Halstrom, E. A. N. "Design of Experimental Apparatus for the Study of Two-Phase Flow in Circular Straight Pipes", M.S. Thesis, Princeton University, 1953.

35. Briggs, L. W. Unpublished Report of Western Precipitation Division, Joy Manufacturing Co., Los Angeles, 1945.

36. Lumley, J. L. "The reduction of Skin-Friction Drag", Fifth Symposium--Naval Hydrodynamics--Ship Motion Drag Reduction, Office of Naval Research, Department of the Navy, ACR-112 (1968).

37. Fabula, A. G. "The Toms Phenomenon in the Turbulent Flow of Very Dilute Polymer Solutions", Proceedings of 4th International Congress Rheological Brown, (1963).

38. Frank, W. G. As compiled in ASHRAE Handbook of Fundamentals, 1967, p. 163.

39. Walters, R. R. "Experiments on the Aerodynamic Turbulent Damping of a Flat Membrane with Fluid Substrate", M.S. Thesis, University of Oklahoma, 1966.

40. Looney, W. R. "Skin-Friction Coefficients of Compliant Surfaces in Turbulent Flow", M.S. Thesis, University of Oklahoma, 1966.

41. Nikuradse, J. "Gesetzmäßigkeit der turbulenten Strömung in glatten Rohen", Forschungsheft 356 (1932).

42. Szymanski, F. "Quelques solutions exactes des équations de l'hydrodynamique de fluide visqueux dans le cas d'un tube cylinderique", J. de math. pures et appliquées, Series 9, 11, p.67, (1932).

43. Vennard, J. K. Elementary Fluid Mechanics, Edition 4, New York: John Wiley and Sons, Inc. 1961, pp. 306-307.

44. Pope, A. Wind Tunnel Testing, Edition 2, New York: John Wiley and Sons, Inc., 1961, p. 89.

45. Landau, L. D., and Lifshitz, E. M. Fluid Mechanics. Oxford: Permagon Press, 1963, pp. 76-79.

46. Vincenti, W. G. and Kruger, C. H. Introduction to Physical Gas Dynamics. New York: John Wiley and Sons, 1965, p. 54.

47. Day, J. M. An Introduction to Fluid Mechanics and Heat Transfer. Cambridge: The University Press, 1957, p. 180.

48. Einstein, A. The Theory of Brownian Movement. New York: Dover, 1956; also see Ann. Physik 19(1906) p. 289 and Ann. Physik 34 (1911) p. 591.

49. Proudman I. and Pearson, J. R. A. "Expansions at Small Reynolds Numbers for the Flow Past a Sphere and a Circular Cylinder", Journal of Fluid Mechanics, 2, 237 (1957).

50. Hirschfelder, T. O., Curtiss, C. F., and Bird, R. B. Molecular Theory of Gases and Liquids. New York: Wiley (1954).

APPENDIX I

TIME DELAY SYSTEM

TIME DELAY SYSTEM

Capacitor C_1 is charged through resistor R_1 to approximately the supply voltage. As the flash contacts on the camera shutter are closed C_1 is discharged through the primary of the pulse transformer T_1. The gate of SCR_1 then becomes more positive than the cathode and SCR_1 fires, discharging the first strobe light.

At the time C_1 discharges a negative pulse is applied to the base of Q_1. This pulse is inverted and directed to the input of OS_1. OS_1 is a one-shot multivibrator with a period of 4 milliseconds. The positive going 4 m.s. pulse from OS_1 is inverted by Q_2 and applied to the input of OS_2. OS_2 triggers on the positive going trailing edge of the 4 m.s. pulse, and produces a positive going 1 m.s. pulse at its output. The 1 m.s. pulse is applied to the base of Q_3. This pulse discharges capacitor C_4 which is charged through R_9. When C_4 discharges through the primary of T_2, SCR_2 is turned on and the second strobe light is fired 4 m.s. after the first. The time interval can be adjusted by trimming capacitor C_2.

The time delay system was tested on a Monsanto frequency counter which had an accruacy of 1 part in 10^7. The system was found to have a time delay of 4010 milliseconds.

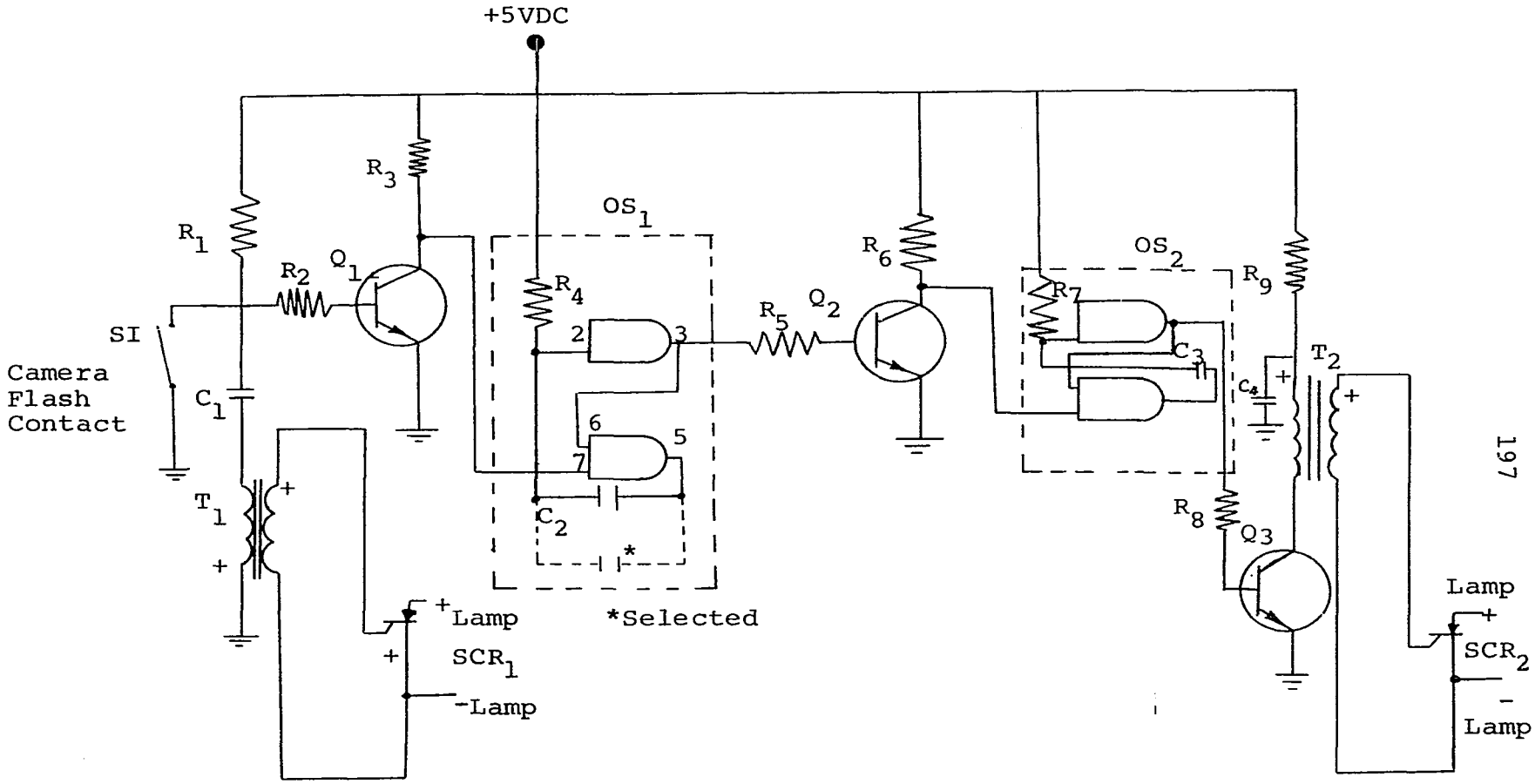

Figure (A1.1) Circuit Diagram for Time Delay System.

APPENDIX II

COLOR DEVELOPMENT PROCESS

COLOR DEVELOPMENT PROCESS

The processing of the color film had to be changed slightly from the standard "Kodak Process E-4" due to inadequate separation of colors. This change consisted of increasing the time in the first developer by 70 percent. This, in effect, increased the ASA rating from 160 to 320 and gave good color separation. The steps taken to process the film are shown in Table (A2.1).

Solution Procedure	Remarks	Temperature °F	Temperature °C	Time in Minutes*	Total Minutes
Prehardener	First 4 steps in total	85±1	29.5±½	3	3
Neutralizer	darkness.	83-87	28-31	1	4
First Developer		85±½	29.5±¼	12	16
First Stop Bath	Don't use Second Stop Bath here.	83-87	28-31	2	18
Wash**	Running water.	80-90	27-32	4	22
Color Developer		83-87	28-31	9	31
Second Stop Bath	Don't use First Stop Bath here.	83-87	28-31	3	34
Wash	Running water.	80-90	27-32	3	37
Bleach		83-87	28-31	5	42
Fixer		83-87	28-31	6	48
Wash	Running water.	80-90	27-32	6	54
Stabilizer		83-87	28-31	1	55
Dry	Dry film off reel.	<110	<43		

* Timing: Include time required to drain tank in total time for each processing ste.
** This step and the following may be done in normal room light.

Table (A2.1) Modified Kodak Process E-4.

APPENDIX III

NOMENCLATURE

NOMENCLATURE

Symbol	Description
A =	Area
a =	Particle diameter
B =	Constant
C =	Constant
$\overline{C}$ =	Average Molecular Velocity
C_d =	Drag Coefficient
C_f =	Skin-Friction Coefficient
$\overline{C_f}$ =	Average Skin-Friction Coefficient for Flat Plate
C_ℓ =	Lift Coefficient
D =	Drag Force
d =	Pipe Diameter
F =	Force
f =	Fanning Friction Coefficient
G =	Torque
g =	Gravitational Constant
g_e =	Newtonian Constant
h =	Measured Pressure Drop
K =	Constant
L =	Length Parameter
ℓ =	Length Parameter

Symbol	Description
ℓ_m =	Mixing Length
M =	Mach Number
m =	Mass Flow Rate
M_o =	Moment
N =	Number of Particles per Constant Volume
Nu=	Nusselt Number
P =	Pressure
Pr=	Prandtl Number
Q =	Volume Flow Rate
r =	Position Along Radii
Re=	Reynolds Number
T =	Temperature
t =	Thickness
u =	Velocity in X Direction
V =	Velocity
v =	Velocity in Y Direction
w =	Weight
w_d =	Width
x =	Abscissa
y =	Ordinate

Greek Symbol	Description
α =	Constant
β =	Constant
ε_h =	Turbulent Diffusivities of Heat

Symbol	Description
ε_m =	Turbulent Diffusivities of Momentum
δ =	Boundary Layer
ζ =	Effective Slip Coefficient
λ =	Mean Free Path Length
μ =	Viscosity
ν =	Kinematic Viscosity
ρ =	Density
σ =	Relaxation Time of Dust Particles
τ =	Shear Stress
ϕ =	Volume Ratio
ψ =	Constant
κ =	Universal Constant

Subscripts	Description
g =	Gases
gp=	Gas-Particle
p =	Particles